RESTRAINED SHRINKAGE BEHAVIOR OF HIGH PERFORMANCE CONCRETE REINFORCED WITH SYNTHETIC AND STEEL FIBERS

By

GREGORY BREWER

A thesis submitted to the

School of Graduate Studies

Rutgers, the State University of New Jersey

In Partial Fulfillment of the requirements

For the degree of

Master of Science

Graduate Program in Civil and Environmental Engineering

Written under the direction of

Dr. Hani H. Nassif

And Approved By

_____

_____

_____

New Brunswick, New Jersey

May 2018

ABSTRACT OF THESIS

RESTRAINED SHRINKAGE BEHAVIOR OF HIGH PERFORMANCE CONCRETE REINFORCED WITH SYNTHETIC AND STEEL FIBERS

By GREGORY BREWER

Thesis Director:

Dr. Hani H. Nassif

High performance concrete (HPC) is generically categorized as the type of concrete having both high strength and durability compared to conventional concrete. This is often achieved with the addition of cementitious materials such as fly ash, silica fume, and blast furnace slag as well as admixtures. This type of concrete is often also accompanied with a lower water:cement ratio. HPC mixes can be optimized in terms of strength, durability, workability, shrinkage, and commonly used around the world, but it is not without its flaws. A common problem seen in using this concrete in bridge decks specifically is its high cracking potential.

This research is aimed to investigate an effective tool that reduces and mitigates the cracking potential in bridge decks. Steel and synthetic fibers are implemented to address this issue. Fibers will be dosed into HPC mixes and the effects on fresh properties as well the strength development and shrinkage over time.

The experimental work will occur in two phases. The first section will be lab-based and compare the contributions of fiber additions and blending. Blending is implemented to promote pumpability and fibers are added to reduce cracking potential. Three fiber types will be analyzed in the lab. Two synthetic macro fibers and one steel hooked fiber, all with equivalent lengths of 2". Class A will also be compared for the data set. The second phase will involve the implementation of fiber reinforced HPC to a bridge in New Jersey. Blended HPC and blended FR-HPC will be cast in an alternating pattern for eight three span continuous bridge decks. The same tests will be run on the concrete sampled from these mixes and the bridge decks are also crack mapped and analyzed.

Fiber implementation proved effective in the reduction of cracking potential for HPC. The addition of steel hooked fibers and Euclid macro PPE fibers into this concrete reduced the cracking area of an AASHTO restrained ring by 26.3% and 23.2% respectively. The results were further reinforced in the field, both through the rings and through the crack surveys of the deck. The addition of fiber to blended HPC in the field resulted in a 42.5% reduction in cracking area when poured and a 79.5% reduction when pumped. These results translate to the actual bridge decks as well, where a 33.4% reduction in cracking area and 16.7% decrease in average crack width was observed when PPE Macro fibers were introduced to the mix.

ACKNOWLEDGEMENTS

I would like to first and foremost thank Dr. Hani Nassif for the support throughout this process. I was given an opportunity to prove myself as an undergraduate student and was fortunate enough to have the opportunity to continue my studies here at Rutgers University under his mentorship. Without this leadership and guidance, none of this would be possible.

I would also like to thank Dr. Adi Abu-Obeidah and Dr. Peter Jin for being members of my graduate committee. They have also provided excellent guidance and mentorship through both my undergraduate and graduate studies and research.

I also want to give credit to the numerous students who have helped with this research along the way. Giuseppe Liberti, Mirelle Alktaish, Jonathan Rodriguez, Christopher Sholy, and Elie Haddad have all been vital to this project's success. Without their help in the extensive labor portion of this project, it would not have been possible. I would also like to thank Dr. Adi Abu-Obeidah for his help throughout my time here at Rutgers. He has always been present to assist in whatever capacity was needed and provide advice and motivation along the way. His leadership has been invaluable. I would also like to thank my friends and family for their love and support throughout this process.

Lastly, I would like to thank Euclid Chemical, Clayton Concrete, Sika, BASF Chemical, and LaFarge for their material donations to accomplish this effort. I also need to thank the New Jersey Turnpike Authority for sponsoring this project and Rutgers Civil and Environmental Engineering department for this great opportunity.

Table of Contents

List of Figures

List of Tables

1. Introduction

1.1. Problem Statement

Concrete is the one of the most common building materials in the world, mainly for its versatility, strength, ease of use, and cost effectiveness. High Performance Concrete is considered a step above conventional concrete due to its increased strength properties, overall durability, and improved shrinkage. Even with lower average shrinkage, these effects can still be seen as significantly adverse in some applications due to the potential for cracking (Aitcin 2004). Shrinkage, paired with some other factors like loading, weather conditions, restrained conditions, and low tensile strength can make cracking a real issue. The case being viewed specifically here is for bridge decks. Cracking on bridge decks is an extreme concern, especially in colder climates, because of the widespread use of deicing salts. When these salts are used, there is the distinct possibility that they form into a solution with the snow or ice they are set to melt and infiltrate these cracks. When solutions of this type reach the steel, they can cause corrosion. This will cause deterioration to occur at a faster rate. For this reason, crack prevention and mitigation is vital to improving the lifespan of these decks.

The restraining of this concrete, paired with concrete shrinkage, is what causes cracks to occur. For instance, a sample that is free to shrink at its own will without any restrictions will not crack. When the concrete is somehow obstructed, the shrinkage will induce tensile stresses in the material and these stresses are what result in cracks. Restrain

and shrinkage are always present in reinforced concrete, so reductions in cracks and crack widths must be approached from a different perspective.

High performance concrete is an improvement on conventional concrete due to additions and adjustments in design. The first of those additions is the use of alternative pozzolan materials such as fly ash and silica fume. Fly ash is a byproduct of the coal industry which comes from crushing the used coal material into a fine powder. It is commonly used in the concrete industry. The addition of this fly ash is proven to increase strength over time, reduce shrinkage, reduce permeability, and it needs less water than cement so the water:cement ratio can be reduced (Aitcin 2004). Silica Fume is an extremely fine particle that is a byproduct of the production of silicon metals. Its main use is in concrete materials as a pozzolan. It is proven to result in an increase of strength and a decrease in permeability. It also results in a decrease in workability due to the large amount of surface area introduced to the concrete mixture (Aitcin 2004). These additions are also paired with the inclusion of air entraining agents and super plasticizers to further increase the materials effectiveness. This combination gives HPC an increase in durability, strength, and shrinkage when compared to conventional concrete.

HPC on its own does reduce cracking potential by increasing tensile resistance and reducing shrinkage, but the cracking is still a problem due to the corrosive nature of deicing salts. An effort will be made to specifically reduce the cracking potential, maximum crack width, and crack area in this study by introducing fiber additions. Euclid 2” macro polypropylene (PPE) fibers, Sika 2” macro synthetic fibers, and Sika 2” steel hooked fibers were introduced to the blended HPC mix and studied for effectiveness.

1.2. Research Objectives

The addition of these fibers needs to be studied from multiple viewpoints. Its overall performance must first be tested and compared to its counterpart without fibers. Compressive strength, tensile strength, modulus of elasticity, free shrinkage under multiple curing conditions, rapid chloride permeability and surface resistivity were all be compared in addition to the results from restrained shrinkage testing. Compressive strength must meet the minimum requirements. Tensile strength should not show significant reduction. Modulus of Elasticity is expected to decrease due to the fibers but cannot be reduced by any significant margin. Permeability is monitored with both RCPT and SRT and must also meet minimum requirements and is expected to remain similar to the blended HPC. Restrained shrinkage testing is monitored in a few ways. The most important way, which was primarily investigated, is the crack propagation over time. These tests will were followed up by crack mapping the physical decks that were replaced on the bridge in question to truly compare the effects that fiber additions have on the cracking potential of HPC.

1.3. Thesis Organization

This thesis will consist of six chapters which will be briefly described below.

Chapter 1 serves as an introduction to the problem at hand as well as the research objective containing the methods in which the problem will be addressed. It also briefly outlines the organization of the thesis.

Chapter 2 will contain a detailed literature review on both the problem statement and the implemented solution by looking at similar work and other successful cases.

Chapter 3 will give a detailed outline on the experimental procedure for both phase 1 and phase 2 all the way from acquiring materials to mixing and casting to the last test to be done.

Chapter 4 will cover the results of the laboratory work that is done and offer insight into these results. It will include results for all testing from fresh properties to material properties.

Chapter 5 will look at the results from the field work done with fiber reinforced concrete. It will compare the results in a similar fashion as the previous chapter

Chapter 6 will offer conclusions, some insight and recommendation, and a scope for future work.

2. Literature Review

2.1. Introduction

High Performance Concrete (HPC) has been an integral building material for modern society. Its combination of favorable initial workability, strength, durability and ductility make it an extremely versatile material. HPC attains these properties using substitute cementitious materials (SCMs) such as fly ash, silica fume, and slag, various admixtures, and lower water:cement ratios. Proper mix designs of HPC can increase tensile and compressive strength while simultaneously decreasing shrinkage and permeability (Aitcin 2004).

This material has proven to be susceptible to cracking and this cracking has been thoroughly investigated over time. The major causes for these cracks are often a combination of concrete shrinkage, poor ambient conditions (temperature, wind, etc.), traffic, poor curing techniques, improper or immature loading, and degrees of constraint (Folliard and Berke, 1997). This cracking can cause severe issues and shorten a structure's, specifically a bridge deck's, lifespan dramatically. This cracking often exposes the rebar inside the slabs to corrosive materials such as deicing salts (Liu and Weyers, 1998).

The addition of a multitude of fiber types is a relatively new technique being applied in multiple types of concrete to address critical issues, including cracking in terms of both prevention and mitigation. Fiber reinforced high performance concrete (FR-HPC) aims to

improve upon HPC by meeting all strength and permeability requirements as well as addressing crack prevention and mitigation.

2.2. High Performance Concrete

High performance concrete began its development off the back of the high strength concrete movement. Pierre Claude Aitcin's book on HPC starts with the introduction of plasticizers and fly ash into concrete production in the 70's. These additions allowed for a decrease in the water cement ratio and an increase in strength as a result. As the quality of both the plasticizers and fly ash improved over time, strength and durability properties also further improved (Aitcin 2004). Aitcin also explains how the concrete industry introduced silica fume into the general production of concrete in the 1980's. This was the next step towards improving what would be known as high performance concrete. Silica fume was accepted and adopted into the industry relatively quickly after being researched (Aitcin 2004). These additions have made great improvements to the durability, workability and strength of HPC, but Aitcin also stresses that it is far from a perfect material. It has made strides and is extremely versatile and useful, but further research and improvements are still needed (Aitcin, 2004).

HPC began to be used as a material for bridge decks in the 1990's. Subsequently, research on these bridge decks and their effectiveness gained traction around the same time period. The Indian Concrete Journal published a comprehensive look into these bridge decks which cited many research projects into this very subject (Mehta and Burrows 2001). The section studying bridge decks cites a section of a report from Krauss and Rogalla in 1996. This report encompassed the results of surveying 200,000 newly constructed bridge decks in both the United States and Canada. It also announces the

startling result that over 100,000 of these decks showed transverse cracking soon after construction (Krauss and Rogalla 1996). Krauss and Rogalla concluded that HPC mixes with high total cement contents, high range water reducers, and silica fume result in concrete with high strength and increased brittleness. This brittleness showed itself to be a leading factor observed in the early cracking of these newly constructed bridge decks (Krauss and Rogalla 1996). The report goes on to make further conclusions on how an increase in strength shows direct correlation to an increase in cracking in bridge decks (Mehta and Burrows 2001). So, the benefits of decreased permeability are essentially null and void due to the dramatic cracking seen in the early HPC bridge decks. The deterioration seen in these structures needed to be addressed in some way.

One of the major areas still to be researched at this point was the cracking potential of HPC mixes and the effects of various admixtures, aggregates and pozzolans on cracking. In 2005, a paper was published by Rambod Hadidi and M. Ala Saadeghvaziri that researched cracking mechanisms, specifically in bridge decks. The issues they discovered to be the primary causes for transverse cracking of bridge decks include, but are not limited to; restrained conditions, environmental conditions, volume changes over time (shrinkage), and improper loading (Hadidi and Saadeghvaziri 2005). These conclusions were made based on a comprehensive literature review on previous studies into the same issue. In 2009, a FHWA report looked deeper into the use of HPC in bridge decks by studying a plethora of structures (Graybeal 2009). Their conclusions emphasize that HPC is an extremely useful material in these circumstances. They also list ways to prevent cracking (water:cement ratio between 0.35 and 0.4, 600-700 pounds cementitious material). These mixes exhibit and improvement to cracking potential (Graybeal 2009).

By combining what is known about cracking in general when it comes to bridge decks and cracking specifically in terms of HPC, the scope refines itself within these factors. Now that this subject matter has been improved, further research can be made into more additives to improve the cracking potential of this material.

In 2012, a comprehensive study was done by Ray, Gong, Davalos, and Kar on the cracking of various HPC mixes to study the effects of varying SCMs, water content and aggregates on inherent shrinkage and cracking properties associated with each mix design (Ray et. al. 2012). This study used four types of coarse aggregates, three distinct SCM combinations (utilizing fly ash, slag, silica fume, and metakaolin), and three water:cement ratios to investigate the effects each attribute has. The results offer insight into each variables effect on the outcome in terms of mechanical properties, shrinkage, and cracking tendencies. To analyze cracking tendencies, AASHTO rings were implemented. Each mix was compared by the date which cracking onset occurred. One thing that was noticed was a decrease in modulus leads to an increase in the age of cracking. It also showed that cracks appear earlier in mixes with lower water:cement ratios. The effects of various SCMs are shown as having no significant effect on the age at which cracking begins in the specimens (Ray et. al. 2012). These observations can lead into many ways in which cracking potential of HPC can be improved upon and opens new avenues of research by defining optimal properties to reduce the cracking potential in this use case.

The cracking can be approached from a multitude of directions, but each has the same end goal. Researchers have been attempting to solve this issue for years. In 2011, it was shown that the addition of pre-saturated lightweight aggregate shows positive effects in

terms of cracking potential (S. Slatnick et. al. 2011). Also in 2011, shrinkage reducing admixtures were shown to have a positive effect on the shrinkage induced cracking of HPC (Saliba et. al. 2011). In 2016, a comprehensive finite element model determined that in bridges where traffic reduction must be minimal and adjacent lanes are opened at six hours, compressive strength must meet a 1200 psi minimum to minimize cracking (Abu-Obeidah et. al. 2016). These ideas have seen marginal success but are by no means perfect. The addition to be further investigated is the use of fiber reinforcement in HPC to prevent and mitigate cracking in HPC bridge decks.

The mix design to be reviewed in the following research also involves the use of blended aggregate. The blending of coarse aggregates is done to improve the pumpability of concrete. A study in 2011 researched the effects of varying aggregate gradation on the workability and compressive strength. These mixes ranged from ACI standard design methods to using band gradation. Band gradation is determined through a sieve analysis of the proposed aggregate mixes. The individual percent retained is graphed and must meet the given requirements or bands to be considered acceptable. In total, eight mixes were cast with various blends created by adjusting or adding aggregates to the concrete (Ashraf and Noor 2011).

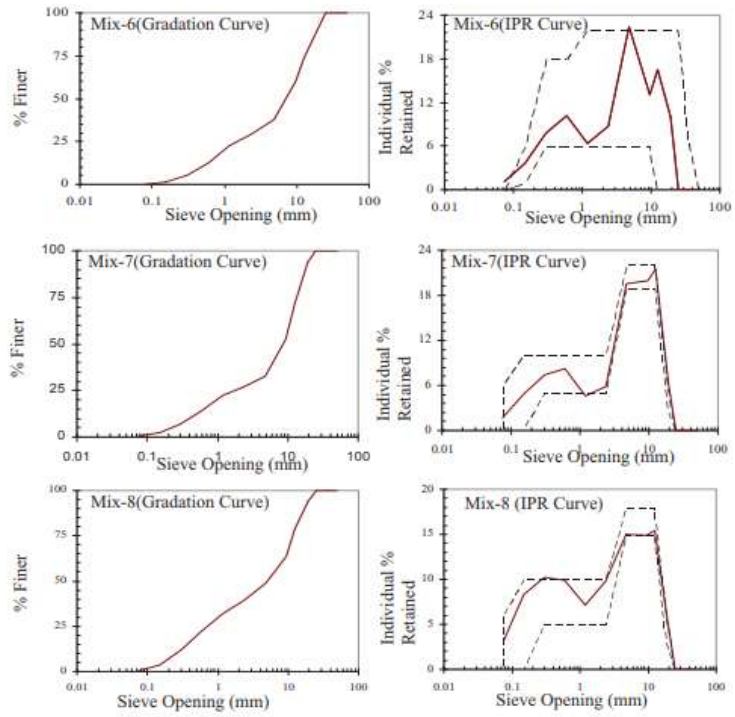

Figure 2.1 Aggregate Band Gradation

The previous figure gives a few examples of the aggregate gradations attempted. It also depicts the band gradation. The solid lines show the actual gradation of the aggregate while the dashed lines show the acceptable bands or ranges that the IPR curve is attempting to comply with. The results suggest that changing the IPR of a mixes aggregate can influence the compressive strength by more than 50%. It also states that the workability can be improved by gradation, but the fineness modulus has a more influential effect on this property (Ashraf and Noor 2011). Aggregate gradation is being used to improve the pumpability of the concrete. Increasing the workability while not affecting the strength of the concrete is the goal, and this research proves the effectiveness of proper aggregate blending.

2.3. Concrete Shrinkage Performance

The analysis to be done in this investigation is primarily focused on the cracking potential and the mitigation of cracking in concrete slabs. This fact makes shrinkage one of the most important factors. A comprehensive report from the Federal Highway Administration (Brown et. al. 2001) gives the following graphic that depicts causes of cracking in bridge decks.

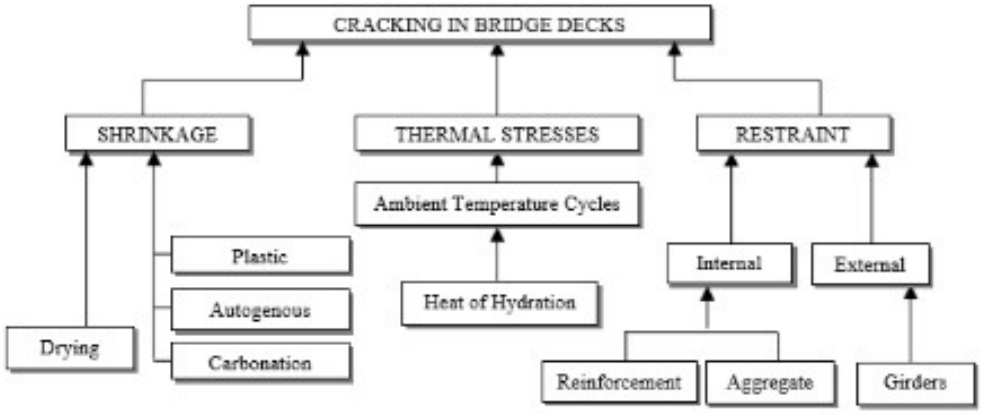

Figure 2.2 Causes of Bridge Deck Cracking (Brown et. al. 2001)

The purpose of this FHWA report is to investigate and elaborate on the most common causes for transverse cracking in bridge decks (Brown et. al. 2001). The mechanisms that lead to cracking must first be understood before solutions can be examined. Drying, plastic, autogenous and carbonation shrinkage are all compounded into one and these combined shrinkage effects often contribute to the transverse cracking seen in many modern-day structures, specifically bridges (Brown et. al. 2001). A further understanding of why and how concrete shrinks overtime and the effects this shrinkage has on concrete that is often restrained due to rebar will lead to a better formulation of

conclusions and possible solutions to improve upon the downside that these materials have been proven to display.

2.3.1. Types of Shrinkage

The four types of shrinkage to be reviewed in this section are drying shrinkage, plastic shrinkage, autogenous shrinkage, and chemical shrinkage. Each shrinkage type is accompanied by its own unique process, timeline, and effects on the bigger picture in terms of cracking. Understanding the individual mechanisms and ways to address the issues associated with them can help with the further reduction of cracking potential in HPC. Each method commonly seen in concrete production will be carefully looked at.

Drying shrinkage is present for all variations of ordinary concrete. This shrinkage is a factor in the cracking of slabs. This cracking must be addressed to improve the durability of concrete members (Pigeon and Saucer 1992). Drying shrinkage transpires when the concrete material is subjected to an environment in which the relative humidity is lower than the internal humidity. This set of conditions causes the water contained in the concrete pores to diffuse from the specimens until there is an equilibrium established between the internal and external humidity. This process results in the deformation known as drying shrinkage (Baroghel-Bouny and Aitcin 2000).

Autogenous shrinkage is the term given when a reduction in volume occurs for concrete or cement compounds after casting. It is caused by the initial setting and hardening of a concrete or cement specimen. It is also noted that the autogenous shrinkage is increased by the reduction of the water:cement ratio and the higher total cement content. Both are key factors when discussing this subject in terms of high

performance concrete. This process is a form of self-desiccation. Unlike specifically in drying shrinkage, the excess water located in the pores is used in the hydration of cementitious material and the final volume is less that the starting volume (Tazawa 1998).

Plastic Shrinkage occurs in the time frame very close to casting. It is a short period of time that occurs between when the water gloss disappears from the surface of the concrete and ending on average two hours after. The mechanism that causes plastic shrinkage is the quick evaporation of surface water. When the surface begins to dry, pressure begins to build in the capillaries of the concrete until a maximum pressure is reached. At this point there is a pressure release. Plastic shrinkage occurs as the pressure is building in the concrete. There is enough force to make the specimen contract slightly and the strain of this contraction can be measured (Cohen et. al. 1990).

The last method of shrinkage in question is the chemical shrinkage. It refers to a broad group of reactions and mechanisms that are chemical in nature and effect the overall shrinkage of the concrete. The mechanisms of this spectrum include, but are not limited to hydration, thermal, dehydration, crystallization, carbonation and conversion shrinkage. The general mechanism for these involves some type of reaction which is the cause of a change in volume for the substance in question (F. H. Wittmann 1982).

2.4. Fiber Reinforced Concrete

Fiber reinforced concrete (FRC) was first patented in 1971 by J.L. Sherard as a composite cementitious material containing a matrix of distributed fiber elements (Sherard 1971). Research on the use of various fibers in concrete materials is still

occurring today. Thousands of papers have been written on the subject matter. A paper by Ronald Zollo, published in 1996, provides a resourceful overview of FRC and its breakthroughs and applications over time. The same report also stresses on the fact that the industry oversimplifies the use cases of FRC and more research needs to be done to break down the nonspecific perception of fiber into more effective subsections (Zollo 1996). FRC has been proven to act in different ways based on a host of factors including mix design, fiber type, concentration, dispersion, or orientation. It's not outrageous to assume totally different outcomes to be possible for some of these variations, so the application list is endless. One of the most important concepts comes from the idea of fiber reinforcements effects on crack growth in terms of the energy these fibers absorbed (Zollo 1996).

Many fiber types have been researched through time. Steel, glass, natural, polypropylene, kevlar and nylon are just a handful of what has been and is still being investigated. These FRC variants have been used in pavements, runways, tunnel linings, blast resistant features, thin pipes and shells, dams, and tanks (Wafa 1990). These avenues have demonstrated to be useful and successful in their own regard, and this proves a certain degree of versatility with the use of FRC in structural elements. While most of these fibers have proved useful, this paper and research will specifically be geared towards the use of polypropylene macro fibers, synthetic macro fibers and steel hooked fibers.

This leads to the implementation of fibers to high performance concrete mixes. In 2000, Guerrini published a paper on his findings on the applications of high performance composites containing fiber reinforcement. To classify in this category, these materials

had to be developed with toughness, ductility, and energy absorption in mind (Guerrini 2000). The combination of HPC materials and the fiber matrices that displayed improvements in these facets in FRC mixtures seemed like the most obvious route to go. The paper goes on to discuss the results of these inquiries. This testing resulted in a better understanding of how this combination of two ideas proved effective. It concludes that, in optimal proportions, significant strength and ductility can be established in fiber reinforced composites (Guerrini 2000). These results are focused on all types of high performance cementitious composites and not just HPC, but they show a progression of thinking and application leading to a broad spectrum of conclusions that can be further researched.

As FR-HPC started becoming a more readily available and provenly effective construction material, more issues were addressed along the way. Rigid fibers offered increased flexural strength while micro fibers offered significant shrinkage improvements. Hybrid fiber mixtures began to be utilized to address both issues simultaneously (di Prisco, Plizzari, Vandewalle 2009). Synthetic macro fibers came into the fold much later than steel fibers. These fibers were lighter, offered a more even distribution and corrosion resistance on top of similar benefits seen when adding steel fibers such as crack resistance and increased flexural strength (Deng and Li 2006). When the fiber materials began to be broken down into categories, more effort was put forth in identifying the advantages of each individually and in a multitude of combinations. Since the focus of this experimental examination is polypropylene macro fibers and steel fibers, advancements of these will be addressed next.

2.4.1. Polypropylene Macro Fibers

Synthetic fibers have gained a large amount of traction over time in concrete applications. A study from 2011 investigated the use of macro fibers in varying concentrations (Hasan et. al. 2011). Four batches of concrete were produced and tested with fiber concentrations from 0 to 0.51% by volume. The results point out an insignificant change in terms of compressive strength, a 10-15% increase in tensile strength as well as a unique failing mechanism in which the fibers absorb some amount of energy after cracking and before total failure, a 15-65% increase in shear strength, and an increase in strain capacity (Hasan et. al. 2011). The direct results show promise immediately, but it is the failure mechanisms in both the shear test and tension test that imply an inherent ductility caused by the energy absorption of fibrous materials after cracking that shows the most promise of any results or conclusions. Another study performed by Buratti in 2011 further verifies the use of macro synthetic fibers. Although the performance of an individual fiber is less significant that a steel fiber, the rigid fibers experience a tougher time to equally disperse during the mixing process. The flexible fibers (polypropylene) show a much higher degree of homogeneity (N. Buratti et. al. 2011). The fact that these fibers are more evenly dispersed during the concrete production promotes a more consistent result as compared to the poor distribution of stiff fibers. Even with a significantly lower modulus of elasticity when compared to steel fibers, appropriate sizing, proportions, and dosages can drastically improve the ductility and durability of concrete materials (Soutsos et. al. 2012).

Lots of research has been conducted looking at the mechanical properties of concrete with fiber additions. Research has shown that macro fiber additions can cause a

decrease in compressive strength at higher dosage points. Appropriate dosing can also cause an increase in tensile strength (Fallah and Nematzadeh 2017). Research in 2014 conducted by Bolat et. al. delves in to the effects of fiber reinforcement on mechanical properties of FRC mixtures. Both steel and polypropylene fibers are investigated in this research for a more comparative result. The research points to an increase in air content, a reduction in water absorption, and a decrease in workability because of the addition of polypropylene macro fibers (Bolat et. al. 2014). These benefits and issues are important to note in terms of application of FRCs.

An investigation in 2014 from Pujadas et. al. looked specifically into the orientation of macro synthetic fibers when being poured. Understanding how the fibers naturally lay is important in rationalizing the benefits they bring to the table as well as gauging the effectiveness in some uses. The investigation studied the natural orientation these fibers would fall into when being cast into slabs (Pujadas et. al. 2014). The results point out strong tendencies of these fibers in form work and in free flow. In form work, it is said that the fibers arrange themselves parallel to the form walls when being poured. When being poured in free flow, the plastic fibers orient in the direction perpendicular to the flow of the concrete (Pujadas et. al. 2014). This is important because it proves that fibers will naturally orient themselves in favorable directions both in free pours and in concrete frameworks. There will of course be outliers, but the majority of fibers will lie perpendicular to crack openings and will naturally gain the ability to absorb stress once crack faces begin to open. The same result can be assumed for steel fiber orientation during placement.

In the application in question, the biggest concerns and points to be researched are the durability, permeability, and cracking performance of this type of fiber. There is a plethora of research on micro polypropylene fibers, but information on these characteristics are extremely limited when it comes to macro fiber usage. A test was completed in 2017 by Plaugue investigating the impact of different fiber types and fiber orientations in terms of cracking and permeability. This test was done with a polypropylene, polyethylene mixture instead of only polypropylene macro fibers. Hooked steel fibers were also tested in this experimental regime and will be described in the following section. It was found the FR-HPC with synthetic fibers is less permeable than a generic HPC mix design. This specific fiber combination was also found to be less effective in crack control than the steel hooked fibers. Its ultimate tensile strength was also 25% less than the FR-HPC with hooked steel fibers. The overall result suggests that the blend used in this experiment was less efficient than steel fibers properly oriented (Plague et. al. 2017). The fiber types show an immediate improvement in post cracking capacity as well as post cracking permeability. The combined restrained ring testing and bridge deck crack mapping of this research directive aims to clarify the effects of these fibers in terms of cracking.

2.4.2.Steel Fibers

Steel fibers were the first to be implemented in FRCs. Early research was extremely limited and often lead to more questions than answers. From this era on, plenty of research has been conducted to analyze the behavior of these fibers. They come in a multitude of shapes and sizes. The most common fiber shapes are straight, crimped, twisted, hooked, ringed, and paddled (Wafa 1990). Each variation comes with slightly

different results, but the overall trends remain similar. P.S. Song and S. Hwang researched the mechanical properties of steel fiber additions at varying dosages (0.5% - 2.0% volume fraction) of hooked steel fibers. Their findings indicate a 7-15% increase in compressive strength, 19-98% increase in tensile splitting strength, and 28-126% increase in the modulus of rupture (P.S. Song and S. Hwang 2004). The initial results here show more positive effects that have been seen with the polypropylene microfibers. Improved performance along with the general understanding of fibers vast improvement in post-crack behavior have caused fiber reinforced composites to become both readily available and frequently used in construction. These effects have lead steel fibers to be the more popular choice in structural concrete projects where concrete crack control is of important (Buratti et. al. 2011). The widespread use of this material is a clear indication of its strength and versatility, but that does not mean it is not without flaw.

The downside to steel fibers is their inherent corrosive tendencies. When exposed to corrosive elements or environments, long term concerns come into play. A study on this issue in 2005 by Granju and Balouch lead to a further understanding on how these fibers react in severe conditions. The fibers become exposed through cracking of said concrete. Cracks smaller than 0.1 mm (~.003 in.) displayed no corrosive action after a year of exposure. Some corrosion was experienced in cracks wider than .5 mm (~.015 in.) without reduction of cross sectional area. Cracks of 2-3mm (.08-.11 in.) displayed severe corrosion over the same time period (Granju and Balouch 2005). This leaves a fine line in terms of bridge decks, especially because of all the independent random variables that cannot be controlled in construction, weather and even in loading. The steel fibers clearly show their effectiveness across the board for an abundance of applications, but the

corrosive properties can dramatically decrease expected lifespan if not approached with precision and care.

The recent 2017 study conducted by Plague, Desmettre, and Charron specifically looks at the concrete permeability when fibers are involved. Using steel fibers at favorable, average, or unfavorable orientation angles, tests were done on the permeability of steel fiber reinforced HPC. It was found that less favorable fiber orientation can lead to up to 33% decrease in tensile strength, but lead to improved permeability of the cracked sections. Both fiber types drastically reduced the permeability of the cracked molds being used, but long-term corrosion was not taken into consideration by these tests (Plague et. al. 2017). Even though this conclusion proves the effectiveness of fibers, its neglects the key idea of long term corrosion.

3. Experimental Program

3.1. Introduction

The experimental portion of this study occurred in two sections and followed a very similar outline with few discrepancies. The first portion of this study occurred in the laboratory. Fresh concrete was mixed using the proper tools in the lab. In terms of fresh concrete, the slump and air content were tested for and recorded. Samples were then casted properly with the assistance of vibrating tables and be placed in the environmental chamber for the first twenty-four hours to begin curing. The samples taken were enough to test for the following array of data:

- Compressive Strength (1, 3, 7, 14, 28, 56 days)
- Tensile Strength (1, 3, 7, 14, 28, 56 days)
- Modulus of Elasticity (1, 3, 7, 14, 28, 56 days)
- Free Shrinkage (14-day wet cure and dry cure)
- Restrained Shrinkage (with crack maps at 28, 42, 56 days)
- Surface Resistivity (7, 14, 28, 56 days)
- Rapid Chloride Permeability (28 and 56 days)

At the one-day mark, all samples were demolded. All cylinders not being tested are placed in lime tanks stored in a room with 100% humidity at all times. Three free shrinkage samples are also kept with the cylinders in the tanks, while the remainder of the free shrinkage samples go immediately to the environmental chamber and remain there

for the entire testing cycle. The restrained shrinkage rings were demolded and set up in the environmental chamber as well. Samples for the RCPT and SR testing are kept in a separate tank for the entirety of their testing cycles. The samples not being used for RCPT or SR were removed from their respective lime tanks at the age of 14 days and subsequently placed in the chamber for the remainder of their testing regimes. The first cycle is a set of seven distinct mixes (Class A, HPC, FR-HPC, HPC-b, FR-HPC-b(1), FR-HPC-b(2), FR-HPC-b(3)). The three FR-HPC-b mixes contain three different fiber types (Euclid 2" Macro Fibers, Sika 2" Macro Fibers, Sika 2" Steel Hooked Fibers). The FR-HPC will only be tested with the Euclid fiber type. Due to the variations in aggregates and fiber contents, HRWR was also varied to receive appropriate workability conditions. All testing procedures comply with ASTM and AASHTO standards.

The second part of this testing procedure was field based instead of lab based. The majority of the outline for the first procedure remained true for the field work as well, but the fresh properties were measured by an independent contractor and the samples remained on site in similar conditions to the slabs they are casted with for close to 24 hours before being transported back to the lab for demolding, testing, and storage. From this point forward, the steps listed previously remained true for this testing set as well.

3.2. Material Properties

The materials in question are primarily locally sourced with little exception. The availability of each material is very important if it is to be implemented by agencies in the area. All coarse and fine aggregates, along with cement and silica fume, were acquired from Clayton Concrete in Edison, New Jersey. Admixtures and Fibers are obtained

through the likes of BASF, Euclid, and Sika. Each material used is listed with a source for easy interpretation in the following table.

Material	**Specifics**	**Source**
Fine Aggregate	Concrete Sand	Clayton
Coarse Aggregate	#8 and #57 Aggregates 3/8" and 3/4"	Clayton
Portland Cement	Type I/II	Clayton
Silica Fume	Densified	Clayton
Fly Ash		LaFarge
Fibers	2" Synthetic Macro 2" Synthetic Macro 2" Steel (Hooked)	Euclid Sika Sika
Air Entrainer	Master Air VR10	BASF
High Range Water Reducer	Master Glenium 7620	BASF

Table 3.1 Materials and Sources

A variety of simple testing must be done on the aggregates before any mixing is done. The aggregates underwent a sieve analysis according to ASTM C316. The aggregate properties were also obtained, and the moisture content is measured individually before each mix to ensure accuracy. The testing for both coarse aggregate properties and fine aggregate properties is done in accordance to ASTM C127 and ASTM C128 respectively.

Sieve analyses were conducted on all the aggregates to be used and cumulative distributions based on the mix designs were also formulated. The following table depicts

the individual percent retained amounts for each aggregate and each mix design proportion.

Sieve Opening (in.)	#57	#8	Sand	HPC	HPC-b
1.00000	0.00%	0.00%	0.00%	0.00%	0.00%
0.75000	7.30%	0.00%	0.00%	4.51%	1.72%
0.50000	51.50%	0.00%	0.00%	31.82%	12.16%
0.37500	25.60%	7.70%	0.00%	15.82%	10.01%
0.18701	5.20%	76.30%	0.80%	3.52%	40.72%
0.09291	4.90%	14.40%	2.90%	4.14%	9.29%
0.04646	0.70%	0.30%	10.00%	4.25%	2.81%
0.02362	0.90%	0.10%	22.40%	9.11%	5.84%
0.01181	1.50%	0.00%	43.00%	17.36%	11.06%
0.00591	0.00%	0.10%	19.40%	7.41%	4.88%
0.00295	0.00%	0.10%	1.60%	0.61%	0.45%
0.00000	2.30%	0.90%	0.00%	1.42%	1.01%

Table 3.2 Aggregate IPR

The sieve analyses were done first to make sure each aggregate complies with its respective standard, but also to gauge the gradation effects seen in each mix design. The following graphs show both the individual percent retained and cumulative percent retained to show the variances in gradation. First the aggregates will be shown independently, followed by the combinations used in the mix designs.

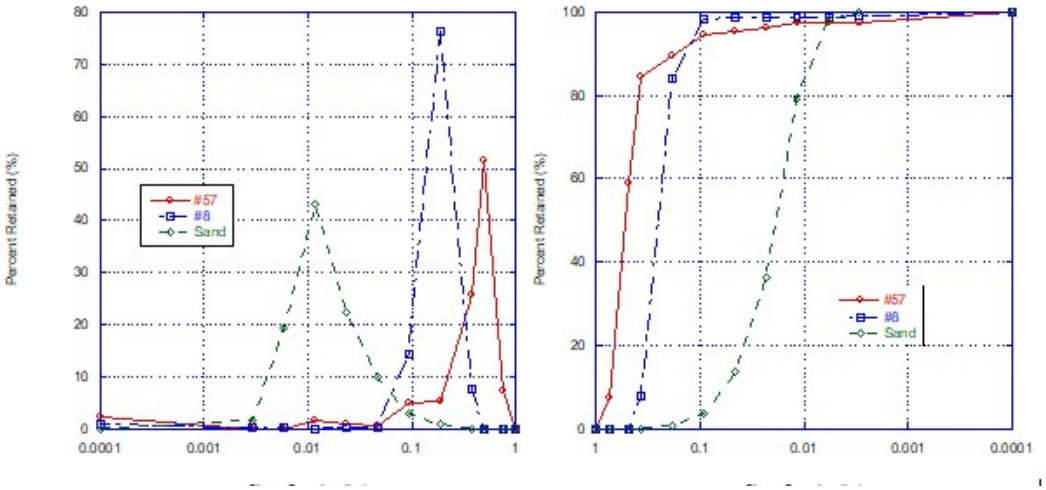

Figure 3.1 Aggregate Independent and Cumulative Percent Retained

The three aggregates shown are used in the appropriate proportions during the mixing phase of this research. The cumulative gradation for each mix design was also looked at. This difference in gradation has been proven to be beneficial when used properly. When looking at the full mix design, the improvement in gradation can be seen. In this case it is not drastic. However, it could be further optimized if deemed necessary. The inclusion of a small portion of #8 rock was first and foremost used to assist in pumpability during placement. Side effects of this can also include a reduction in shrinkage, stiffer concrete (higher modulus), and an increase in compressive strength. The adjustment to gradation is slight, so no major changes should be seen.

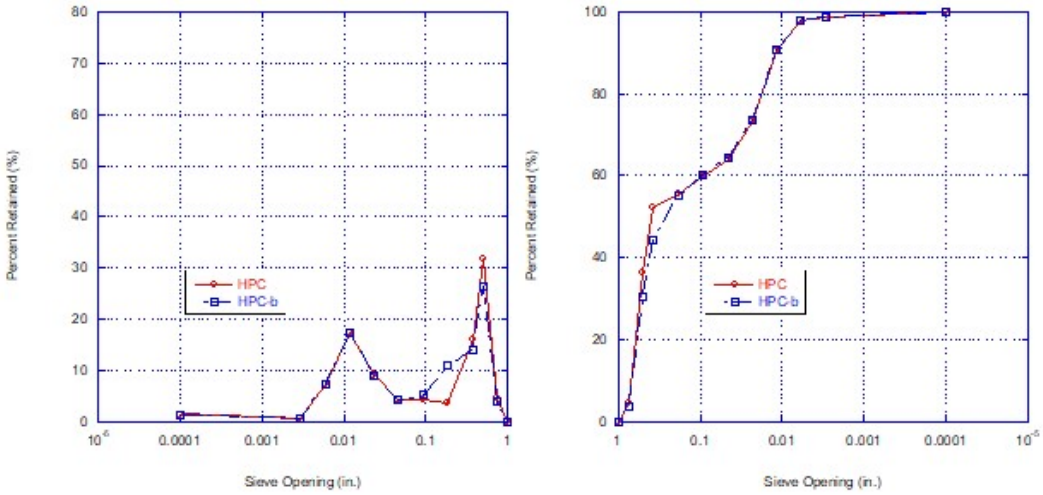

Figure 3.2 Mix Design Independent and Cumulative Percent Retained

All cementitious material is ensured to meet all governing requirements by the manufacturer. Cement must be tested and comply with ASTM C150. Silica Fume must be tested and comply with ASTM C1240. Fly Ash must be tested and comply with ASTM C618. Manufacturer's testing assures the validity of all three of these materials for this use. All three fiber types used comply with ASTM C1116. Each fiber is verified again through the manufacturer, who also provides all necessary physical and chemical properties to the consumer. For the admixtures, high range water reducer must be in used in accordance to ASTM C494-F and air entrainer must be used in accordance with ASTM C260. All physical and chemical properties are verified and assured by the supplier.

Figure 3.3 Fiber Types

The three fiber types procured for this study come from two manufacturers. Sika provided a 2" steel fiber which was hooked at both ends as well as a macro synthetic 2" fiber. Euclid provided a 2" macro polypropylene fiber. Each fiber was added to the base HPC blended mix in a proportion within the manufacturers' acceptable range. Both synthetic fibers were added at five pounds per cubic yard, and the steel hooked fibers were added at twenty-five pounds per cubic yard.

3.3. Mix Designs and Procedure

Seven mix designs were used in the first portion of this study, and two of them were repeated in the field for further validation. Mix proportions were kept as similar as possible, and all samples were cast from singular batches to ensure a valid comparison. Each lab mix was approximately 5.2 cubic feet. Each field mix was taken from trucks

pouring slabs. The mix proportions are shown in the following table, with the highlighted mixes being the ones used in the field as well, with some variation noted specifically in the water content of the field mixes. The mixes chosen were all approved NJTA designs with fiber additions.

3.3.1. Designs

Basic Mix	HPC	**HPC-b**	FR-HPC	**FR-HPC-b**	FR-Sika(1) - Synthetic	FR-Sika(2) - Steel	Class A
Cement, Type I (lb/cy)	520	**520**	520	**520**	520	520	658
Fly Ash, Class C (lb/cy)	130	**130**	130	**130**	130	130	-
Silica Fume (lb/cy)	25	**25**	25	**25**	25	25	-
Total Cement (lb/cy)	675	**675**	675	**675**	675	675	658
w/b ratio	0.382	**0.382**	0.382	**0.382**	0.382	0.382	0.410
#57 (lb/cy)	1,800	**1,500**	1,800	**1,500**	1,500	1,500	1,800
#8 (lb/cy)	-	**300**	-	**300**	300	300	-
Sand (lb/cy)	1,113	**1,113**	1,113	**1,113**	1,113	1,113	1,205
HRWR (oz/cwt)	2.5	**2.0**	2.5	**3.5**	2.5	2.5	2.0
AEA (oz/cwt)	1.0	**1.0**	1.0	**1.0**	1.0	1.0	1.0
Other admixture	-	**-**	2" PPE (5 lb/cy)	**2" PPE (5 lb/cy)**	Sika - Synthetic (5lb/cy)	Sika - Steel (25 lb/cy)	-

Table 3.3 Mix Designs

3.3.2. Procedure

The mixing of these concretes was done in the lab in a rotating mixing drum according to ASTM C192. First, all of the coarse aggregates were added into the mixer. The aggregates are mixed together for one minute with some of the required water before half of the cement and pozzolans are added. After this addition, a portion of the sand is placed on top of the cementitious materials in order to prevent material from building up on the walls of the drum. The mixer was sealed and turned on for an additional two minutes. At this point, half of the water was added to the mixer. The mixer was again turned on and this time mixed for two minutes. The previous two steps are repeated for the remainder of the cement, pozzolans, sand and water. The cement was added in two

segments due to the large amount needed and the restrictions created from the size of the mixer being used. The air entrainer is added into the water for the mix. Once this was all properly mixed, a minimum amount of super plasticizer is added. This was most generally between 2.0 and 2.5 ounces per hundred pounds of cementitious material. The mixer is sealed and let rest for two minutes before beginning mixing again. When the mixing began, any fiber additions were slowly made at this time. The fibers are added gradually in an attempt to avoid any unwanted clumping. Once all of the fibers are added, the mixer remains on and sealed for an additional three minutes at minimum. It is at this point that the mixer can be turned off and the fresh property testing can begin. It is important to note that any failure for fresh property testing will lead to additional use of admixtures, which will be added and again thoroughly mixed.

3.3.3. Fresh Property Testing

Fresh concrete properties tested include slump and air content. Slump testing is done in accordance with ASTM C143. Slump testing was done by filling the slump cone in equal thirds by volume. Each layer was rodded with a 5/8” tamping rod 25 times. The rod should penetrate the previous level by 1 inch and should never strike the bottom in a hard manor. After the third layer is rodded, the tester levelled the top surface of the concrete sample and wiped away any excess concrete around the base of the slump cone. Once these steps had been completed, the slump cone was raised slowly from the sample. Vertical slump was measured by the difference in height from the slump cone to the concrete sample after the cone is removed. For all mixes, a range of 4”-8” was considered acceptable. All mixes were tested at minimum one time. Any discrepancies resulted in retesting of the mix with a new sample.

Air content testing was also performed, in accordance with ASTM C231. Air testing was done using a pressure device. First, the bowl of this device must be filled in equal thirds. After each third, the bowl was rodded 25 times in a similar fashion to the slump samples. After each layer was consolidated, the bowl was also struck with a mallet 10-15 times around its circumference. Once the bowl was filled, the top layer was struck off and leveled with a strike off bar. After all excess was removed, the lid was attached and clamped in to place. Water was pumped through the petcock valves until air bubbles could not be seen. These valves were then closed and the meter was pumped to its designated initial pressure mark. After this, the lever controlling the pressure was released and the reading remaining was taken as the value for air content. Some of these test results appear controversial, possibly due to the fiber additions. The readings were taken as is for the results. Anyone testing slump and/or air content had obtained their ACI certification for the testing of fresh concrete properties.

Figure 3.4 Slump and Air Content Testing

3.3.4. Sampling and Curing

The sample size for a general mix included fifty 4” by 8” cylinders, six 3” by 3” by 11” free shrinkage molds, two AASHTO Rings (one with vibrating wires embedded, one without), a slump test, an air test, and 10% excess. This cumulated to approximately 5.2 cubic feet per lab mix. Consolidation for these samples was achieved by using vibration tables for an appropriate amount of time depending on the sample.

After the sampling was completed, each mold is sealed and cured for 24 hours within its mold. The rings were also cured in this one-day period using burlap covered by plastic wrap to keep the evaporation to an absolute minimum. These samples were stored in the environmental chamber at a consistent 74 degrees Fahrenheit with 50% humidity. Just before 24 hours, the samples are all removed from their respective molds. The rings and three free shrinkage samples are to remain inside of the environmental chamber. The process of demolding the rings starts with removing the samples from the wooden

frames. After this and before removing the sonotube, the tops of the rings are covered with paraffin wax. After this, the sonotube is removed and the ring is placed in its final position. The ring is also wired into the data logger at this time, as well as sealed at the base with silicon caulking. The remainder of the samples not to be immediately tested are labeled and placed in lime water curing tanks. These samples are all removed at 14 days with the exception of the RCPT and SR samples that remain in lime curing for the duration of the necessary testing. The removed samples are hereinafter stored in the environmental chamber until they are to be tested.

Figure 3.5 Environmental Chamber

3.4. Laboratory Testing

Laboratory testing was performed at a multitude of time periods for each mix and testing regiment. All testing mechanisms that are used in the lab will be outlined here. This includes some of the material already covered, such as the sieve analysis and fresh concrete properties. Each testing procedure is listed and outlined based on its ASTM (or other standard(s)) specification. The tests to be outlined in this section will include compressive strength, tensile strength, modulus of elasticity, free shrinkage, restrained shrinkage, surface resistivity and rapid chloride permeability. All curing techniques were previously covered in section 3.3.4. The time frames for testing will be noted in the following table.

Test	**Standard**	**Age for Testing**
Compressive Strength	ASTM C39	1, 3, 7, 14, 28, 56
Tensile Strength	ASTM C496	1, 3, 7, 14, 28, 56
Modulus of Elasticity	ASTM C469	1, 3, 7, 14, 28, 56
Free Shrinkage – Dry Cure	ASTM C157	1-56 (as often as possible, especially during days 1-14)
Free Shrinkage – Wet Cure	ASTM C157	1-56 (as often as possible, especially during days 14-21)
Restrained Shrinkage	AASHTO PP34	1-56 (crack mapping at 28, 42, and 56 days)
Surface Resistivity	AASHTO T 358	7, 14, 28, 56
Rapid Chloride Permeability	AASHTO T 277	28, 56

Table 3.4 Lab Test Summation

3.4.1. Compressive Strength Testing

Compressive strength testing was done in accordance with ASTM C39. Testing was done at 1, 3, 7, 14, 28, and 56 days. The test is simply summarized by saying that the specimen, a 4” by 8” cylinder, was loaded axially at an appropriate rate until failure. The compressive strength is defined as the maximum load divided by the cross-sectional area of the cylinder used for testing. The cylinders were also capped, using a sulfur compound, in accordance with ASTM C617. The capping compound was used to ensure a level surface during testing. Cylinders were tested using a one million-pound Forney compression machine as seen in the figure below. For each test, a minimum of two cylinders must be broken for accuracy purposes. Any outliers resulted in further testing.

Figure 3.6 Sulfur Capping and Compression Testing

3.4.2. Tensile Strength Testing

Tensile Testing was accomplished according to ASTM C496. Testing occurred at the same time as the compression tests described in the previous section. A cylinder being tested was placed horizontally into the Forney compression machine to be tested. The specimens were then loaded at an appropriate rate, according to the standard. Failure in this case was indicated by cracking through the material and a release of load capacity. This could be easily detected when the concrete to be tested does not contain fibers, because the maximum tensile load will coincide with the specimen's maximum load. With the addition of fibers, the concrete can tend to take additional residual load after tensile failure. Testing concluded at the point where the load began to release for the individual specimen. For this test, a minimum of two samples was again be used.

3.4.3. Modulus of Elasticity Testing

Figure 3.7 Tensile Splitting Test

Testing for modulus of elasticity was done in accordance with ASTM C469. These samples were also capped, like the compression samples, in accordance with

ASTM C617. The testing also fell on the same days as compression and tension testing. The modulus of elasticity cannot be tested for until after compression tests are complete. The samples had to be loaded to 40% of the average compressive load during this test. The initial step of this process was to attach a modulus cage to the cylinder being tested. This was accomplished using a handful of screws. This cage also had a length comparator built in, which was crucial to the testing. The first step was to preload the sample to the 40% compressive load specified earlier. After this, the sample must be measured. This was accomplished by measuring the cage on opposite sides with a caliper. After this, the cylinder was loaded again, while measurements were taken from the length comparator at appropriate load increments. This test was to be repeated two times for each cylinder, and two cylinders are to be tested for every mix. Taking the load and the displacement into consideration, the modulus of elasticity can be calculated for each test.

Figure 3.8 Modulus of Elasticity Test

3.4.4. Free Shrinkage Testing

Free shrinkage testing was accomplished following the ASTM C157 standard. Six free shrinkage samples were cast from every mix. This was accomplished by using 3” by 3” by 11” molds. At each end of said molds, steel plates were placed with shrinkage gage studs screwed in to them. During demolding, these steel plates were removed, leaving a sample with two shrinkage gage studs embedded for measuring. Six samples were cast with each mix to be able to test two separate curing scenarios that represented the best-case and worst-case scenarios. This showed an accurate envelope of what can be expected, because best case scenarios are often hard to replicate in the field. All six

samples were measured shortly after being demolded, before they are placed where they were to be cured.

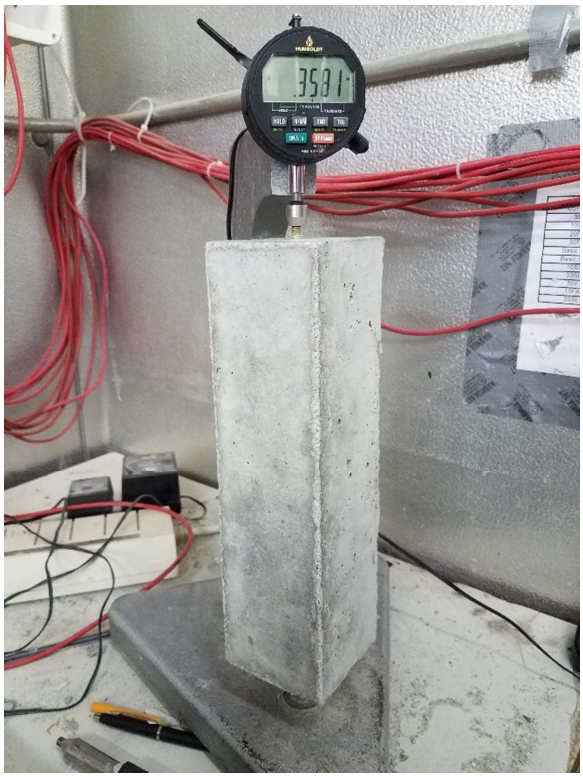

Figure 3.9 Free Shrinkage Testing

The first three samples were cured in the lime tanks along with the majority of the samples for 14 days. This emulated the best-case scenario. They were periodically removed from the tanks to be measured. At 14 days, the samples were removed from the tanks along with the rest of the cylinders. From this point on, they were kept in the environmental chamber at a consistent temperature and humidity. The samples must be measured as frequently as possible when first moved into the environmental chamber. They were measured periodically up until 56 days.

The second three samples were not cured after the initial day. They were immediately placed in the environmental chamber. No additional curing imitated the

worst-case scenario. These samples were measured frequently in the first two weeks and again periodically up until the 56-day point. The combination of these two shrinkage patterns produced an envelope of what can be expected for the shrinkage of the mixes in question and a relative comparison from mix to mix.

3.4.5. Rapid Chloride Permeability and Surface Resistivity

Rapid chloride permeability testing (RCPT) was done by following the ASTM C1202 standard. It was considered a measure of how well a concrete specimen can resist chloride ion penetration. Seeing as the concrete in question is most applicable for bridge decks, the concrete's ability to resist the penetration is vital to its long-term success in application. The testing was accomplished by taking cylinder samples and cutting them at an appropriate length with a concrete saw in discs. These discs are then allowed to dry before being placed in a vacuum saturation pump apparatus. The vacuum ran for a minimum of one hour and the discs were left within the water filled container for approximately 16-20 hours. At that point, the samples had to be removed and placed into the RCPT cells in the lab. After each cell was securely fastened around its specimen, solutions of sodium chloride and sodium hydroxide were used to fill opposite designated ends of the cell. The cell was then rigged to a machine with a computer interface, and the test began. The test involved running a current across the cell and monitoring the output through the computer. The output was finalized at the 6-hour mark. At this point, the cells are emptied, taken apart, and cleaned out. The results of this test will be compared with other mixes and with the NJTA specifications. A minimum of two specimens were to be tested each time.

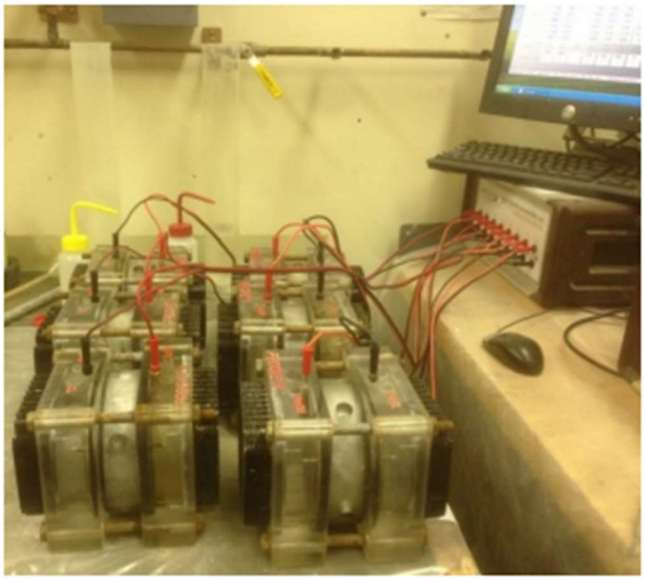

Figure 3.10 RCPT Testing

Measuring the surface resistivity (SR) of concrete has proven to be correlated to rapid chloride permeability testing at a highly reduced cost with much less effort in testing. This testing mechanism was not fully adopted by the state at this time, but it is in the process of receiving its own standard for use. The test was applied by using a method known as a Wenner four electrode method. Four equally spaced electrodes are pressed against a concrete cylinder in 90 degree increments until eight readings are recorded. The reading comes from running alternate currents through the two end nodes and measuring the voltage between the inner electrodes to produce a reading. The eight values were averaged and the testing was done for at least two cylinders for each test. The average between the cylinders was taken as the surface resistivity for the appropriate time frame for the concrete in question. This test is much simpler and extremely cost effective when compared to RCPT, and the results have proven to be accurate through extensive comparison.

Figure 3.11 Surface Resistivity Testing

3.4.6. AASHTO Restrained Shrinkage Testing

In addition to all of the previous testing, restrained shrinkage rings were casted and monitored in accordance with AASHTO PP34. For the majority of these mixes, two rings were cast. One of the rings would only have been monitored with foil strain gages attached inside the steel ring, while the second ring was monitored by both these and vibrating wires connected to each other by way of bolts embedded in the concrete at the time of casting. There were a few mixes that are an exception to this rule, and these will be noted at a later point in this paper. Both of these methods have been proven to give insight on when cracks are forming, where they are forming, and an idea as to the significance of these cracks. The standard for this type of ring testing does not include vibrating wires, so these rings are considered "modified" going forward.

For each ring, there are four foil strain gages attached to the inner surface equidistantly from each other. These sensors were wired into a permanent data collection

system after final placement. They monitored the strain changes of the steel which can be correlated to the strain in the concrete. They can also show indications of cracking, which usually come in the form of significant strain jumps for large cracks and small jumps for micro cracks. For the modified rings, a hexagon of vibrating wires was attached to the embedded bolts and tightened, as seen below:

Figure 3.12 Typical Vibrating Wire with Plucking Coil and VWSG Ring

The vibrating wire sensors are then monitored by plucking coils, which are wired again into the permanent data collection system. These sensors are comprised of a metal string encased inside of the hollow structure of the sensor. The plucking coils to be attached to each vibrating wire cause the wire to vibrate at a certain frequency. The frequency, more importantly the change over time, is monitored over the entire testing period. Any change in length of the tube due to shrinkage (shortening) or cracking (elongating) will cause a change in the frequency of the wire. These can also be converted into strains and tracked in this manner. The fluctuation in these sensors can be extremely helpful in locating and measuring cracks the concrete rings experience. Both

the foil strain gage data and the vibrating wire data should be routinely checked for the duration of the testing period.

Figure 3.13 Ring Set-Up Data Collection System

Arguably, the most important part of these rings is the crack mapping surveys. Crack mapping is done at three separate time intervals: 28, 42, 56 days. These surveys are completed by going over the entire ring with a microscopic camera and cataloging all visible cracks as well as measuring them for approximate widths. The camera being used is computer based and works with the DinoCapture software. Each crack is photographed and the photographs are cataloged.

Figure 3.14 DinoCapture Image

These results are interpreted in a few ways. First, the crack widths for each individual crack are summarized and averaged giving a crack area for each crack. The summation of this cracking area divided by the total surface area is known as the crack density. Tracking crack density over time and comparing the results across all mixes gives a lot of insight into the behavior of each mix and each fiber type. The total number of cracks and maximum crack width should also be monitored in these time frames for reference. The maximum crack width is of extreme importance to each concrete sample and can be indicative of the effects fibers have on reducing crack width. The reduction of cracking area and crack width is the primary objective of this testing.

4. Results

4.1. Introduction

An experimental program was set up with the mixes from table 3.2 of this thesis to investigate the variance of certain properties caused by various fiber additions and the blending of aggregates. For each mix in question, approximately 5.2 cubic feet was batched and mixed in the Civil Engineering Laboratory at Rutgers University using a rotating drum mixer. Each mix was appropriately sourced, mixed and cast according to ASTM C192 and ASTM C172. Prior to casting, air content and slump were measured and must have been in the acceptable range to proceed. For each mix, approximately fifty 4" by 8" cylinders, six 3" by 3" by 11" free shrinkage specimens, and two AASHTO rings were prepared and molded. Each sample was sealed shortly after the completion of casting and placed into the environmental chamber for 24 hours. The AASHTO rings also received a layer of burlap for this 24 hours as the standard states.

Shortly before the one-day mark, all samples were removed from the chamber and removed from their molds. From here, all the cylinders and half of the shrinkage molds (after initial measurements) were labelled and placed into curing tanks where they are to remain for fourteen days with the exception of the cylinders to be used for RCPT and SR which stay in curing tanks for the duration of their testing cycle. The AASHTO rings and remaining free shrinkage molds go directly into the environmental chamber. The rings are properly placed and sealed with a paraffin wax coat on the top surface and silicon caulking around the bottom outside edge. The strain gages on the rings are also attached

to the dataloggers. The modified rings with a vibrating wire strain gage hexagon were also outfitted and rigged to the recording software now. The remaining free shrinkage molds are measured and left in the environmental chamber with no additional curing allowed.

The mixes presented will include HPC, HPC with 2” polypropylene macro fibers from Euclid, blended HPC, blended HPC with 2” polypropylene macro fibers from Euclid, blended HPC with 2” synthetic macro fibers from Sika, blended HPC with 2” steel hooked fibers from Sika, and a Class A concrete mix. This array of mixes is intended to differentiate the effects of various fiber types and blending in a basic HPC mix. It is also intended to compare all of mixes to the worst-case scenario, which in this case is presented as the Class A mix. Each mix will be compared in terms of fresh properties, strength, permeability, and relative cracking potential.

4.2. Fresh Properties

The fresh properties measured in this experimental procedure were slump and air. Mixing was done in a contained environment that is kept consistently at the same relative temperature, so ambient temperature and concrete temperature were not tracked for this set. Slump testing was done is accordance with ASTM C143, and air content testing was done in accordance with ASTM C231. It is also important to note that the amount of super plasticizer used in each mix was at times varied to meet the desired slump goal. Therefore, the amount of super plasticizer must also be taken into consideration when analyzing the findings. Air entrainer was kept constant for all mixes. The results are tabulated below.

BASIC MIX	HPC	HPC-B	FR-HPC	FR-HPC-B	FR-SIKA(1) MACRO	FR-SIKA(2) STEEL	CLASS A
HRWR (OZ/CWT)	2.5	2.0	2.5	3.5	3.5	2.5	2.0
SLUMP (IN.)	8"	4"	6"	6.5	6.5"	4.5"	7"
AIR CONTENT (%)	N/A	N/A	8.5%	7%	7%	9%	5.5%

Table 4.1 Concrete Fresh Property Testing

The fresh property testing leads into some insight on how fibers affect workability. It was previously discussed in the literature review portion of this paper that fiber additions to concrete lead to a decrease in workability and an increase in air content due to pockets created by the fibers themselves. The fiber mixes do show a higher air content than that of class A across the board, but this is necessarily a fair or conclusive comparison. The workability issues can be seen in this data. Looking at both the slump achieved and the amount of water reducer needed to achieve the slump clearly shows a trend. Fibrous mixes require more high range water reducer to achieve similar or acceptable slump results. The workability lost from the addition of fibers does however appear easily replaced by slight adjustments to the batch.

4.3. Mechanical Properties

The mechanical properties tested for in this experiment are compressive strength, splitting tensile strength, modulus of elasticity, permeability, and surface resistivity. These were all performed in accordance to their individual standards which are previously listed in table 3.3. The purpose of these sections is to analyze the contributions made by the fiber additions and by blending the aggregates in terms of each property. Having a comprehensive understanding of the benefits and/or consequences these

additions have is crucial in gaging their overall degree of effectiveness for this use case and many other use cases. Each property will be individually analyzed below.

4.3.1. Compressive Strength

Compressive strength testing was done at 1, 3, 7, 14, 28, and 56 days. This testing was done using at minimum two 4" by 8" cylinders and in accordance with ASTM C39. Each sample tested during this program was cured for 14 days in lime saturated water before being placed in the environmental chamber. The numerical results are as follows:

AGE	HPC	HPC-b	FR-HPC	FR-HPC-b	FR-Sika(1) - Synthetic	FR-Sika(2) - Steel	Class A
1	3436	4021	2130	2763	2834	2966	2866
3	4522	4618	3320	3774	N/A	3344	3416
7	5295	5573	4049	5016	4323	3909	3451
14	6409	5852	4538	5016	5016	4857	4172
28	7544	7146	5036	5414	6071	6210	4578
56	8340	7205	5235	6131	6967	6748	4737

Table 4.2 Compressive Strength Results

From the results, a few conclusions can be made. The first would be that this blending of aggregates appears to have a negative effect on the compressive strength of the concrete. From casting until the 7-day mark, they trend very similar to each other. After this point, the blended mix has consistently lower compressive strength than the ordinary mix, culminating in a 13.6% reduction at 56 days. The compressive strength achieved is still within the acceptable range. The second point to be made is that the addition of fibers reduced the compressive strength of HPC and HPC-b, regardless of the fiber type. All fiber reinforced variants are still stronger in compression than the a standard class A mix. All of the mixes fall well within a useable compressive strength range for the application in question. The results are compared graphically below.

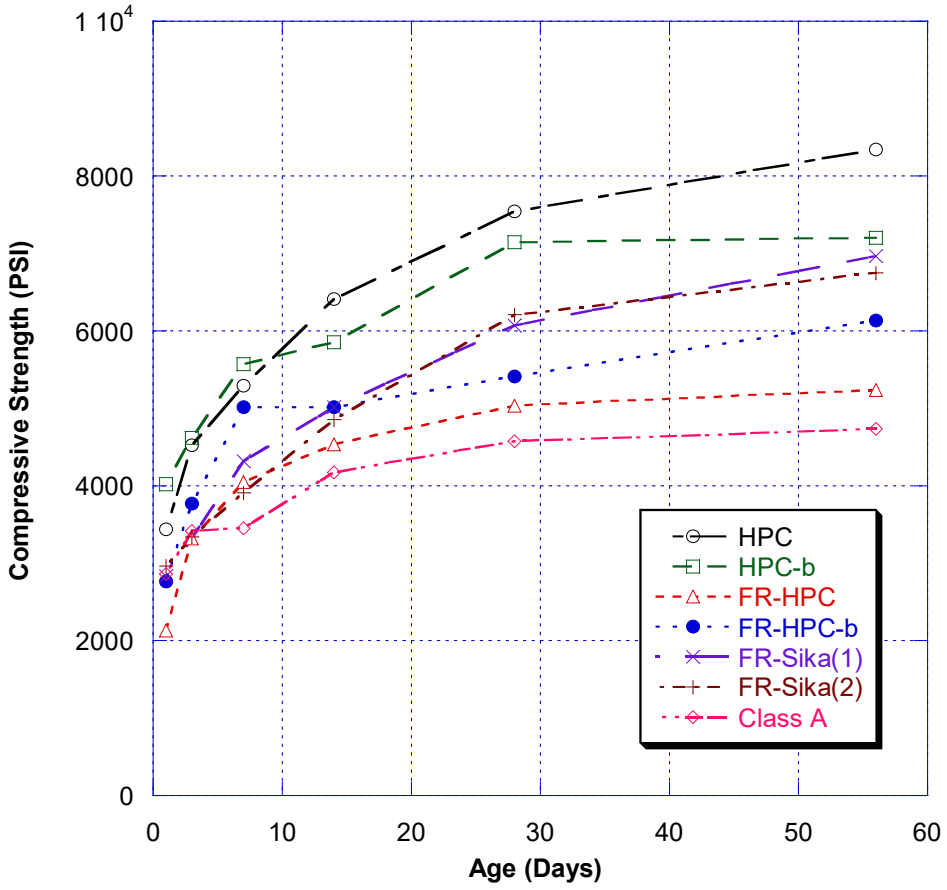

Figure 4.1 Compressive Strength Comparison (Lab)

From the previous data, it is clear that the compressive strength of HPC is reduced by the addition of fibers. The concrete is still relatively strong and strong enough for application in bridge decks. When looking at the blended variants of HPC, the fiber additions result in a 3.3 to 14.9 % reduction in the compressive strength. It has already been proven that increases in compressive strength correlate to an increase in cracking, so the relative reduction should factor in positively. Reducing the compressive strength by increasing the fiber content could further positively influence the final results.

4.3.2. Tensile Strength

Tensile Strength Testing was done at the same time intervals as compressive strength and in accordance with ASTM C496. Each 4" by 8" sample was cured for 14 days in lime saturated water and placed in the environmental chamber. The table below denotes the results from this testing.

AGE	HPC	HPC-b	FR-HPC	FR-HPC-b	FR-Sika(1) Synthetic	FR-Sika(2) Steel	Class A
1	347	346	288	343	212	301	299
3	404	414	393	482	N/A	368	336
7	438	430	398	486	418	394	342
14	508	450	438	504	512	508	424
28	575	615	502	600	N/A	577	483
56	577	653	542	617	617	589	498

Table 4.3 Tensile Strength Results

A few notable trends can be seen in the results above. The first significant conclusion that can be made is that the aggregate blend in use increases the tensile strength of the concrete mix. For both the standard mixes and the fiber reinforced mixes this holds true. The aggregate blending used increased the tensile strength in this HPC variant by 13.2%. In terms of the effects each fiber has on tensile strength, there is a net positive effect of 2.1% to 6.9% when comparing the blended fiber mixes to the base HPC. In terms of individual performance, the differences between fiber types can be described as negligible. Each fiber reinforced, blended HPC mix had negligible differences in splitting tensile strength results. No fiber type proved more effective in this portion of the study. An increase in tensile strength can be viewed as a strong positive in terms of crack prevention. This however does not account for the residual tensile strength

after cracking. The fibers provide great assistance in this case. All HPC mixes outperformed class A. The results are also shown graphically below.

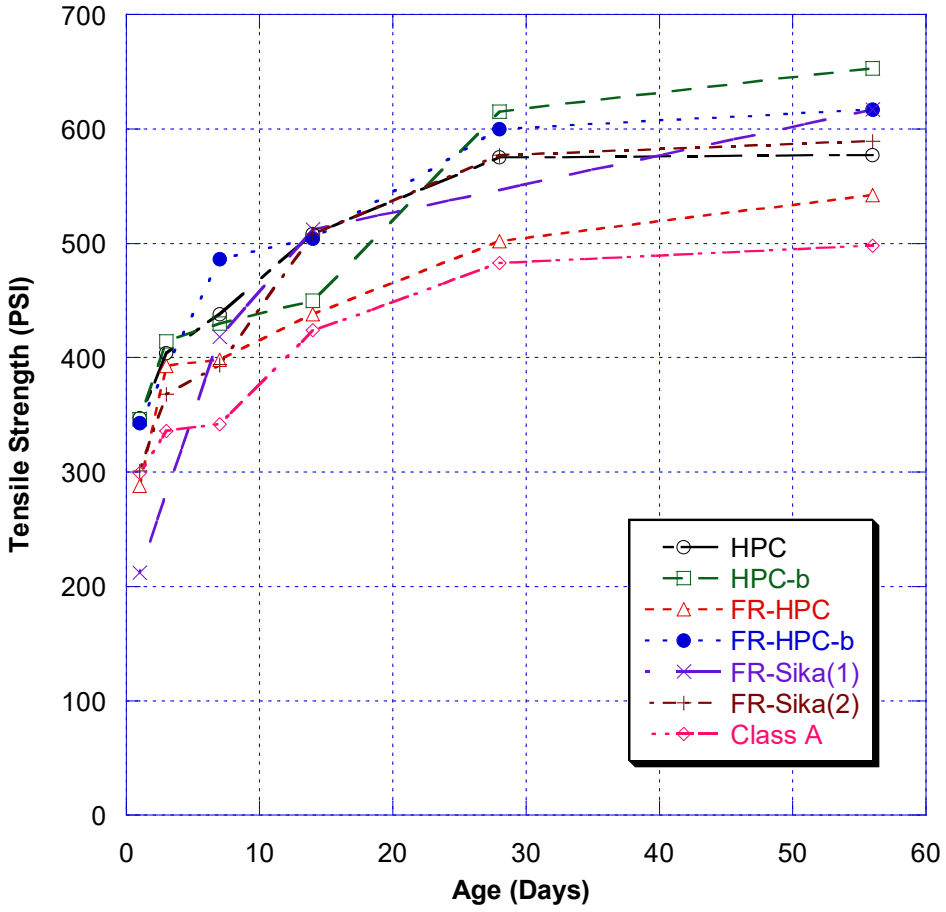

Figure 4.2 Splitting Tensile Strength Comparison (Lab)

The increase in residual strength can be best qualitatively documented with the following set of images. They depict the tensile failure mechanisms for both fiber reinforced concrete and plain concrete. The first figure shows the typical failure of plain concrete. The cylinder being tested reaches a maximum load before cracking. Upon cracking, the cylinder starts to dramatically lose load capacity until the point where it splits completely in two.

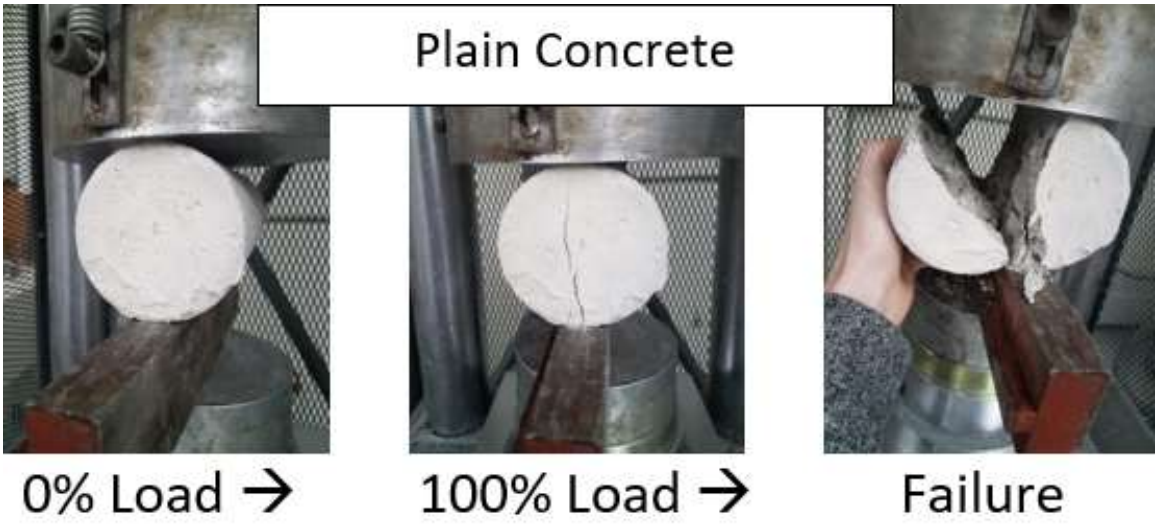

Figure 4.3 Plain Concrete Tensile Failure Mechanism

Contrary to this failure mechanism, Fiber Reinforced Concretes begin cracking slightly before maximum load. They continue to be able to withstand a higher load capacity before the crack fully splits the cylinder. At this point, load capacity begins to decrease, albeit at a much slower rate than what can be seen in plain concrete. The crack expands to a point where the fiber reinforcement is absorbing a majority of the residual tensile stress. This load is generally around 50% of the capacity. The load will fluctuate around this point for a significant amount of time. The fibers act in a tensile capacity while the split concrete crushes and acts in a compressive capacity.

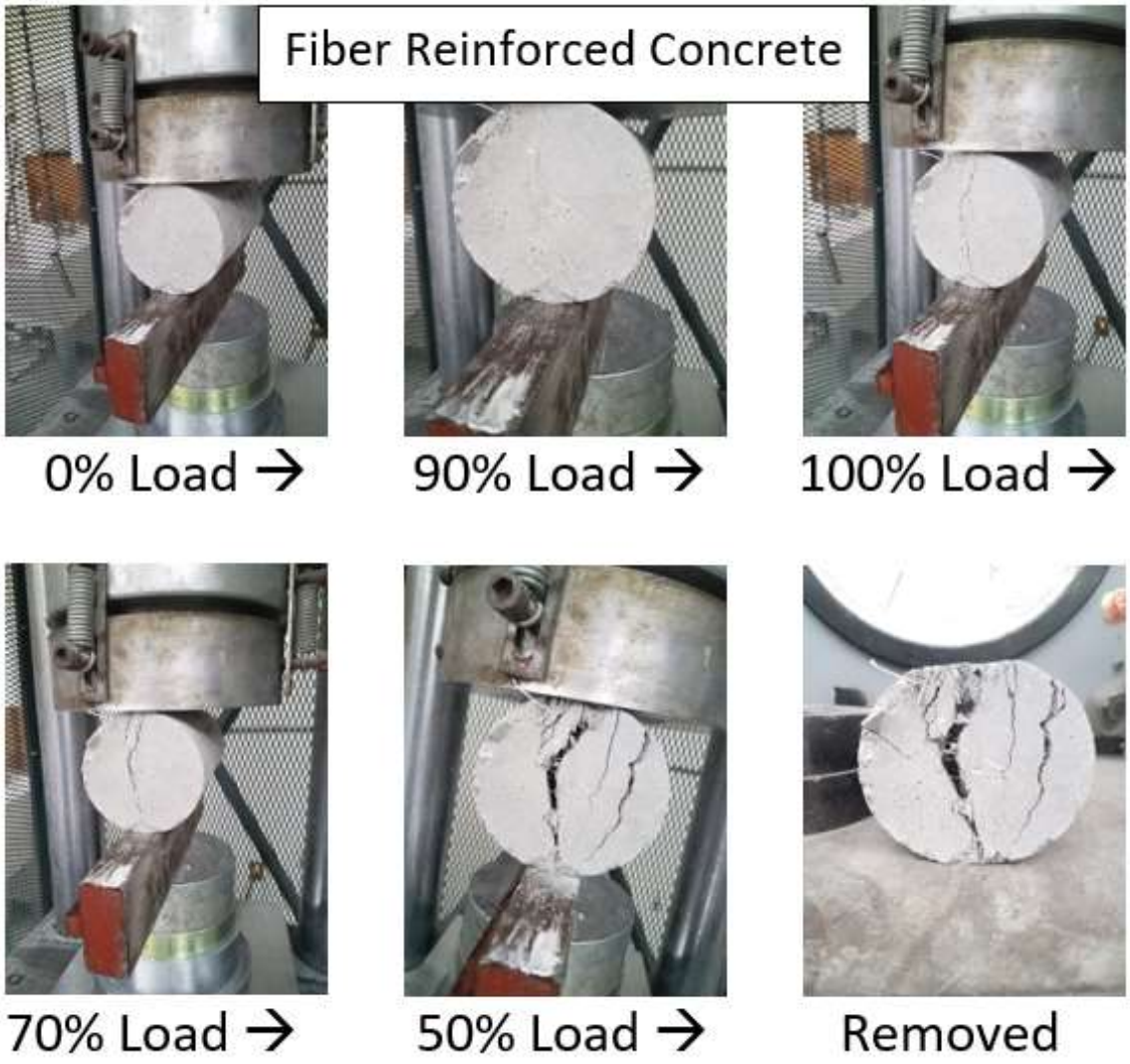

Figure 4.4 Fiber Reinforced Tensile Failure Mechanism

While the desired effect of significantly increased tensile strength was not achieved, further optimization could further improve the results. For one, the fiber content could be increased in each mix to ensure a better distribution. The aggregate blending could also be optimized to increase tensile strength. Even without the perfect outcome, the post cracking action seen in testing could be a huge benefit in this application. The mixes without fibers would essentially fail immediately. There was no residual load to be held after the crack had propagated through the sample. The fiber

mixes however have the ability to absorb more energy and load after what would be considered failure. The concrete begins to work in compression while the fibers take on the tensile strength of the sample.

4.3.3. Modulus of Elasticity

Modulus of elasticity was also tested for at the same time intervals as compressive strength and splitting tensile strength. First, the cylinders are capped with a sulfur capping compound according to ASTM C617. After this, the modulus test is conducted in accordance with ASTM C469. The length displacement is recorded as the load increases and the results are analyzed to determine the material's modulus of elasticity. The following table depicts the values for each mix at each interval.

AGE	HPC	HPC-b	FR-HPC	FR-HPC-b	FR-Sika(1) - Synthetic	FR-Sika(2) - Steel	Class A
1	4279	4198	3742	3719	4120	3658	4035
3	4377	4335	N/A	4149	N/A	N/A	4131
7	4836	4633	4408	4020	5100	4372	N/A
14	4898	4671	3953	4119	4326	4329	4666
28	5028	4746	4213	4358	4193	4459	4370
56	4683	4704	4292	4567	4375	4457	4241

Table 4.4 Modulus of Elasticity Results

From this table, it can be concluded that the minimum amount of blending used in this experimental program does not have any significant effect on modulus. Further blending should result in a stiffer concrete, but this mix is not optimized in that direction. The fibers also show a consistent decrease in modulus. It is most noticeable in the non-blended mix, where the modulus decreases by 8.3%. The blended fiber mixes have a decreased modulus ranging from 2.9% to 7.0% depending on the fiber type. The modulus received from the Class A testing has remained similar to this entire mix set. The fibers

are proven to increase the ductility of the concrete, so a decrease in the modulus of elasticity helps reassure that claim. The fibers are improving the flexibility of the concrete. In the proper application this is a huge advantage. The following graphic represents the change in modulus of elasticity with respect to time.

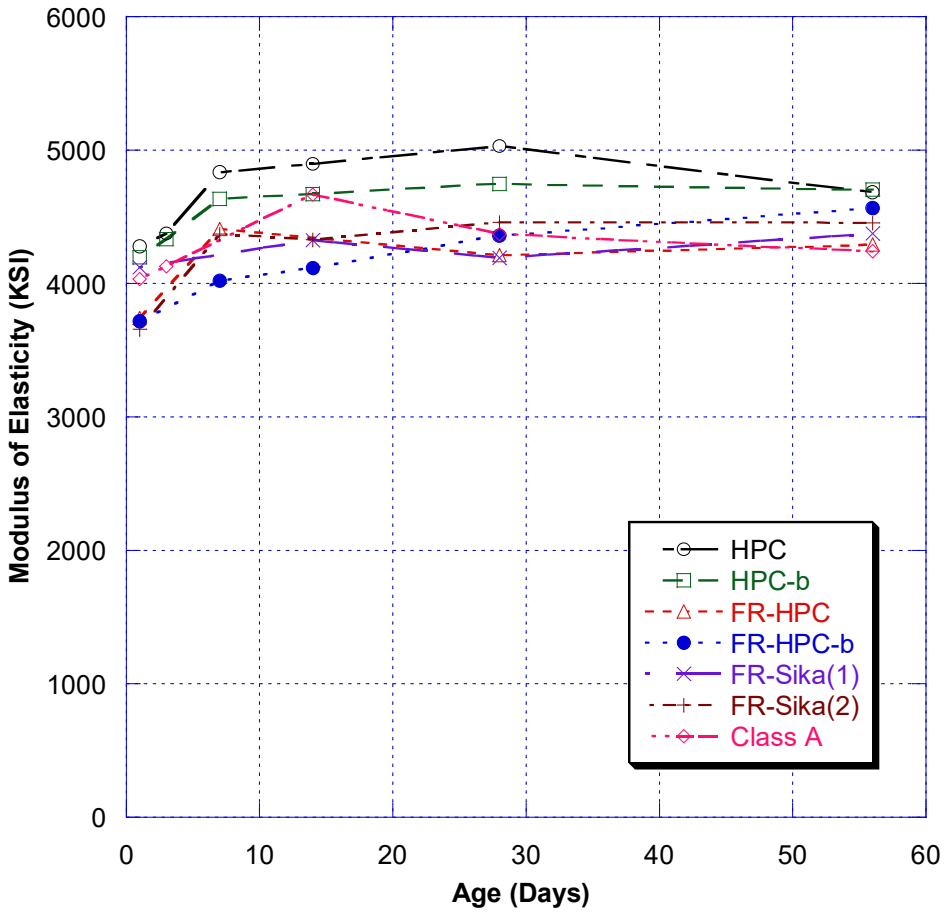

Figure 4.5 Modulus of Elasticity Results (Lab)

The trends described from the raw data seem applicable at any point in time for this testing. Both non-fibrous mixes were stiffer than their counterparts with fiber reinforcement from one day all the way through the testing cycle. Further decreasing the modulus can likely be achieved in a few ways. The fiber content could be increased in each mix, but not further than the point where workability is lost. Hybridization could

also be utilized. Combinations of micro, macro and steel fibers could be optimized for a plethora of use-cases. This could lead to further improvements in this study.

4.3.4. Rapid Chloride Permeability and Surface Resistivity

The permeability of each mix was measured twice at 28 and 56 days for each mix. All samples involved with both tests remain curing in lime water tanks for the duration of their testing respective time. Rapid chloride permeability testing was done in accordance with AASHTO T 277. Samples are cut using a diamond blade saw to the appropriate section. Then they are placed in a vacuum with distilled water for 24 hours. After this the test is set up and run for six hours. Surface Resistivity is completed by following AASHTO T 358. The cylinders to be tested are probed at 90 degree increments for two full rotations and a total of eight readings are recorded for each sample and averaged. The results are as follows.

AGE	HPC	HPC-b	FR-HPC	FR-HPC-b	FR-Sika(1) Macro	FR-Sika(2) Steel	Class A
SRT (kOhm-cm)							
7	11.6	16.3	9.6	11.5	9.4	9.4	9.8
14	17.2	17.7	12.7	20.8	15.1	13.9	12.1
28	25.6	24.2	22.4	31.1	22.5	13.2	14.9
56	34.9	34.1	30.4	59.1	36.2	32.4	15.5
RCPT (coulombs)							
28	1656	1739	1880	1071	N/A	2071	2539
56	1079	1105	1306	601	1144	1633	2085

Table 4.5 RCPT and SR Results

The only issue to be seen in this section comes with the addition of steel fibers. As found during the literature review, the addition of steel fibers is proven to exhibit corrosion. This is reaffirmed by the increase in permeability. This is an issue that can be

addressed, but must be taken into consideration for application and longevity among other things.

4.4. Free Shrinkage

Free shrinkage is an extremely important factor when analyzing the use of these concrete mixtures for use in bridge decks. The level of restraint in the decks is fairly high due to all of the reinforcement necessary. The lower the shrinkage can be kept, the less strain the concrete will experience. Higher shrinkage is one factor than can be directly correlated to cracking in these slabs. Shrinkage was measured in two different conditions. There was the worst-case scenario, which is no curing, and the expected condition which is fourteen days of curing. The idea of this set up is to show an envelope of what can be expected in practice. While by far not the only factor not involved, reducing shrinkage in theory will directly reduce the cracking potential in slabs.

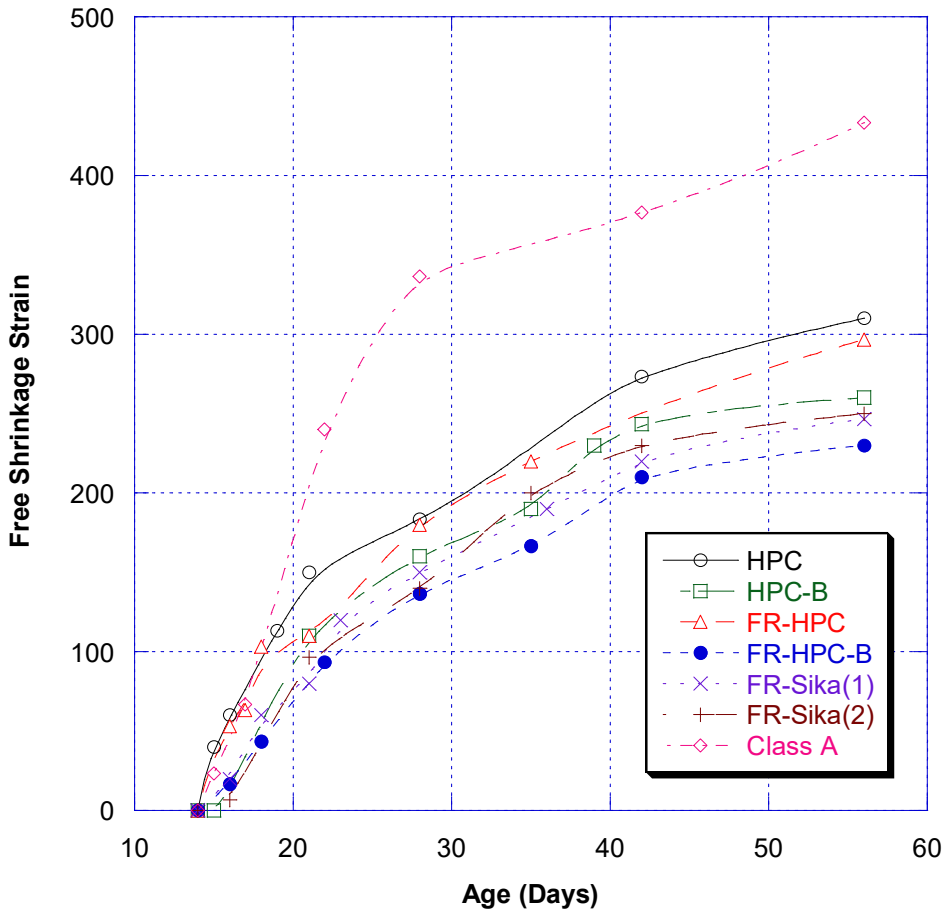

Figure 4.6 Wet Free Shrinkage (Lab)

The 14-day wet cure is considered the best-case scenario and is expected in most cases. This shrinkage data provides great insights on the effects that each adjustment or improvement to the mix design creates. Class A experiences more shrinkage than the HPC mixes. From there, the effects of both blending and fiber reinforcement can be established. Aggregate blending, even in situations like this one where the blending is minimal, reduces shrinkage. From this experiment, it can be seen that the 300 pounds of three-quarter inch aggregate that was replaced with three-eighth inch aggregate reduced the shrinkage at 56 days by 16.1%. The effects from the variety of fiber additions can also be investigated from this set. For instance, the Euclid 2" macro fibers provided a 4.3% reduction in the non-blended mix and an 11.5% reduction in the blended mix. It is

also important to note that the Euclid fiber mix outperformed the pair of Sika Fiber mixes.

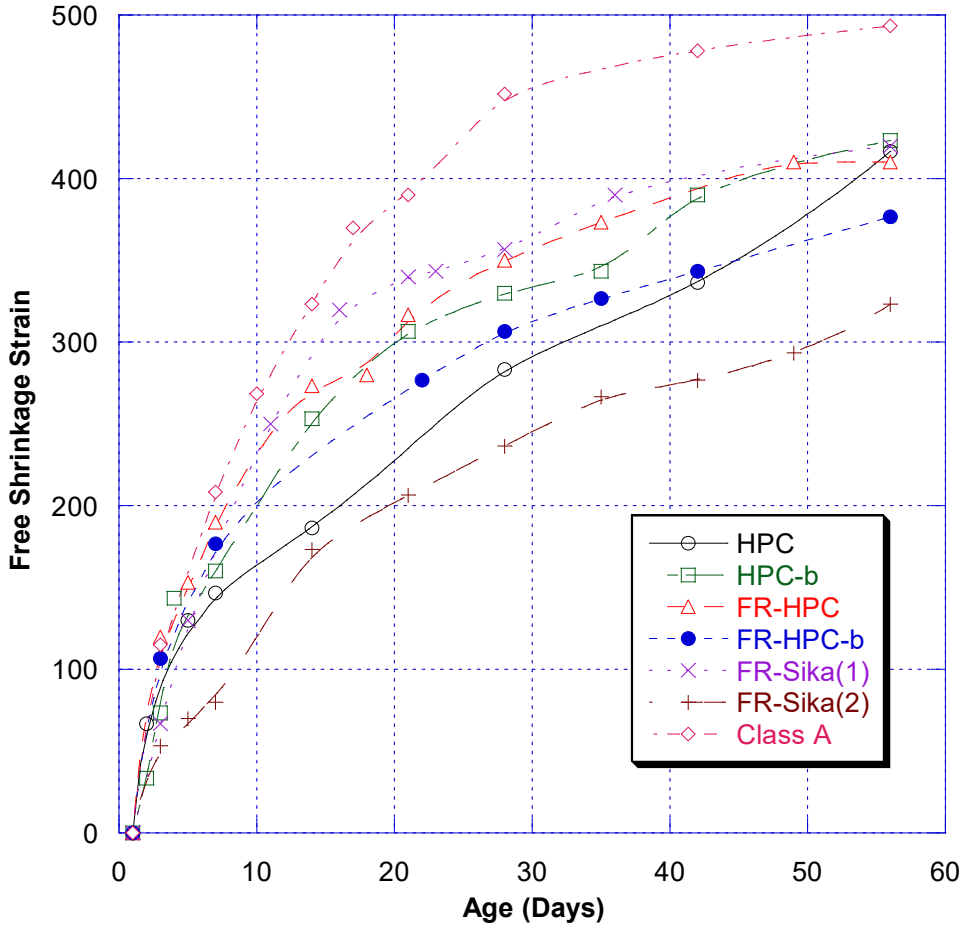

Figure 4.7 Dry Free Shrinkage (Lab)

The dry shrinkage results are a bit more difficult to interpret. Clearly the class A mix still establishes as the worst option. There is no noticeable difference shown from the aggregate blending at 56 days. The Sika synthetic fibers also appear to have no effect on shrinkage in this case. There is a slight reduction in shrinkage in the fiber reinforced base mix and that becomes amplified to an 11.0 % reduction in FR-HPC-b. The best results in terms of dry shrinkage was achieved by the Sika steel fiber mix, which resulted in a 23.6% reduction in shrinkage when compared to the base blended design.

When properly cured, each FR-HPC-b mix offers a reduction in shrinkage ranging from 18.2% to 25.5% at 28 days accompanied by a 19.4% to 25.8% reduction at 56 days when compared to HPC. With no curing, there is a larger disparity. At 28 days, Euclid 2" PPE fibers and Sika 2" synthetic fibers show increases in shrinkage strain of 26.0 and 46.6% respectively while Sika steel hooked fibers show a slight reduction of 2.7%. At 56 days, Euclid fibers and Sika steel fibers show reductions of 9.6% and 22.4% respectively while Sika synthetic shows a slight increase in shrinkage of 0.8%. Fiber additions all have a relatively similar positive influence on shrinkage when a sample is properly cured. When not cured, steel fibers provide the largest reduction in shrinkage, followed by Euclid PPE fibers. Sika's synthetic fiber offered no influence on shrinkage when the samples were not cured after demolding.

It is important to note that all of these results were achieved in a controlled environment and cannot be expected in the field under more adverse conditions. The relativity of these results from tests conducted in the same environment do however establish the effects of each change made to the design. Shrinkage could be even further reduced with some additional adjustments. Improving the aggregate blending, optimizing the fiber content and utilizing fiber hybridization by also including micro polypropylene fibers could all further improve the results seen from this set of tests. These possible improvements could directly relate to and improve upon the cracking performance of these concrete mixes as well.

4.5 Restrained Shrinkage

Each mix was cast with two AASHTO Restrained Rings. In the majority of these cases, one ring was cast according to the standard (AASHTO PP34), and the second ring was cast with a hexagon of vibrating wires to monitor cracking even further. The more accurate depiction of the fiber effects can be seen in the standard AASHTO rings. While the vibrating wires do not affect the time to cracking, they did have an influence on the crack widths and areas. The comparison will focus on the standard AASHTO rings as they have yielded a clear and concise result. Each mix will have one ring chosen for comparison. They will be individually summarized before a comparison is made.

The major points that will be focused on in this comparison include the number of cracks, the maximum crack widths, average crack widths and the total cracking area of the concrete specimen. The number of cracks and the maximum crack width for each sample at each time interval are easily definable. The cracking area is taken as an average of the width of a crack multiplied by the length of the crack propagation. Tracking each of these variables over time should create a firmer understanding of the effects of both the fibers and the blending in terms of their relative cracking potential.

Each set to be used in the comparison will be included individually from section 4.4.1 to 4.4.7. These sections will include the detailed crack maps at each time interval as well as crack width measurements used in the cracking area calculations. The sections will also include tables that track the variables in question for each crack map. Lastly, the strain data for each ring will be shown. This data is primarily used as an indicator for the cracking of concrete. These sets did not form major cracks, so large drops in strain were not experienced by the steel rings. The minor cracking can be visualized as smaller strain

releases in the steel rings over time. Each set will be individually considered before a broader comparison is forged in section 4.4.8.

4.4.1. HPC

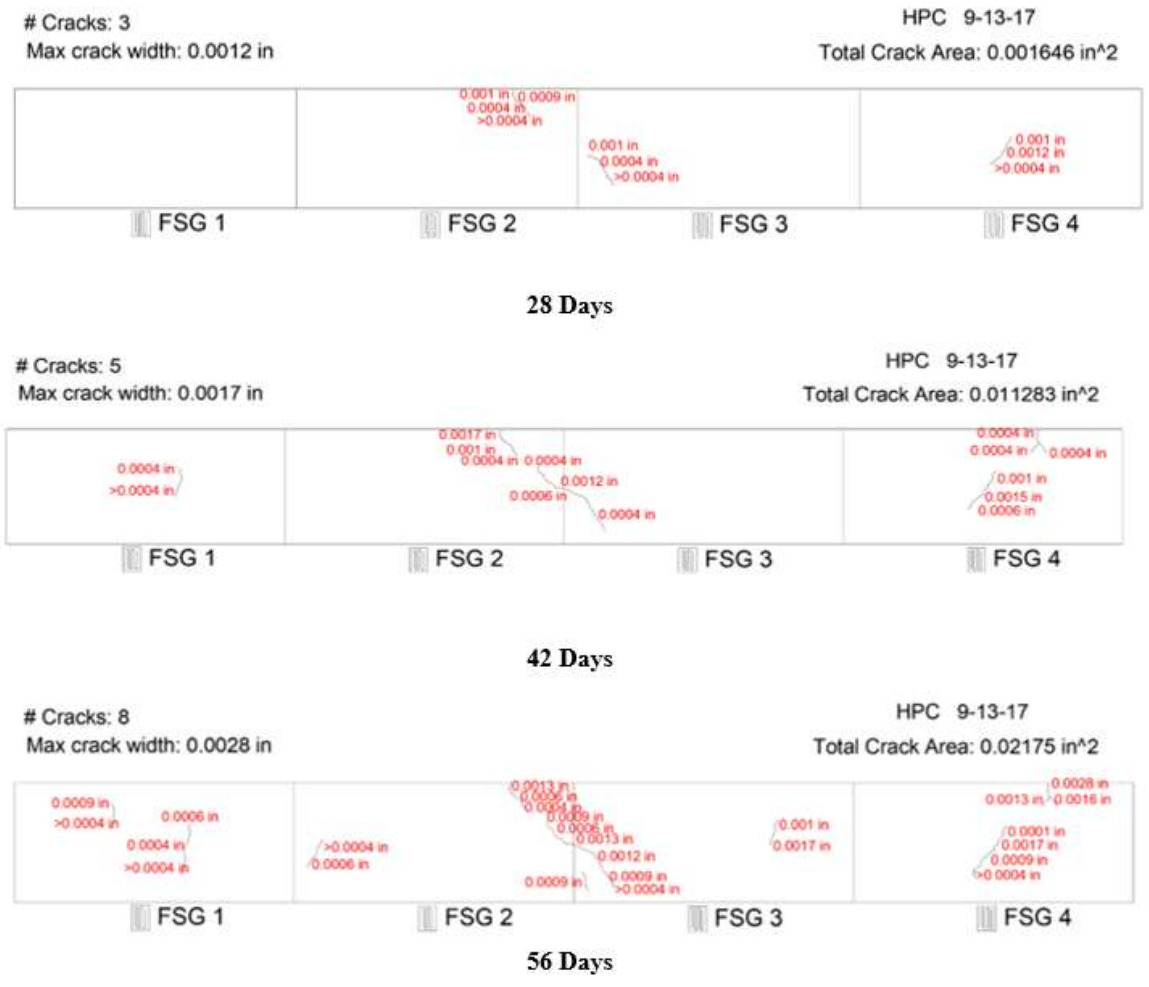

Figure 4.8 HPC Crack Maps

Age	*Crack Area*	*Max Width*	*Average Width*	*# of Cracks*
28 Days	0.001646 in^2	0.0012 in	0.000658 in	3
42 Days	0.011283 in^2	0.0017 in	0.001254 in	5
56 Days	0.02175 in^2	0.0028 in	0.001176 in	8

Table 4.6 HPC Cracking Summary

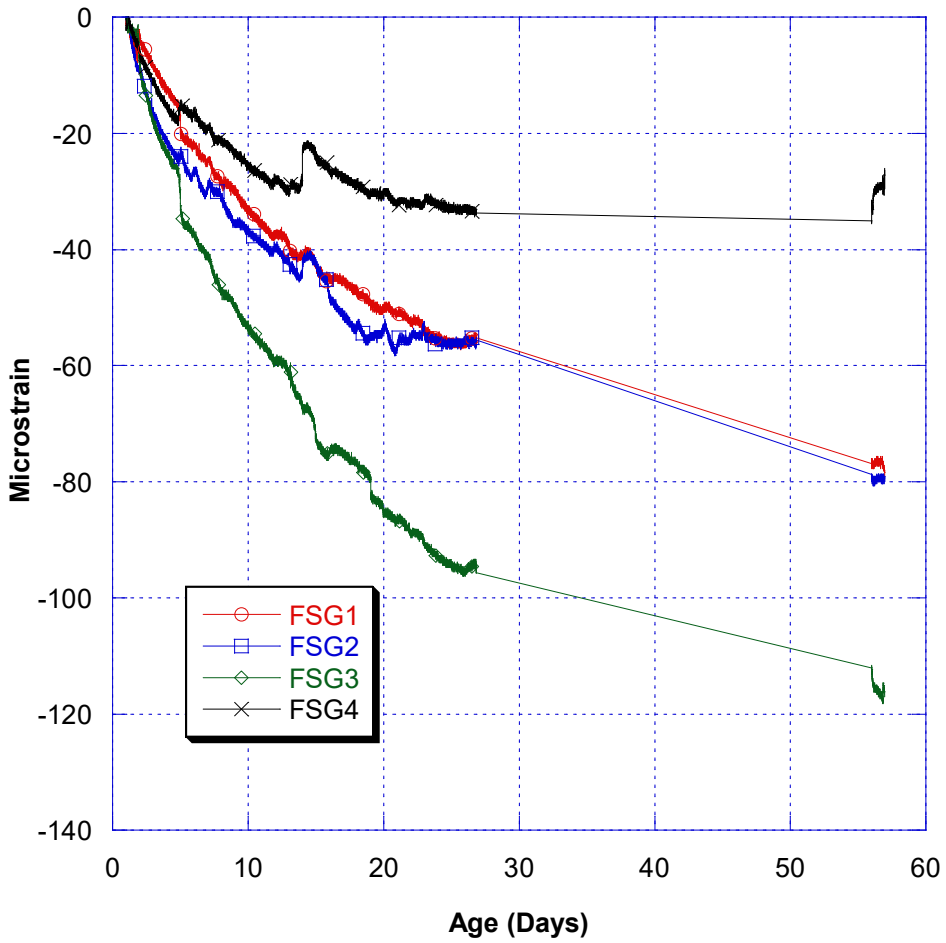

Figure 4.9 HPC Strain Data

The HPC mix performed relatively well. It experiences minimal cracking at the 28-day mark but the propagation thereinafter is at an increased rate when compared to the fiber reinforced variants. The number of new cracks forming between 28 and 56 days is also higher than what is experienced in all fiber reinforced mixes. There is a gap in the strain data caused by an issue with the collection system, but the trends and maximums can still be estimated.

4.4.2. HPC-b

28 Days

42 Days

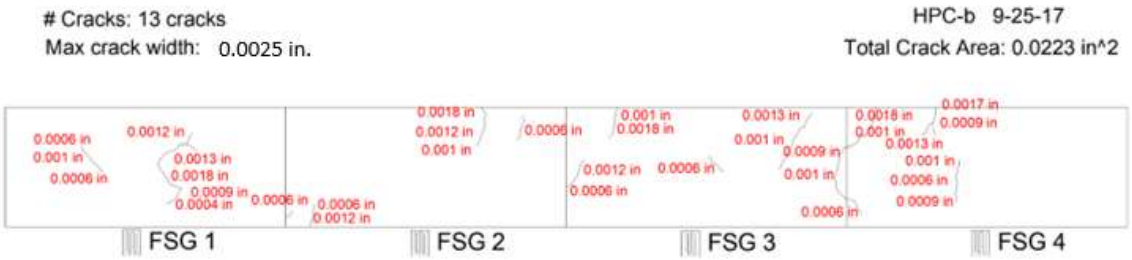

56 Days

Figure 4.10 HPC-b Crack Maps

Age	*Crack Area*	*Max Width*	*Average Width*	*# of Cracks*
28 Days	0.001625 in^2	0.0009 in	0.00038 in	6
42 Days	0.0176208 in^2	0.0018 in	0.00081 in	13
56 Days	0.0223 in^2	0.0025 in	0.00099 in	13

Table 4.7 HPC-b Crack Mapping Summary

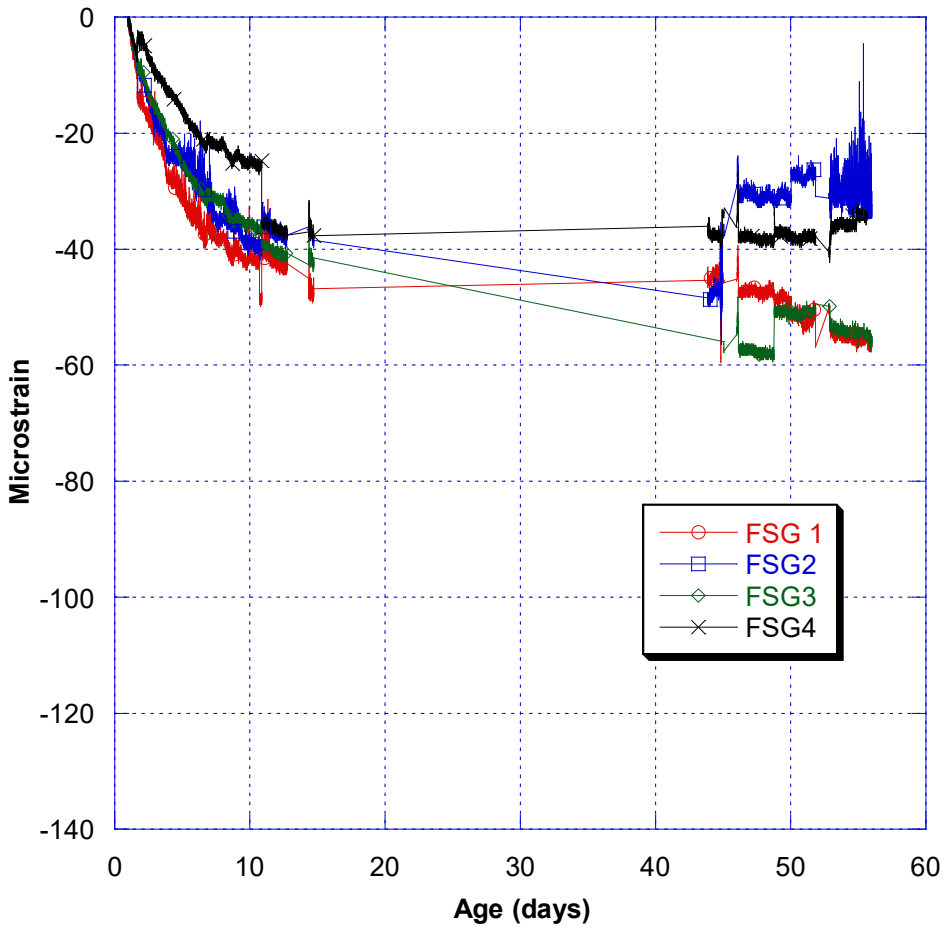

Figure 4.11 HPC-b Strain Data

A similar issue arises with the strain data from HPC-b as well as HPC. A similar trend can also be observed in the formation of cracks over time. A substantial amount form between the ages of 28 and 56 days when compared to the fiber mixes. The substantial number of cracks also leads to a skew in the results for average crack width in this case, because the cracks forming at later ages remain relatively tiny and drive the said average down. This data can still be compared, but the skew created in the result must be accounted for.

4.4.3. FR-HPC (2” Euclid PPE fibers)

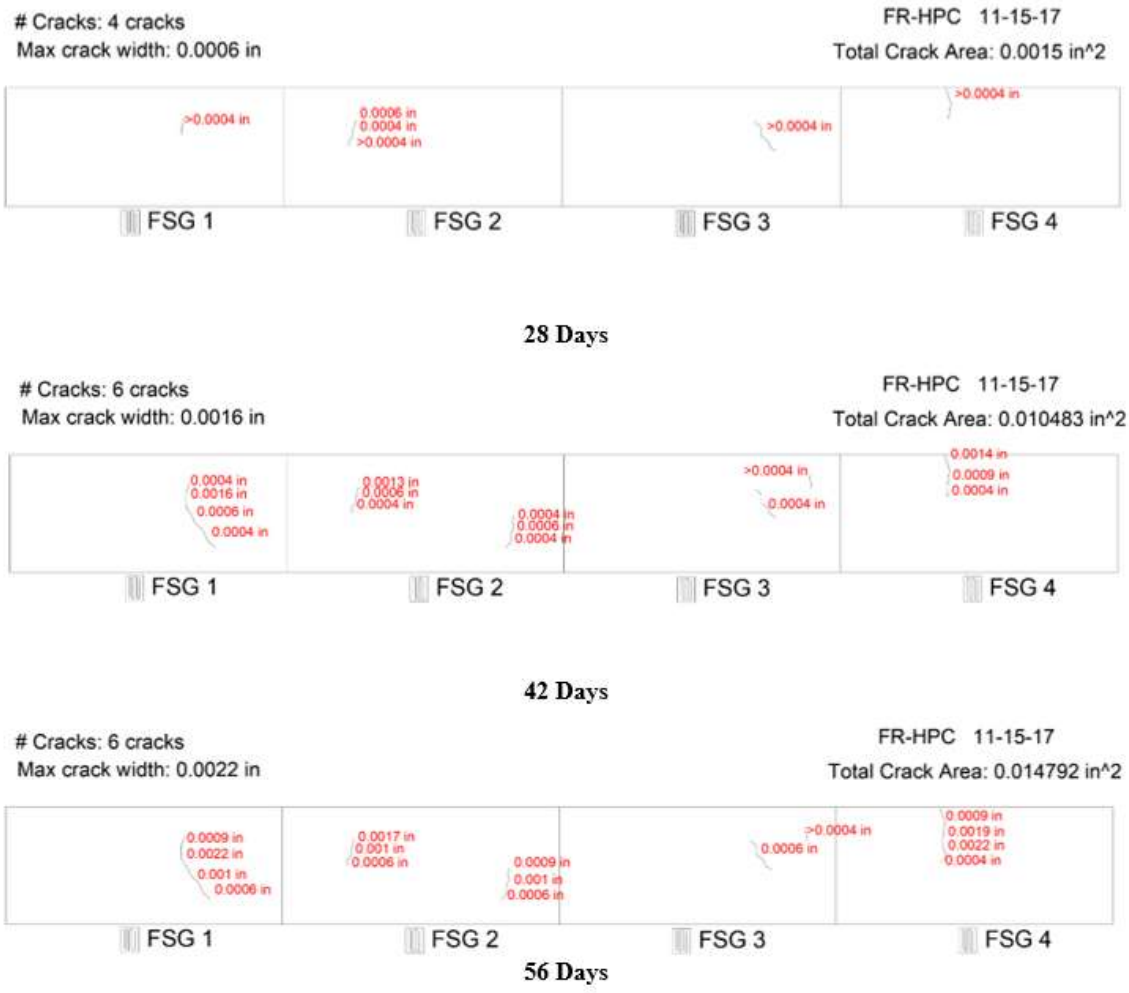

Figure 4.12 FR-HPC Crack Maps

Age	*Crack Area*	*Max Width*	*Average Width*	*# of Cracks*
28 Days	0.0015 in^2	0.0006 in	0.00033 in	4
42 Days	0.010483 in^2	0.0016 in	0.00087 in	6
56 Days	0.014792 in^2	0.0022 in	0.00118 in	6

Table 4.8 FR-HPC Crack Maps

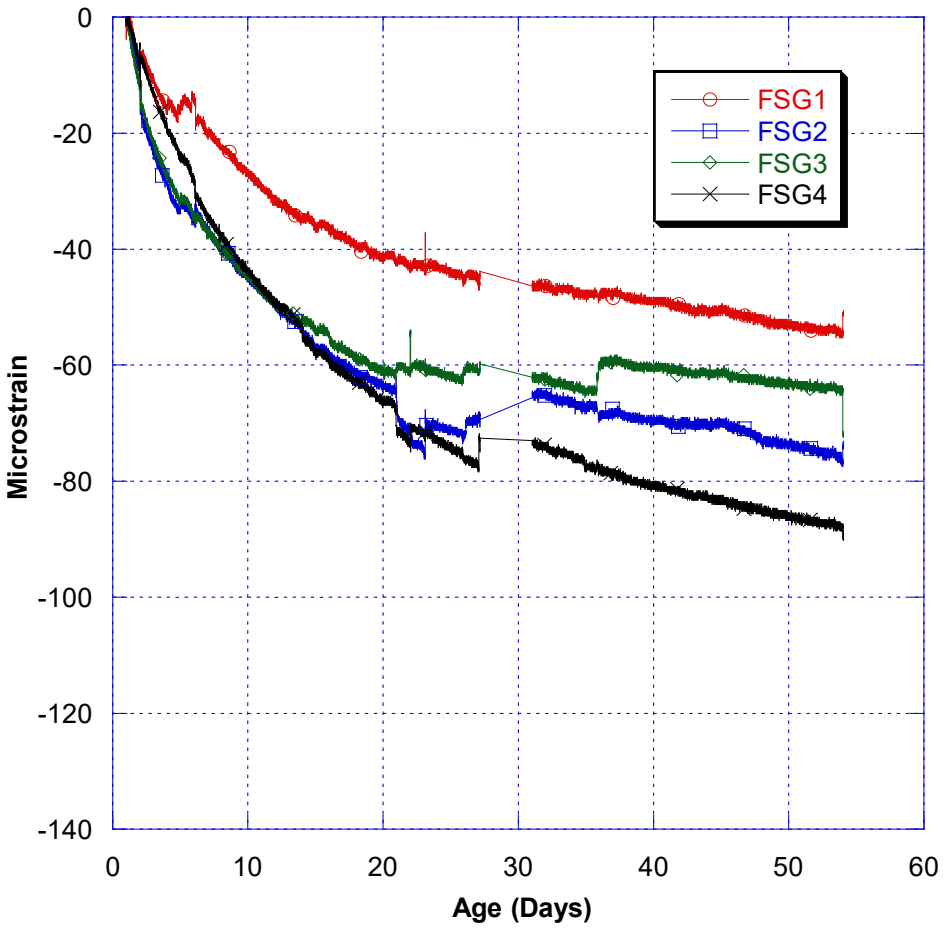

Figure 4.13 FR-HPC Strain Data

FR-HPC represents an improvement in cracking potential when compared to HPC. At 56 days, a 32.0% reduction in cracking area and a 21.4% reduction in maximum crack width are observed. At 28 days, the crack width and crack area are larger than what is experienced in HPC, but the growth rate of the cracks appears to be stinted by the fiber reinforcement implemented. The addition of five pounds per cubic yard proves effective in terms of reducing the cracking experienced in an AASHTO restrained ring over time.

4.4.4. FR-HPC-b (2” Euclid PPE fibers)

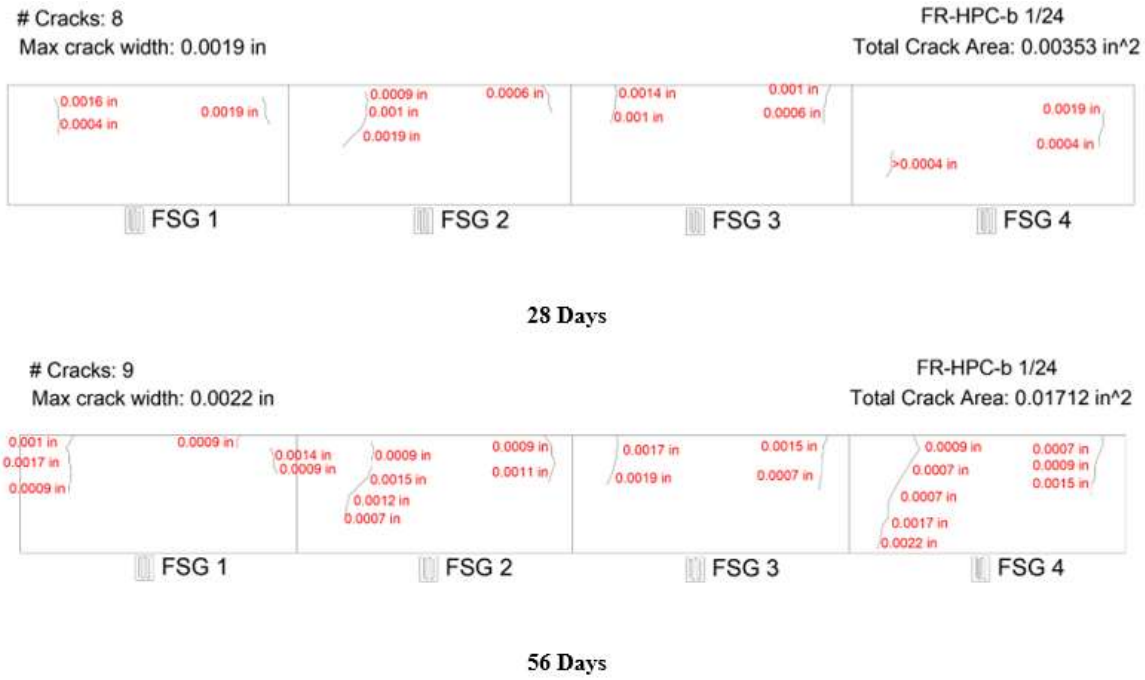

Figure 4.14 FR-HPC-b Crack Maps

Age	*Crack Area*	*Max Width*	*Average Width*	*# of Cracks*
28 Days	.00353 in^2	.0019 in	.00094 in	8
42 Days	N/A	N/A	N/A	N/A
56 Days	.01712 in^2	.0022 in	.00111 in	9

Table 4.9 FR-HPC-b Crack Mapping Summary

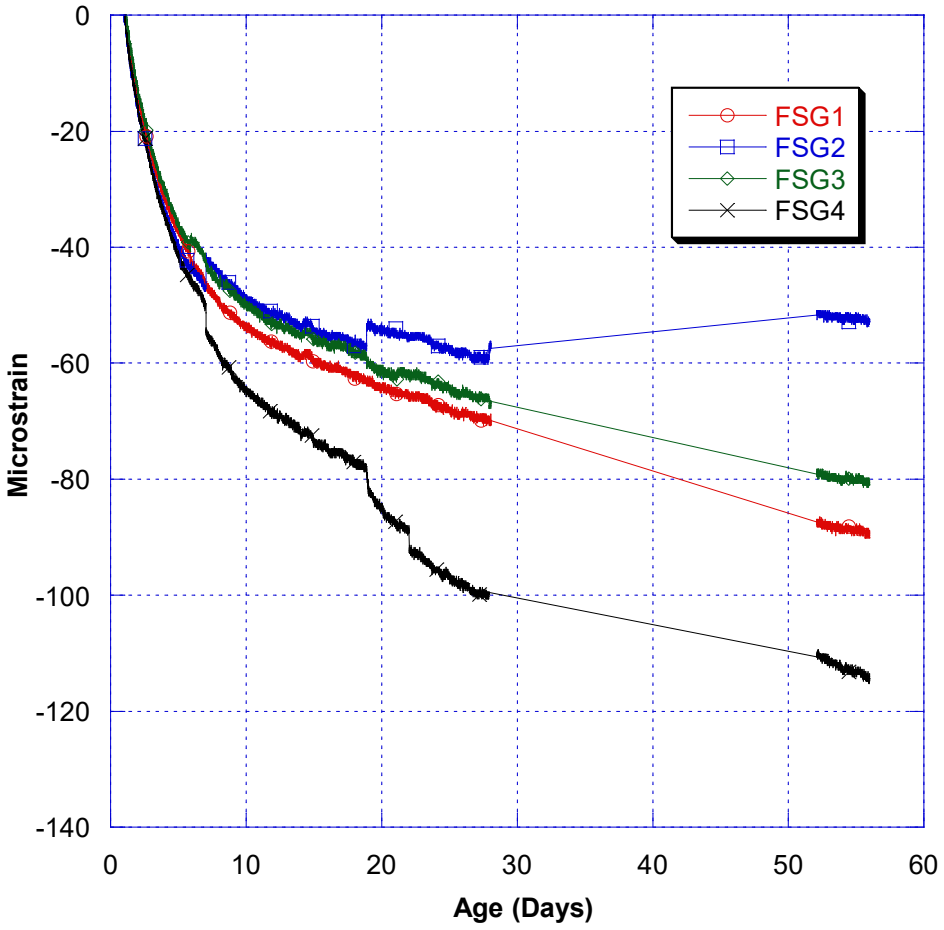

Figure 4.15 FR-HPC-b Strain Data

The addition of Euclid Macro PPE fibers as well as implementation of blending proves to be effective. When compared to the base blended variant, a 23.2% reduction in cracking area at 56 days is observed. A 12% reduction in maximum crack width is also observed. Cracking potential is improved in a similar result as was seen in HPC and FR-HPC. Blending will be used in the field, so the remainder of the fiber types to be investigated will also be investigated in the blended HPC mix.

4.4.5. FR-HPC-b (2” Sika Macro Synthetic Fibers)

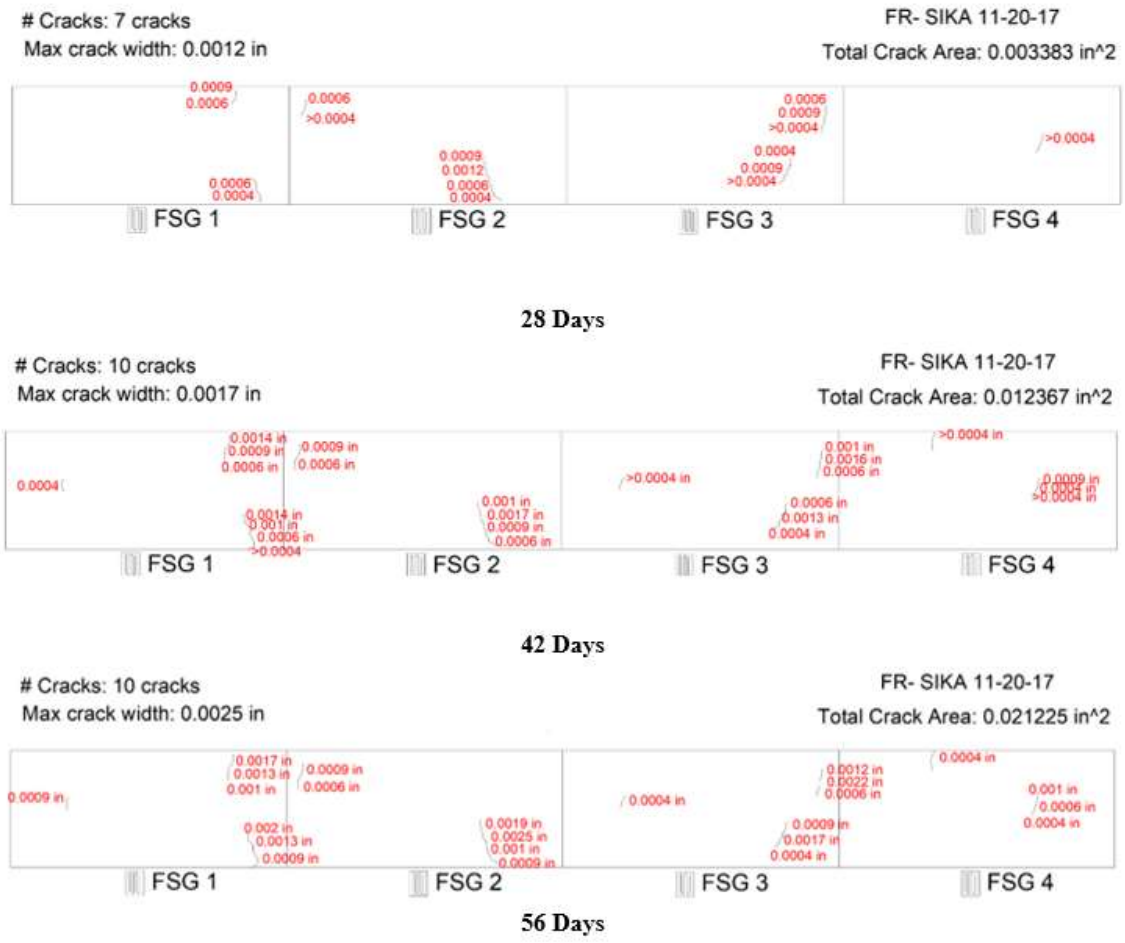

Figure 4.16 FR-Sika(1) Crack Maps

Age	*Crack Area*	*Max Width*	*Average Width*	*# of Cracks*
28 Days	0.003383 in^2	0.0012 in	0.000615 in	7
42 Days	0.012367 in^2	0.0017 in	0.000951 in	10
56 Days	0.021225 in^2	0.0025 in	0.001147 in	10

Table 4.10 FR-Sika(1) Crack Mapping Summary

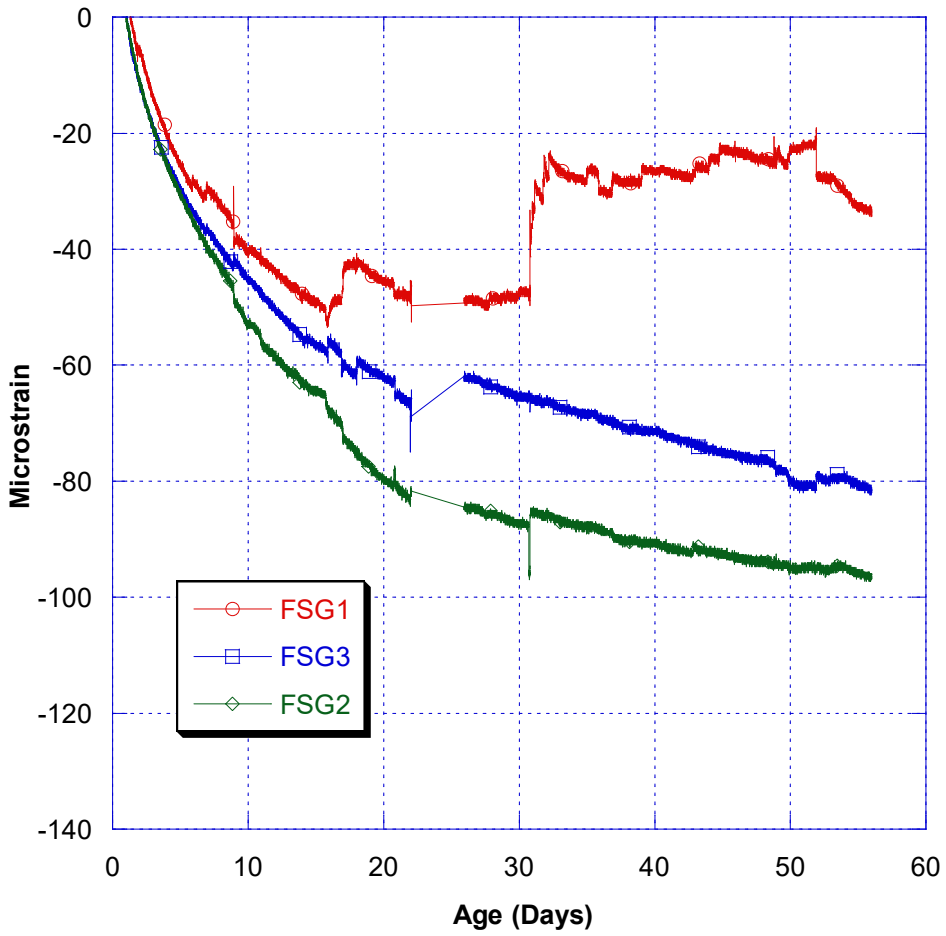

Table 4.11 FR-Sika(1) Strain Data

The Sika macro fibers do not influence cracking potential to the same degree that the Euclid macro fibers have shown. There is no decrease noted in the maximum crack width and a minimal decrease of 4.8% in terms of total cracking area when compared to HPC-b. The fiber type does not improve the results up to 56 days for this mix. This was also the only fiber mix that showed no improvement to HPC-b in terms of free shrinkage when the samples were not cured. A correlation can be established, but not a precise causation.

4.4.6. FR-HPC-b (2” Sika Steel Hooked Fibers)

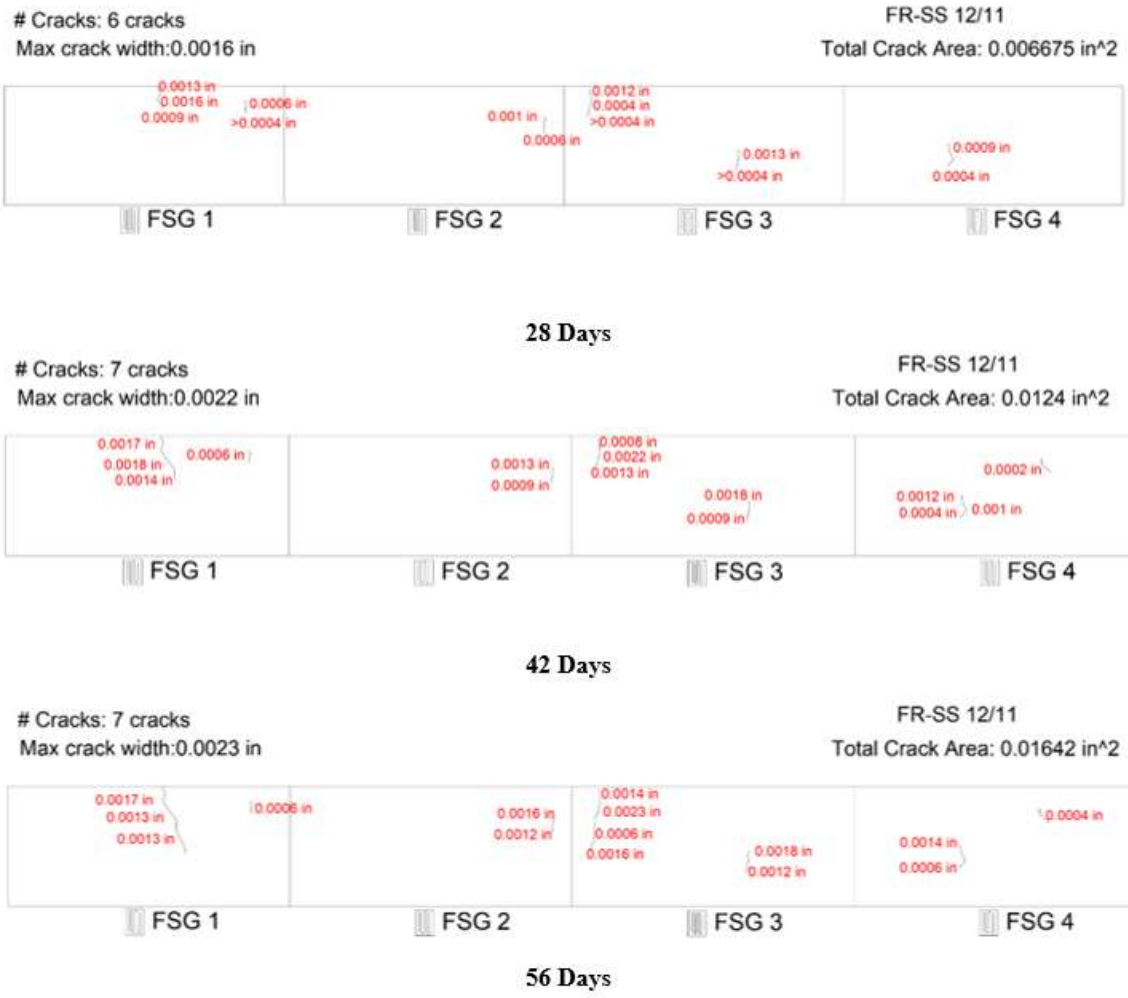

Figure 4.17 FR-Sika(2) Crack Maps

Age	*Crack Area*	*Max Width*	*Average Width*	*# of Cracks*
28 Days	0.006675 in^2	0.0016 in	0.000744 in	6
42 Days	0.0124 in^2	0.0022 in	0.001021 in	7
56 Days	0.01642 in^2	0.0023 in	0.001177 in	7

Table 4.12 FR-Sika(2) Crack Mapping Summary

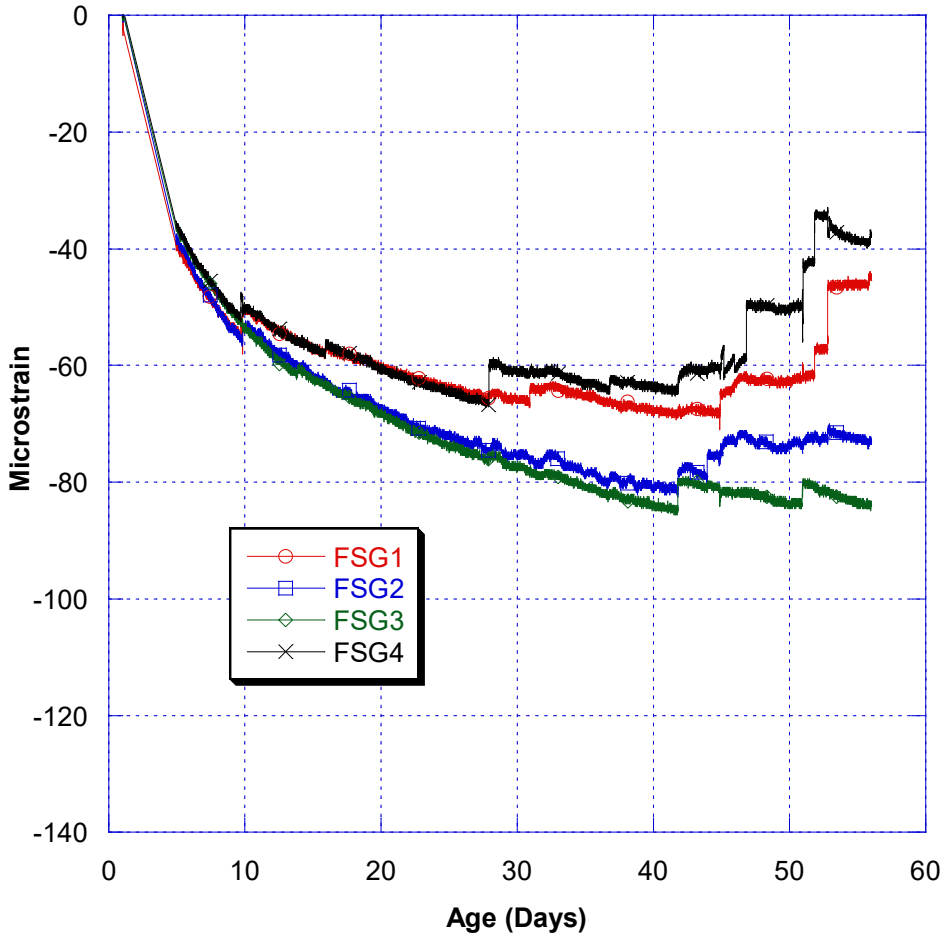

Figure 4.18 FR-Sika(2) Strain Data

The Sika steel hooked fibers also display an improvement in cracking potential. A 26.3% reduction in total cracking area paired with an 8% decrease in the maximum crack width when compared to HPC-b provide merit to the steel fibers. The issue remains however that these fibers are prone to corrosion over time, which is not accounted for here. This corrosion can also be accelerated in harsh environments. Because of this, the Euclid 2" fibers would be preferred over steel fibers for use in bridge decks.

4.4.7. Class A

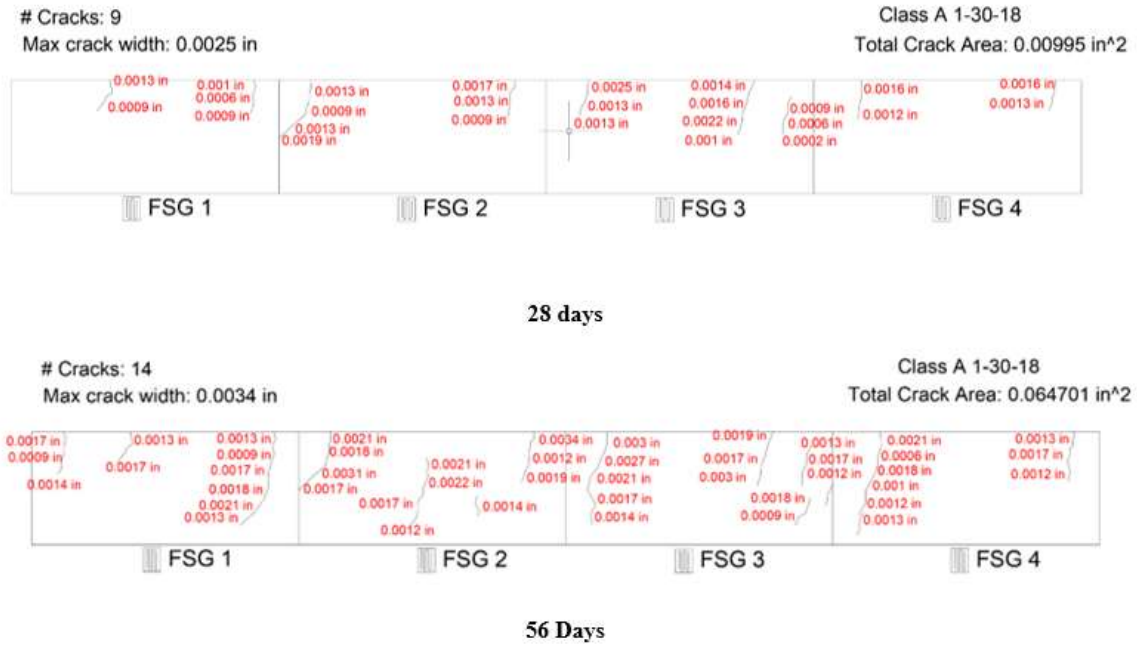

Figure 4.19 Class A Crack Maps

Age	*Crack Area*	*Max Width*	*Average Width*	*# of Cracks*
28 Days	.00995	.0025	.001279	9
42 Days	N/A	N/A	N/A	N/A
56 Days	.06470	.0034	.001644	14

Table 4.13 Class A Crack Mapping Summary

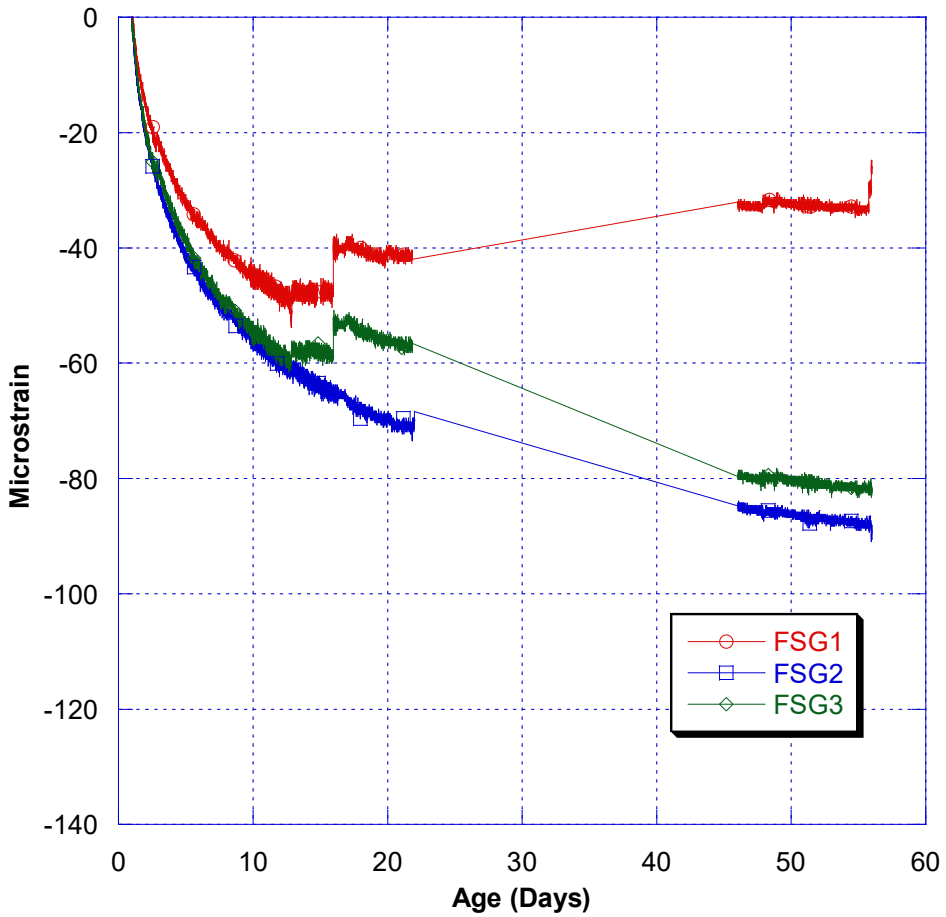

Figure 4.20 Class A Strain Data

Class A experienced significant cracking over time. At 56 days, it showed an increase in cracking area of 197.5% when compared to HPC. The maximum crack width was increased by 21.4%. This ring also experienced the highest number of cracks and the highest average crack width compared to the rest of the data set.

4.4.8. Crack Mapping Comparison

The first comparison will be made in terms of cracking area. This is a broad way to generalize the overall affects each change to the mix design produces. Cracking area was calculated by averaging the width of each crack across its respective face and

multiplying the result by the length of the individual crack. This takes all factors into account and generates a scale of effectiveness for each design change.

Age	*HPC*	*HPC-b*	*FR-HPC*	*FR-HPC-b*	*FR-Sika(1)*	*FR-Sika(2)*	*Class A*
28	0.00164	0.00162	0.0015	.00353	0.00338	0.00667	0.00995
42	0.01128	0.01762	0.01048	N/A	0.01236	0.01240	N/A
56	0.02175	0.02230	0.01479	.01712	0.02122	0.01642	0.06470

Table 4.14 Crack Area Comparison (in^2)

While this comparison does not necessarily tell us why using fiber is effective or the facets in which it facilitates, it does give a general sense that the fiber additions have a resounding positive effect on the cracking potential of the HPC variant in question. The variation seen when comparing blending versus not blending is minimal, but it should be noted that the blended mix had an overall cracking area that was 2.5% higher than the base mix at 56 days. In terms of the effects of each fiber, there are a few trends to point out. The first note to make is the progression of the cracking area appears much slower through 56 days when comparing the fibrous mixes to the blended and nonblended HPC. The cracking area at 28 days shows the fiber mixes having a higher amount of cracking, but as time proceeds these cracks are not widening at the same rate as the base mixes. By 56 days, large reductions in cracking area are already noticeable. For the nonblended mix, the Euclid 2" PPE fibers provide a 31.2% reduction in cracking area. For the blended mixes, each fiber performed differently. The Sika synthetic fiber provided little to no assistance in the mitigation of crack propagation (4.8% reduction compared to HPC-b). The Sika steel fibers proved effective with HPC-b, with a cracking area reduction of 26.3%. The Euclid PPE fibers provided an area reduction of 23.2% to the blended HPC mix.

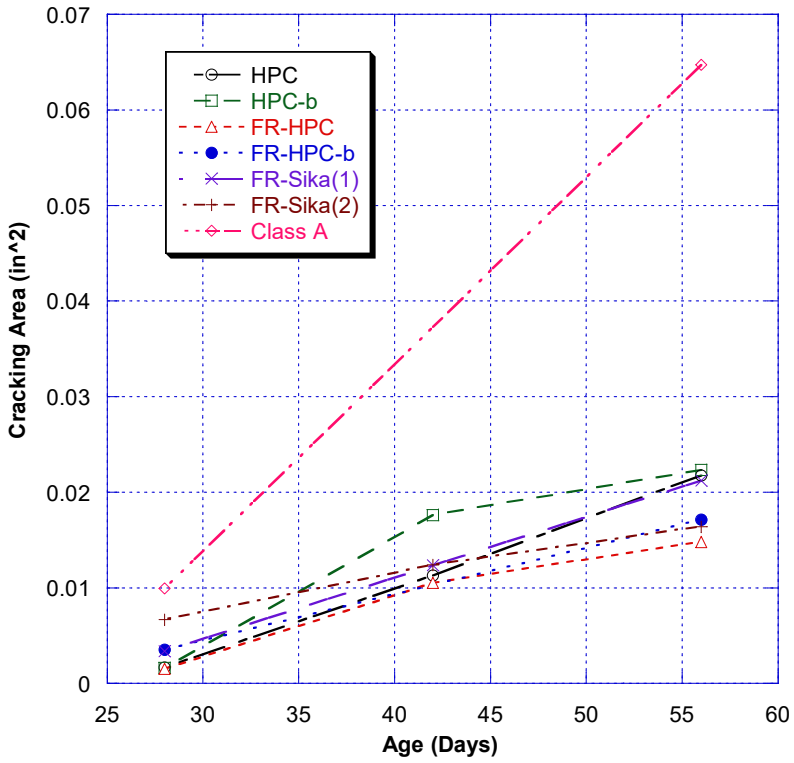

Figure 4.21 Cracking Area Comparison

These results prove that the concept is effective, but they do not show why that is. For this reason, further comparisons must be made. The maximum and average crack widths will be compared, as well as the number of cracks for each specimen. All of this will be done in an attempt to gain a better understanding of the mechanism that makes this concept effective. The crack widths will be investigated first.

Age	*HPC*	*HPC-b*	*FR-HPC*	*FR-HPC-b*	*FR-Sika(1)*	*FR-Sika(2)*	*Class A*
28	0.0012	0.0009	0.0006	0.0019	0.0012	0.0016	.0025
42	0.0017	0.0018	0.0016	N/A	0.0017	0.0022	N/A
56	0.0028	0.0025	0.0022	0.0022	0.0025	0.0023	.0034

Table 4.15 Maximum Crack Width Comparison (in.)

In terms of the maximum crack widths, minimal differences are noted. The blending of aggregate resulted in a 10.7% reduction of the maximum, but both FR-HPC

and FR-HPC-b had equivalent maximum widths at 56 days. The Sika synthetic fibers offered no reduction in crack width, while the Euclid PPE fibers offered a 12% reduction in maximum width and the Sika steel fibers resulted in an 8% reduction to the maximum width. It should be noted that the propagation of these cracks again appears to be slower with the addition of fibers. This can be visualized by the figure below. It is clearly shown that, even while beginning at a higher crack width from 28 days, the progression of these cracks is clearly stunted by the fiber reinforcement.

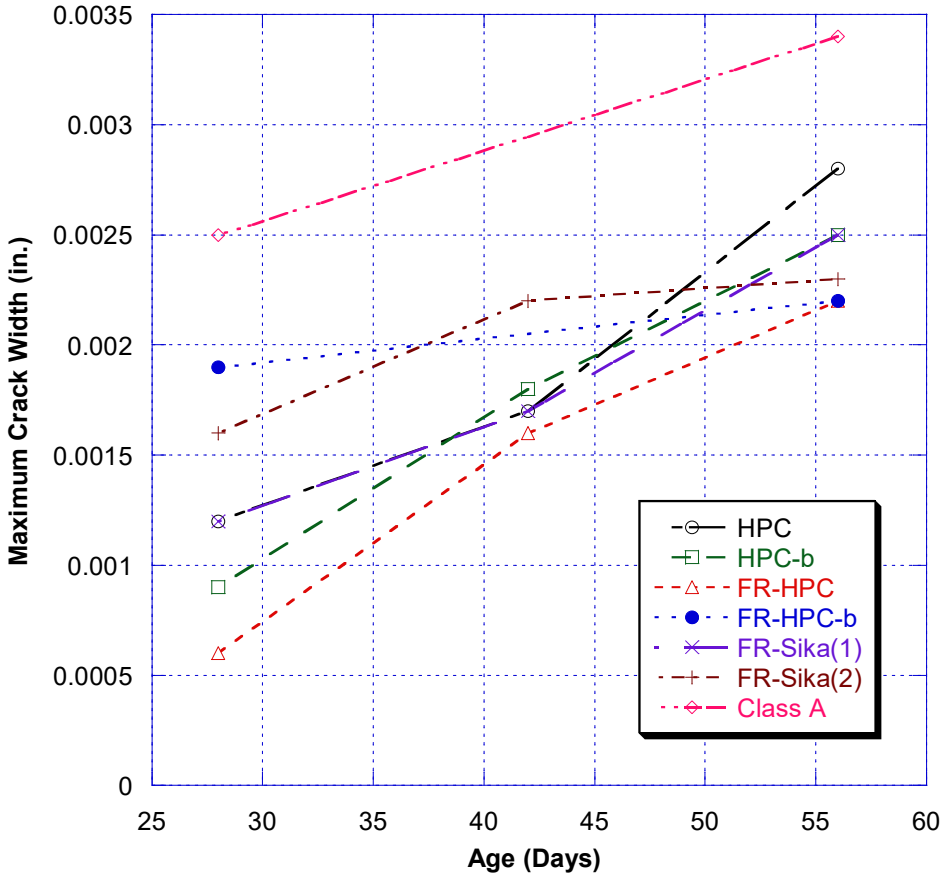

Figure 4.22 Maximum Crack Widths

Both the maximums and the averages should be seen as viable, comparable values. For this experimental set up, the only notable difference seen from average crack widths comes with the blended HPC. While all other HPC variants fall in a range

between .00111 and .00118 inches at 56 days, blended HPC shows an average of .00099 inches at 56 days. The reasoning for the smaller average and larger total area is explained in by the number of cracks in each ring which will be observed after the average crack widths.

Age	*HPC*	*HPC-b*	*FR-HPC*	*FR-HPC-b*	*FR-Sika(1)*	*FR-Sika(2)*	*Class A*
28	0.000658	0.00038	0.00033	0.00094	0.000615	0.000744	.001279
42	0.001254	0.00081	0.00087	N/A	0.000951	0.001021	N/A
56	0.001176	0.00099	0.00118	0.00111	0.001147	0.001174	.001644

Table 4.16 Average Crack Width Comparison (in.)

The fiber additions show a slight increase in the average crack width. The difference is negligible when comparing HPC to FR-HPC, but a larger difference can be seen when comparing the blended variants. The increases range from 12.1% to 19.2% for the specified mixes. Based on the rate of increase noted in the maximum crack width portion of this comparison and a similar trend in the average crack width comparison shown below, the trend would appear to be on the path of correcting in the favor of fiber reinforced mixes at later ages. Further research must be done to ascertain this hypothesis.

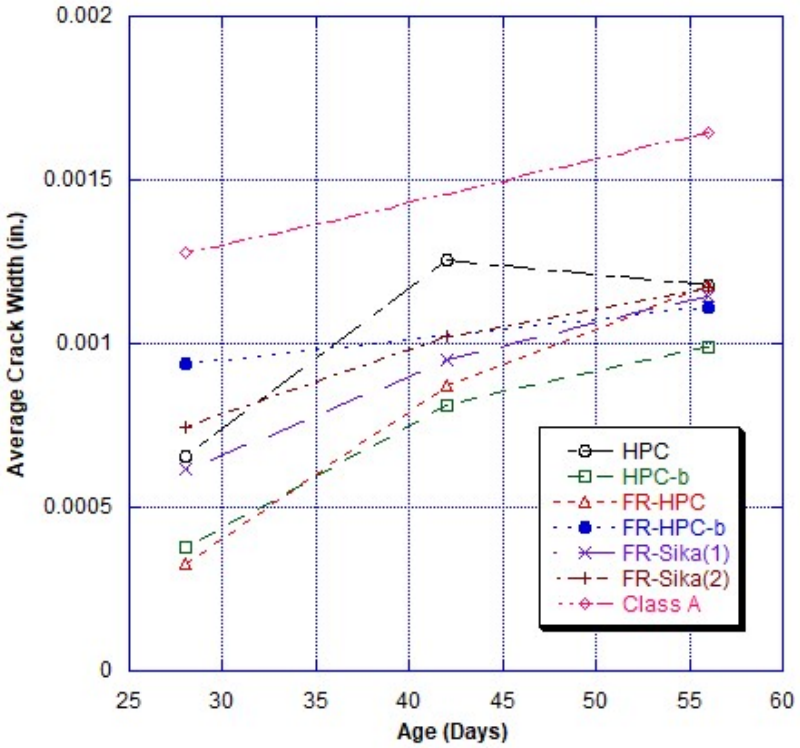

Figure 4.23 Average Crack Width

The other concern with this data set is epitomized in the figure by the HPC results. The average crack width decreased from 42 to 56 days. The simple explanation for this is the fact that new cracks have formed over this time. Those cracks remained relatively small up to the point where the ring was mapped. Therefore, they bring the average lower that what it was at fourteen days prior. This issue can skew the results if it is the only thing being considered. For this reason and as another comparative method, the number of cracks over time will also be observed.

Age	*HPC*	*HPC-b*	*FR-HPC*	*FR-HPC-b*	*FR-Sika(1)*	*FR-Sika(2)*	*Class A*
28	3	6	4	8	7	6	9
42	5	13	6	N/A	10	7	N/A
56	8	13	6	9	10	7	14

Table 4.17 Number of Cracks

Adding this parameter clearly shows why HPC-b has more cracking area even though its average crack width is significantly lower than the rest of the HPC variants. The number of cracks observed for HPC-b is a minimum of three cracks higher than every other HPC mix. The trends to be noticed here are clear. Blending aggregates results in a higher number of cracks. This is noticed in both fiber reinforced and plain concrete. Also, less cracks appear to form over time when fibers are introduced. From 28 to 56 days, both HPC and HPC-b more than doubled in terms of the number of cracks observed. All the fiber mixes increased by less than 50% over the same time period. This is another metric that bodes well for the long-term outlook of the implementation of fiber reinforcement into bridge decks.

5. Case Study

5.1. Introduction

The polypropylene fiber reinforcement proved effective enough to be tested as an actual bridge deck. Before any pours on the actual deck, a trial slab was cast below the bridge. From this slab, samples were taken to test for all mechanical properties as well as restrained shrinkage. The bridge in question is in New Jersey. A deck replacement was needed. The decks in question are all three-span continuous and match in dimension and loading. For appropriate comparison, these slabs were cast alternatively as blended HPC and blended FR-HPC. Samples were collected from the trial slab, two blended HPC pours (slab #1, slab #3), and one blended FR-HPC pour (slab #2). It is important to note that the trial slab and slab #1 were not pumped, while slab #2 and slab #3 were pumped to pour. This is important because the contractors added more water and super plasticizer to the mix, which in turn weakened the concrete. For the best comparisons, each set (pumped and not pumped) must be compared separately. The concrete was tested for compressive strength, tensile strength, modulus of elasticity, rapid chloride permeability, surface resistivity, free shrinkage, and restrained shrinkage.

5.2. Mix Designs

The mix designs from this section are analogous to the mix designs from the laboratory experiments. All four mixes are listed. These are standard approved NJTA mix designs, with the exception to that being the addition of macro synthetic polypropylene fibers. The designs are kept as similar as possible in order to truly investigate the

resulting effects of the fiber addition. The high range water reducer for the fiber reinforced mixes is notably higher because of the fibers inherently negative effect on the workability of concrete. Results for slump testing, air content testing, ambient air temperature and concrete temperature are also shown at the bottom of the table.

Basic Mix	FR-NJTA-TR Trial Slab	HPC-b	FR-HPC-Pump	HPC-b-Pump
Date	7/5/2017	7/10/2017	7/11/2017	7/12/2017
Cement, Type I (lb/cy)	520	520	520	520
Fly Ash, Class C (lb/cy)	130	130	130	130
Silica Fume (lb/cy)	25	25	25	25
Total Cement (lb/cy)	675	675	675	675
w/b ratio	0.360	0.374	0.374	0.374
#57 (lb/cy)	1,500	1,500	1,500	1,500
#8 (lb/cy)	300	300	300	300
Sand (lb/cy)	1,113	1,113	1,113	1,113
HRWR (oz/cy)	42	35	42	35
AEA (oz/cy)	7.6	7.6	7.6	7.6
Other admixtures	2" PPE (5lb/cy)	-	2" PPE (5lb/cy)	-
Slump (in.)	5.5	8.0	5.0	7.0
Air Content (%)	6.4	5.5	5.5	5.8
Ambient Temperature (F)	82	81	80	80
Concrete Temperature (F)	84	84	83	84

Table 5.1 Field Mix Proportions

All mixes were within the guidelines set in the NJTA Technical Specification in terms of slump and air content. It is important to note that the concrete trucks hauling the mixes to be pumped for slabs slab #2 and slab #3 had approximate additional 20 gallons of water and 15 ounces of super plasticizer added to account for the slump and air content lost in the pumping process. Slump and air measurements of these mixes were taken directly from the concrete trucks before pumping. The sampling procedure will be discussed in the next section.

5.3. Procedure

The following section will outline the specific procedures followed for the field work of this case study. Rutgers RIME group was deployed to the site on multiple occasions during casting to monitor and collect samples and after casting to crack map each deck individually to compile data for a valid comparison. They were present for the casting of each slab and performed the sampling themselves.

5.3.1. Sampling and Curing

All concrete sampling was performed by the Rutgers RIME group in accordance to AASHTO T23. Concrete samples were taken in the form of cylinders (both 4” by 8” and 6” by 12”), free shrinkage molds (3” by 3” by 11”), and AASHTO TP34 Rings. Vibration was not applicable in the site location so rodding was the chosen method of consolidation. The specimens were left on site to mimic curing conditions of the decks, and transported 24 hours after the fact to the lab. Cylinders and half of the free shrinkage molds were cured for fourteen days in the curing room of the lab. Each sample in the curing room was placed in lime saturated water for the duration of curing. The AASHTO rings and half of the free shrinkage samples were not cured further and immediately placed in the environmental chamber. Within 24 hours the ring samples were demolded, prepared, and connected to the data loggers. Cylinders cast for rapid chloride permeability and surface resistivity testing were placed in a separate tank of lime saturated water where they remained for the duration of the test period (up to 56 days).

Figure 5.1 Casting of the Trial Slab and Field Sampling

5.3.2. Crack Mapping

Crack mapping was performed on both the AASHTO rings and the actual bridge decks cast during construction. The procedure for the crack mapping of the rings followed the exact same outline as previously stated in section 3.4.6. As for the bridge decks themselves, a separate procedure was used due to the massive increase in surface area that needed to be covered. The procedure is more rudimentary than that of the rings, but it still provides an effective comparison of the difference in cracking tendencies for the two mix designs in question.

Figure 5.2 Crack Mapping

There are a few important parameters that must be met before the crack mapping can occur. The deck must be at minimum 14 days old and done curing. The tests must be performed in between this time period and the time when the lane(s) are open to traffic. The deck must also be completely dry when the mapping is occurring. Before crack mapping occurs, a plan view (to scale) must be prepared using drafting software. These will be printed and used by the surveyors during crack mapping. The examiners will proceed to the bridge decks with the plan drawing printed as well as measuring tapes, crack measurement cards, and a writing utensil for the plans and the deck. The crack surveyors will start at one end of the slab and mark off the deck in appropriate segments for reference. The deck at this point shall also be cleaned, whether it be with an air blower or by washing and letting dry. The examiner should, starting at one end, identify all cracks that can be seen while bending at the waist. The location of this crack should be marked on the plan view drawing at its approximate location with an appropriate length.

The maximum crack width of each individual crack should also be measured using the crack cards and recorded. Finding all cracks from a similar reference point (bending at the waist) should help to eliminate subjectivity from the examination. At the end of the slab(s), each section should be accurately mapped on to the plan view drawing using AutoCAD or MicroStation. The individual information of each crack should also be transcribed onto these files and accounted for. From this information, it is possible to calculate crack density and give an accurate depiction of the cracking patterns for the slabs in question.

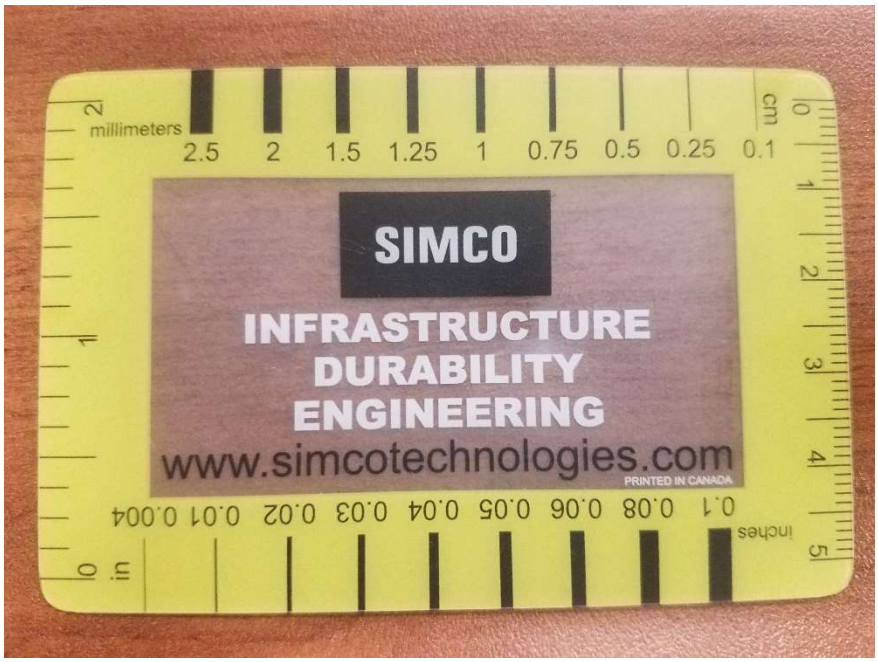

Figure 5.3 Crack Card Measuring Tool

5.4. Results

There will be two sets of mixes presented in this section. Both serve as direct comparisons of fiber reinforced high performance concrete to normal high-performance concrete. There are two fiber reinforced mixes and two mixes without fibers. For each

subset, one mix was pumped while the second was not pumped. The sampling was done as specified in section 5.3.1. Each mix was transported back to the lab and demolded within 24 hours of casting. Each of following testing sections will describe the testing done as well as curing conditions, results, and a brief comparison of the results.

5.4.1. Compressive Strength

Compressive Strength testing was done at 1, 3, 7, 14, 28, 56 days. The testing was done with 4" by 8" cylinders in accordance with ASTM C39. At least two cylinders were tested in compression during each round. The cylinders for this test were all cured for 14 days in lime saturated water and subsequently placed in the environmental chamber until tested. The results are as follows:

Age	FR-HPC-b	HPC-b	FR-HPC-b (Pump)	HPC-b (Pump)
1	3503	3646	3240	3041
3	4419	4220	3774	3670
7	5613	5474	4570	4265
14	6205	6011	5533	5036
28	7723	7604	6648	6529
56	8141	8420	7424	6887

Table 5.2 Compressive Strength Results (Field)

As shown in the results, the difference in compressive strength from the addition of fibers is negligible. As seen in the lab, there is a slight decrease (3.3%) in compressive strength due to the fiber additions for the set of poured mixes. The pumped FR-HPC-b appears slightly stronger than the pumped HPC-b, but this could be due to the undocumented water additions during pouring. The two non-pumped mixes offer a more accurate comparison which depicts a slight reduction in compressive strength from the addition of polypropylene macro fibers. In terms of the effects of pumping versus not

pumping, there is a clear differentiation in results. The pumping, specifically the addition of extra water and super plasticizer, has an adverse effect on the compressive strength. At 56 days, HPC-b shows an 18.2% reduction when pumped while FR-HPC-b shows an 8.8% reduction when pumped. It is also important to note that the result of this pumping is still acceptable in this specific situation when the minimum required compressive strength is 5 ksi at 28 days. The following graph depicts the strength over time of all four mixes to offer a wider view of the comparison between each subset.

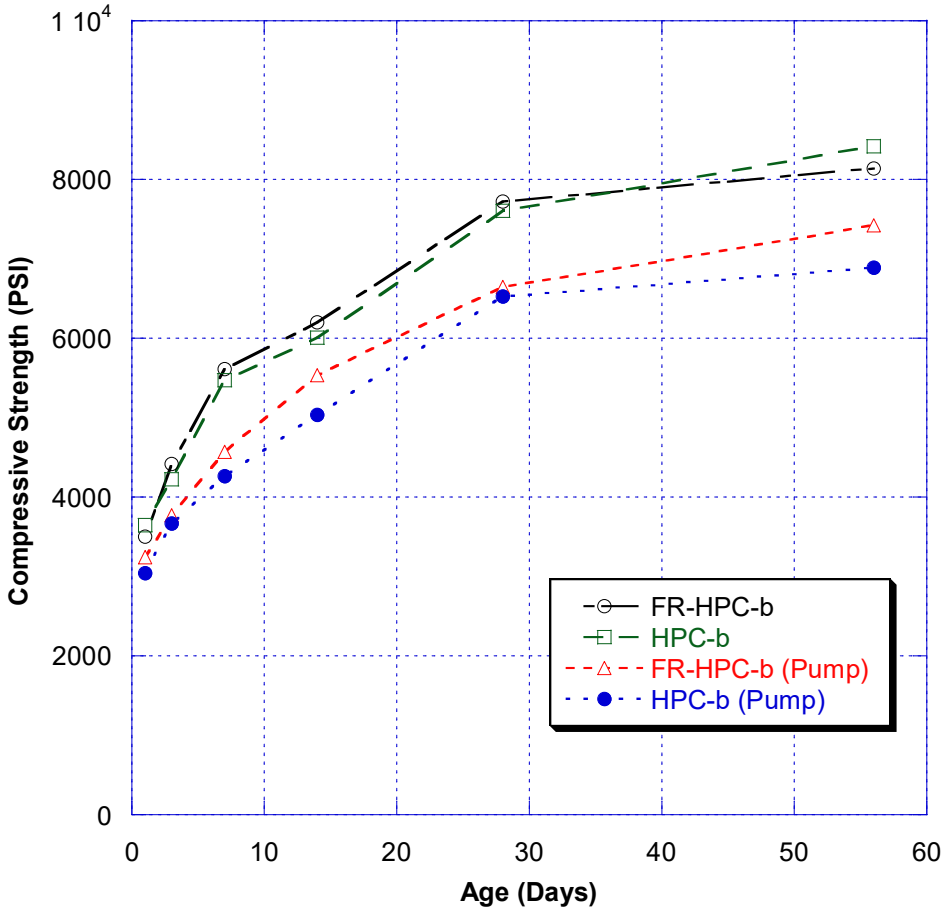

Figure 5.4 Compressive Strength Comparison (Field)

5.4.2. Tensile Strength

Tensile strength testing was done at the same time intervals as the compressive strength testing with the same specimens under the same curing and storage conditions. The testing was done in accordance with ASTM C496 standards. The results from testing are as follows:

Age	FR-HPC-b	HPC-b	FR-HPC-b (Pump)	HPC-b (Pump)
1	360	394	322	307
3	360	402	358	326
7	518	450	426	396
14	537	490	491	482
28	547	671	619	555
56	541	637	557	498

Table 5.3 Tensile Strength Results (Field)

There is a little more disparity in the tensile strength results. It is clearly shown that the addition of materials to promote pumping is taking away from the early age tensile strength. As time goes forward the results between the pumped and not pumped FR-HPC-b mixes begin to converge on each other, while the opposite effect is seen between the HPC-b mixes. In the mixes without additions made, a decrease in tensile strength is observed when fibers are added. This is aligned with the results from laboratory experimentation. The fibers in question seem to have more of an effect on this testing regime after the cylinders are broken. It is repeatedly observed that while the HPC-b mixes fail immediately at the initial cracking load, the FR-HPC-b cylinders seem to be able to withstand some loading after the initial cracking due to the fiber contents. It is as if these fibers intercept the failure mechanism to at least slow the tensile failure process down. This mechanism isn't easily quantified and cannot be seen in the testing results.

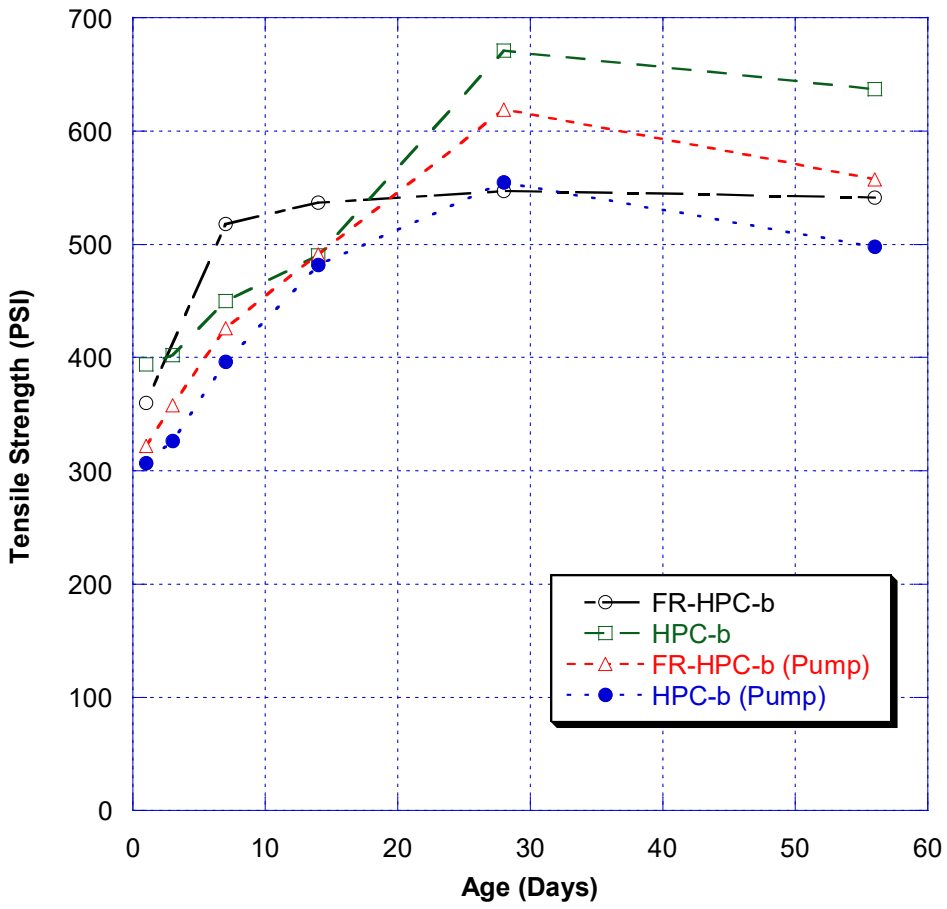

Figure 5.5 Tensile Strength Comparison (Field)

While looking at the tensile strength over time, it is also observed that the fiber mixes both attain higher early age tensile strength than their counterparts. At the later ages of testing however, a decrease in tensile strength is observed when looking at the poured mixes. This is consistent with the results seen in the lab.

5.4.3. Modulus of Elasticity

Modulus of elasticity testing was again done in the same time intervals as compressive strength and tensile strength testing. The samples were kept in the same

curing and storage conditions. The testing procedure was done in accordance to ASTM C469. The results were as follows:

Age	FR-HPC-b	HPC-b	FR-HPC-b (Pump)	HPC-b (Pump)
1	3503	3639	3681	3082
3	3859	4348	3771	N/A
7	4514	4310	3851	3769
14	4392	5227	4318	4425
28	4414	4987	4634	4115
56	4044	4754	4358	4027

Table 5.4 Modulus of Elasticity Results (Field)

The results here help to prove the previous conclusion of fibers decreasing the concrete's modulus of elasticity. When comparing both non-pumped mixes, it is clearly seen that the FR-HPC modulus is lower than that of the HPC. The fibers increase the elasticity of the concrete. On the other hand, the pumped concrete mixes show the opposite effect. This difference is most likely due to the undocumented additions to each batch to make the concrete pumpable in each case. Seeing as the results between pumped FR-HPC-b and FR-HPC-b are very close to each other, these additions could be having a more profound effect on the mixes without fibers. The graph below depicts the variation in modulus of elasticity with respect to time.

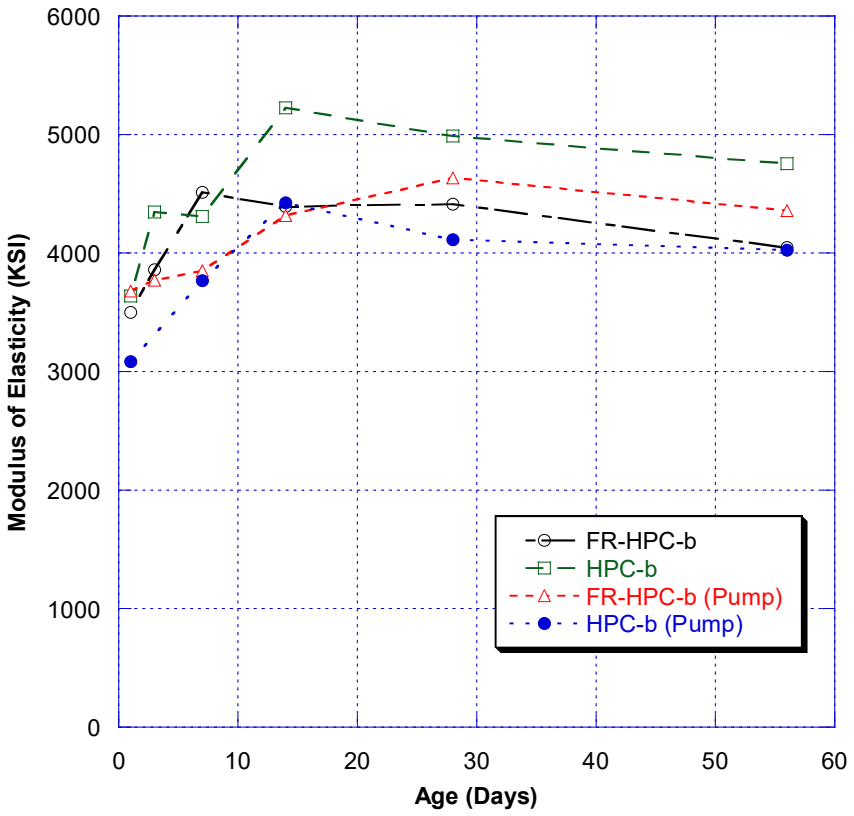

Figure 5.6 Modulus of Elasticity Comparison (Field)

5.4.4. Free Shrinkage

For each field mix, a minimum of six shrinkage samples were cast. They were cast in the field and transported with the rest of the samples. There are two sets of free shrinkage data to be evaluated. One set removed was from the molds and sent directly to the environmental chamber. It received no further curing. The second set is cured in the lime water tanks for 14 days with the remainder of the test samples. These two sets will give an accurate envelope for the shrinkage of each mix depending on the effectiveness and length of the curing mechanism. The dry shrinkage results are depicted in the following graph.

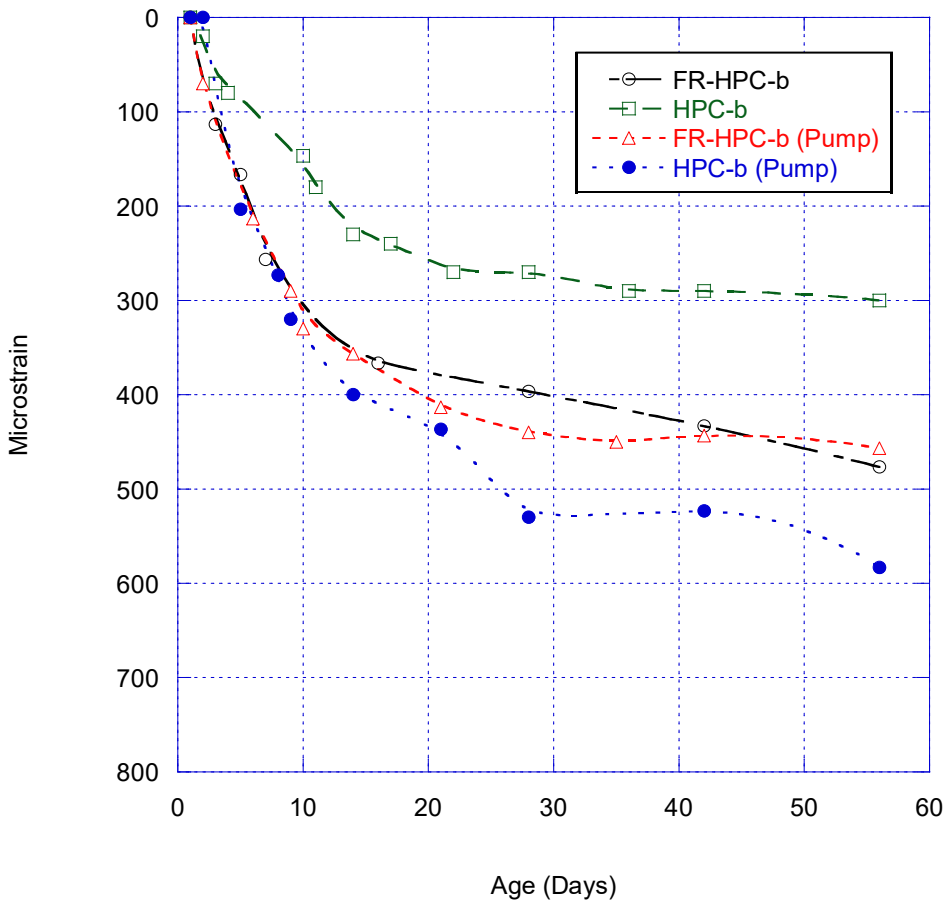

Figure 5.7 Free Shrinkage Comparison (Dry Cure - Field)

The results here further reinforce the thought process that excess water was added to the pumped HPC-b mix to meet the contractor's requirements. While the FR-HPC-b mixes culminate in nearly the same result, The HPC-b mixes vastly differ. The results of the shrinkage samples cured for 14 days in lime tanks will also further reinforce this idea. The fibers, contrary to what was experienced in the lab, do seem to have a slightly negative effect on the results here, but it is not significant enough to cause alarm. This only depicts what is essentially the worst-case scenario for curing. The next graph will give a more accurate picture of expectations.

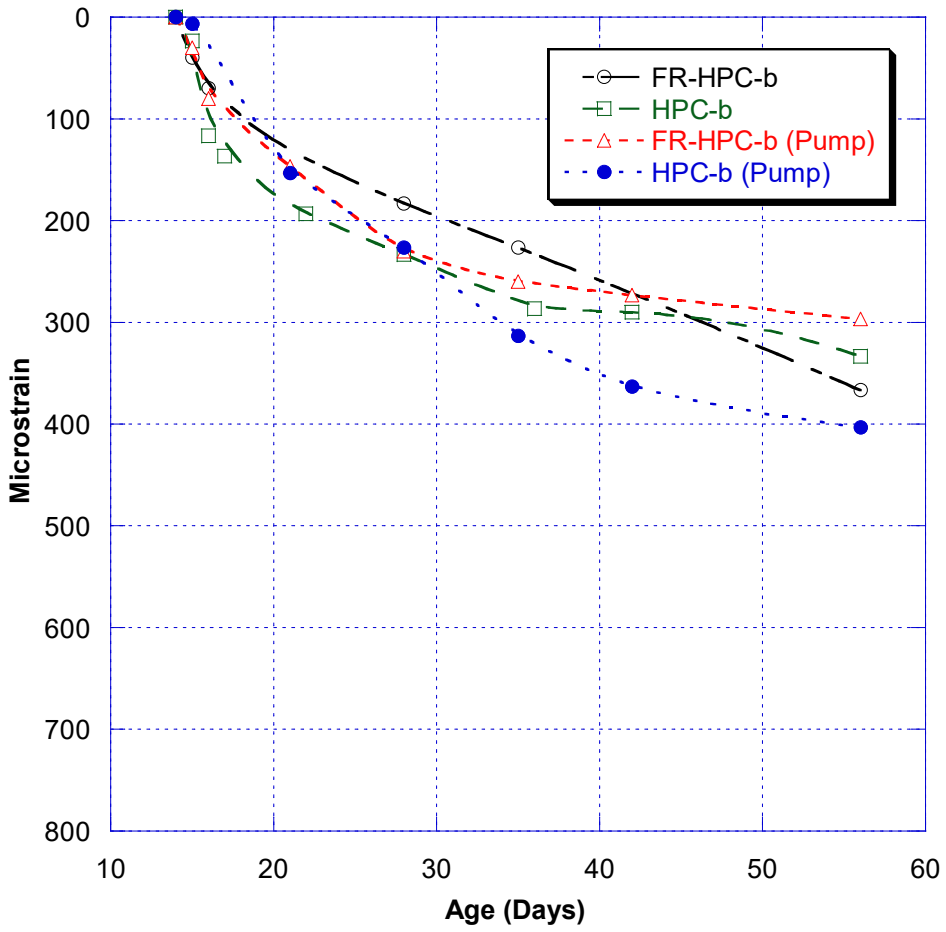

Figure 5.8 Free Shrinkage Comparison (14 Day Cure - Field)

The more accurate depiction shows a minimal disparity between the mixes and again reinforces the idea that there was some sort of extra water addition to the pumped HPC-b mix. From this data as well as the previous lab data, it can be deduced that the specified fiber additions do not have any significant effect on the concrete they are added to. The slight variations here are more likely due to the large volume and certain approximations made in the design and batching of the mixes themselves.

5.4.5. Restrained Shrinkage

In terms of AASHTO restrained shrinkage rings, there were five cast. For the trial slab, two rings were taken (one with FSGs only and one with FSGs and VWSGs). For the

HPC-b mix, two rings were taken with the same sensor arrangements. The last ring was taken from the pumped FR-HPC-b mix and only had FSGs. The procedure is in accordance with AASHTO PP 34. For simplicity in this section, the rings with only FSGs will be considered 'Ring 1', while the rings with FSGs and VWSGs will be considered 'Ring 2' in their respective sets. This only holds true to these specimens. The rings were cast in the field and transported back prior to the 24-hour mark. From there, the surface was promptly waxed to create a seal and the sonotube was cut removed from the rings. Shortly after this, the rings were placed in their final location and all of the sensors were wired into a series of CR1000s rigged to record the necessary data. The last step was the sealing of the bottom edge with silicon caulking compound.

Figure 5.9 Restrained Ring Set Up

From this point, the data was periodically collected and monitored for signs of cracking. The rings themselves were also periodically monitored for cracking. For a more detailed analysis, rigorous crack mapping was also performed on each ring at 28, 42, and 56 days. This crack mapping procedure is explained in section 3.4.6. This data is used to effectively compare the cracking tendencies across the different concrete mixes as well as giving us an accurate depiction of the crack density over time for both fiber reinforced and standard HPC mixes. The mixes are analyzed independently first before being compared to one another.

5.4.5.1. Trial Slab (FR-HPC-b) Rings

Two AASHTO rings were cast during the sampling from the trial slab pour below the bridge. One ring was set up with only FSGs while the other had FSGs and VWSGs. These results become not easily comparable because the bolts imbedded for the vibrating wires create stress concentrations and promote more cracking. The first ring viewed will be the FSG only ring. For this ring, only three of the strain gages were functioning properly. There are some similar issues in the ring strain gages for some of the other field samples. Some damage must’ve occurred to the gages while in the field. The strain data is as follows.

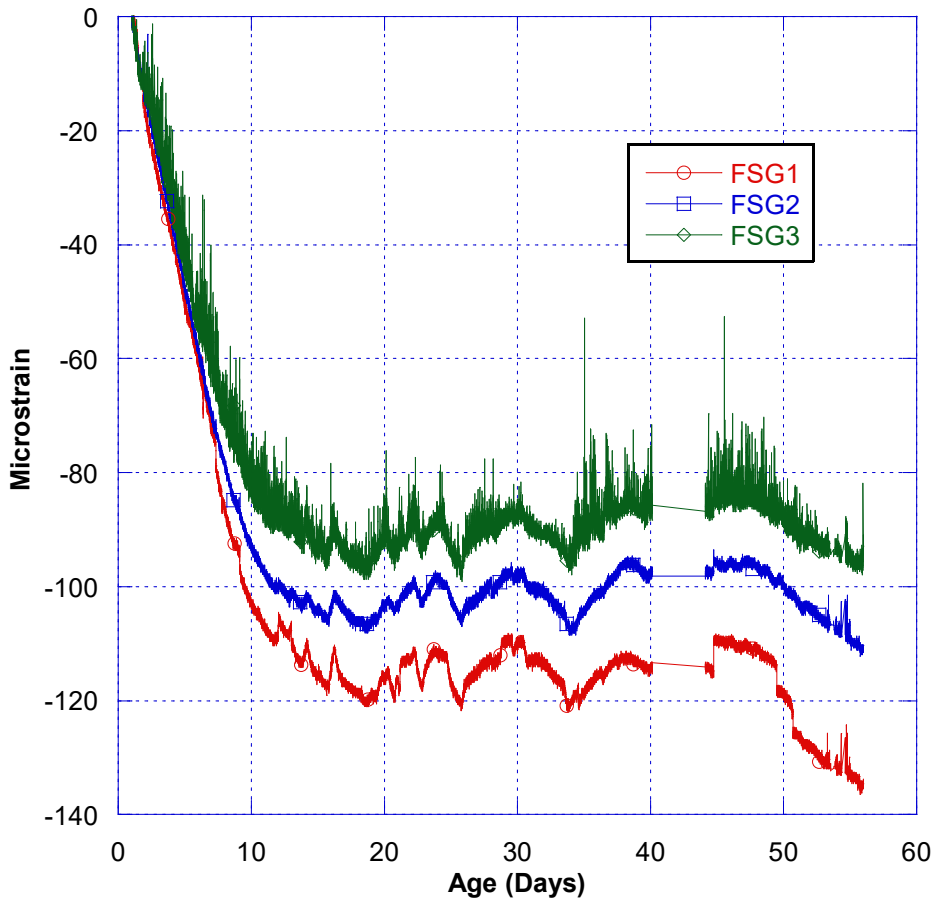

Figure 5.10 FR-HPC-b Ring #1 FSG Data

The strain data here shows no significant cracking of the specimen; however, we can assume that around 11 days micro cracks began to form based on the pattern of the data. Strain begins to essentially release at this point, at least in a small capacity, which points to the beginning of micro cracks. The specimen was also crack mapped at three separate time intervals (28, 42, and 56 days). The results are drawn on AutoCAD as a visual representation and the cracks are analyzed for crack density as well. These strain readings indicate no significant cracking (cracking across the entire plane) throughout the 56-day testing regime. They do however point to the formation of many micro cracks and

cracks that never fully propagated across the entirety of the material surface. The summation of these cracks, both visually and analytically, will occur below.

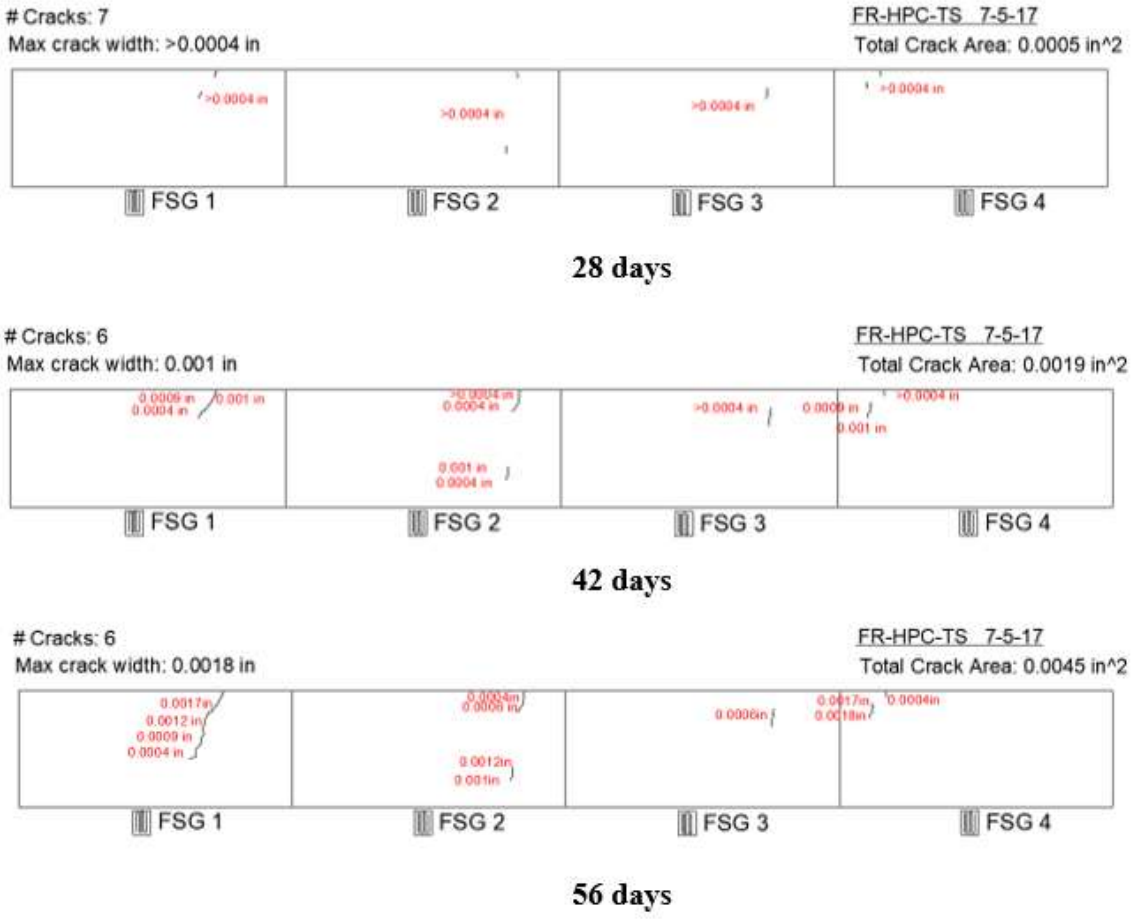

Figure 5.11 FR-HPC-b Ring#1 Crack Maps

At 28 days, the crack density was very minimal. All the cracks were extremely small, measuring less than .0004 inches with the microscopic camera. According to the strain data, larger jumps in strain (indicating larger cracks) occur after the 28-day marker. This is further proven in the 42-day crack map. At 42 days, there is a 280% increase in the crack area and therefore the crack density. No new cracking had formed at this point. Only widening occurred. The maximum crack width reached from <.0004 inches to .001 inches in multiple locations. From this point forward, the propagation rate of the cracks

appears to slow down significantly. After nearly quadrupling on the first-time interval, the crack area only increased by 137% between the second and third cycles. This correlates directly with how the free shrinkage strain behaves over time. The material begins to shrink at a lesser rate, causing the cracks to propagate at a slower pace. This data, along with the rest of the field ring data, will be revisited at the conclusion of this section in a comparative sense to deduce a relationship between the use of fibers and the mitigation of crack propagation.

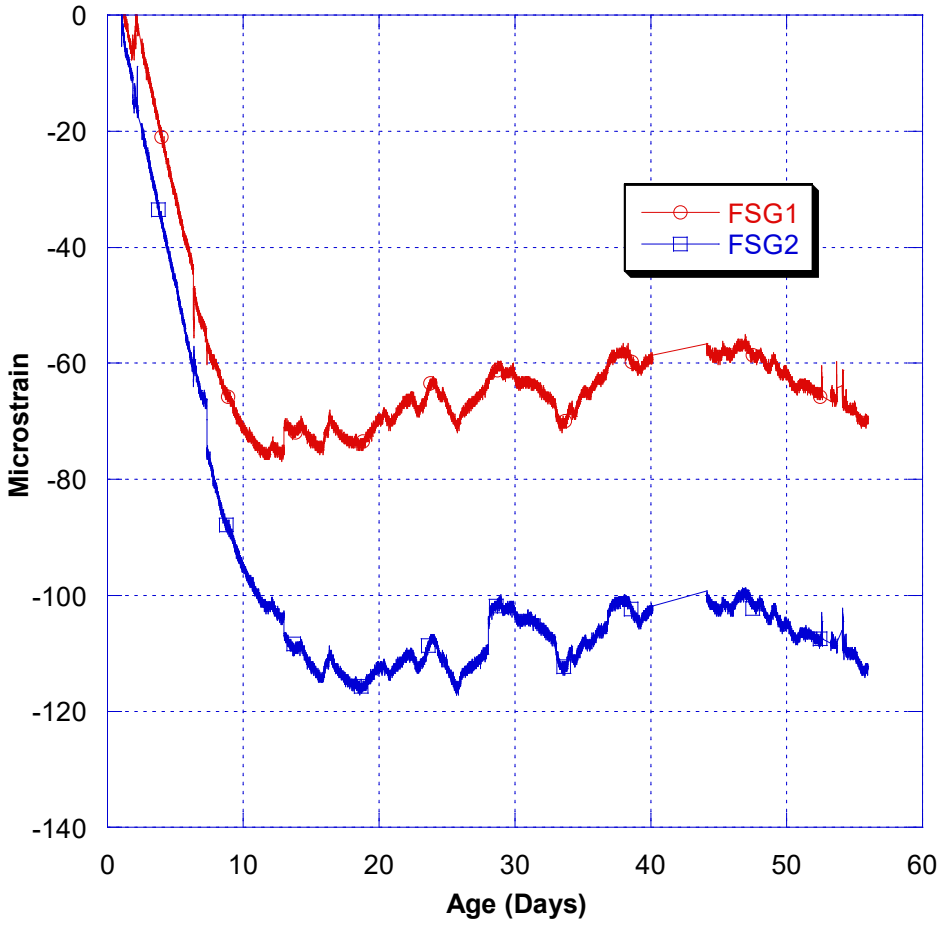

Figure 5.12 FR-HPC-b Ring#2 FSG Data

The strain data for ring #2 paints a similar picture to that created from the strain graphs of ring #1. The earliest signs for cracking (micro cracking) appear in the same time frame as the first ring, which makes sense seeing as they were from the same mix. The overall pattern of these strain gages is very similar to its counterpart. Micro cracking ensues at the 11-day mark and no significant cracking happens within the 56-day testing period. Unfortunately, the vibrating wire data from this set of rings was corrupted due to some temperature concerns and their volatility. The information collected from the strain gages and the crack map surveys will still be sufficient in establishing conclusions from the experimental work. The crack map survey results are as follows:

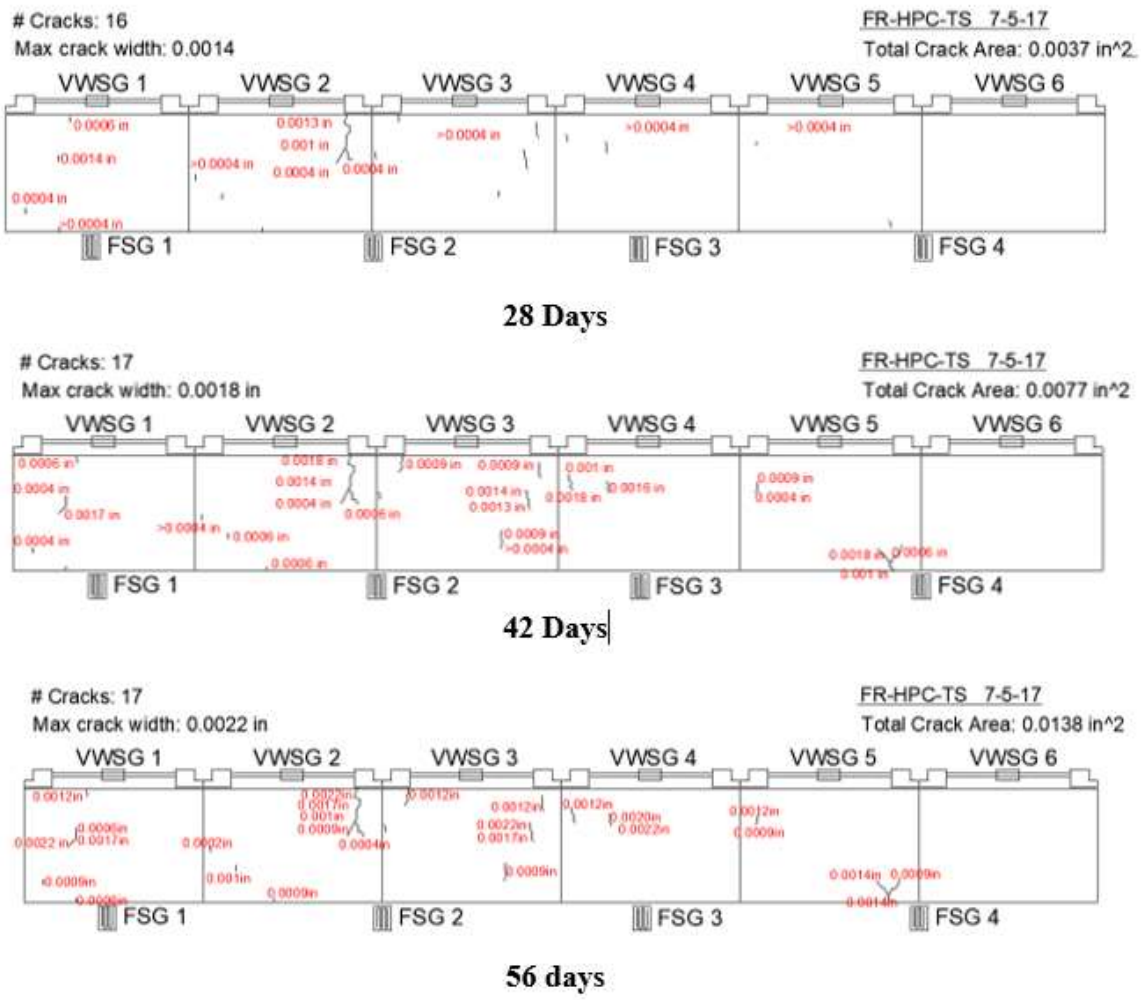

Figure 5.13 FR-HPC-b Ring #2 Crack Maps

The huge disparity in cracking area can be seen by comparing this ring to its counterpart without vibrating wires. At 28 days for the ring with vibrating wires, the crack area is already almost equivalent to that of the 56-day crack area for the ring without vibrating wires. There is also a large disparity in the number of cracks. Ring #1 of this set only had 6 cracks at 28 days, where ring #2 had 16 cracks. The difference in crack width is also drastic. At 28 days, the maximum for ring #1 was less than .0004 inches, whereas for ring #2 the maximum was .0014 inches. For these reasons, the rings with vibrating wires should not be compared to the rings without them. There clearly are

residual stresses being formed by the bolts which can induce more cracks with a faster growth rate.

5.4.5.2. HPC-b Rings

The second set of rings was taken from the slab #1 pour on the bridge. This mix was blended HPC. The mix was not pumped in this specific case. The same arrangement was used as the previous set of rings. There is one ring with only FSGs and one with both FSGs and VWSGs. The same disparity can be seen between the two rings. The rings with embedded bolts for VWSGs have a higher tendency of cracking due to the stress concentrations these bolts create. The results will be depicted in the same order as the previous set, with the FSG ring results being presented before the FSG and VWSG ring. The strain data for Ring 1 is as follows.

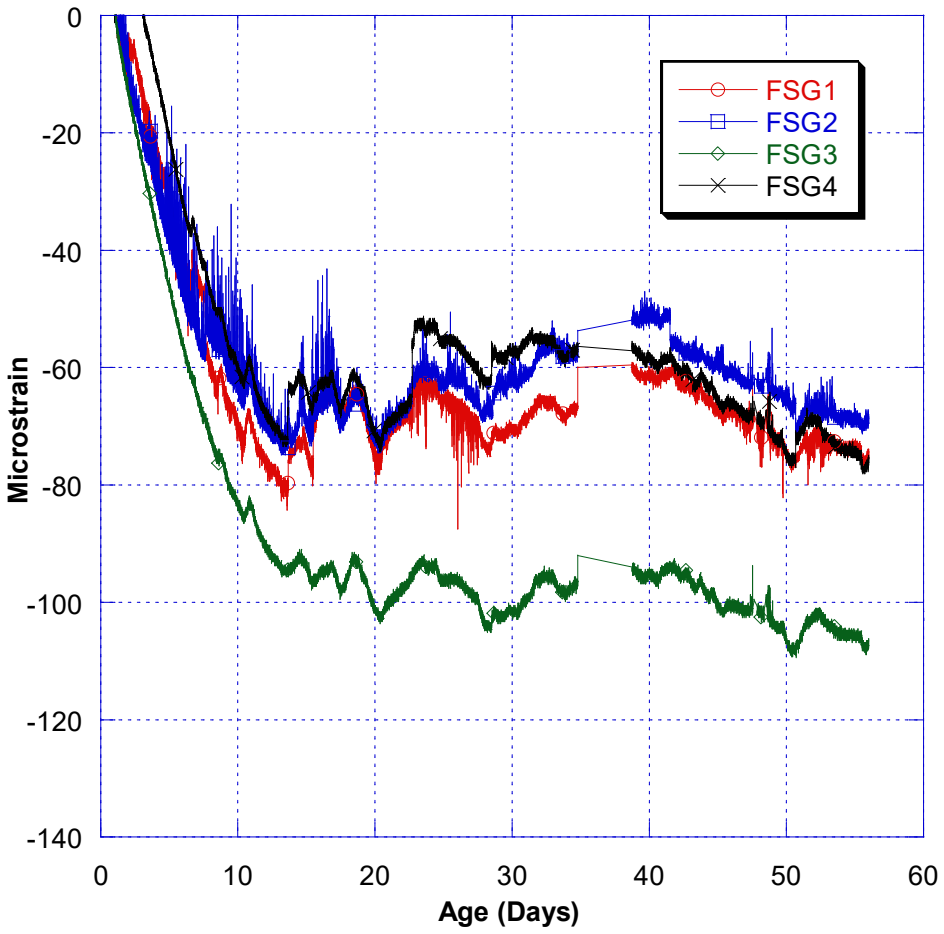

Figure 5.14 HPC-b Ring #1 FSG Data

For this set, there are subtle signs of cracking at 10 days, shortly before its FR-HPC-b counterpart. This again is only micro cracks, as the section did not fully crack during the 56-day monitoring period. Continuing from this point on, many micro cracks continue to form until the ending of the test period. The results also indicate more significant cracking in quadrants 1, 2, and 4. This is further reinforced by the crack map results, which show 0 cracks in the 3rd quadrant of the ring in question.

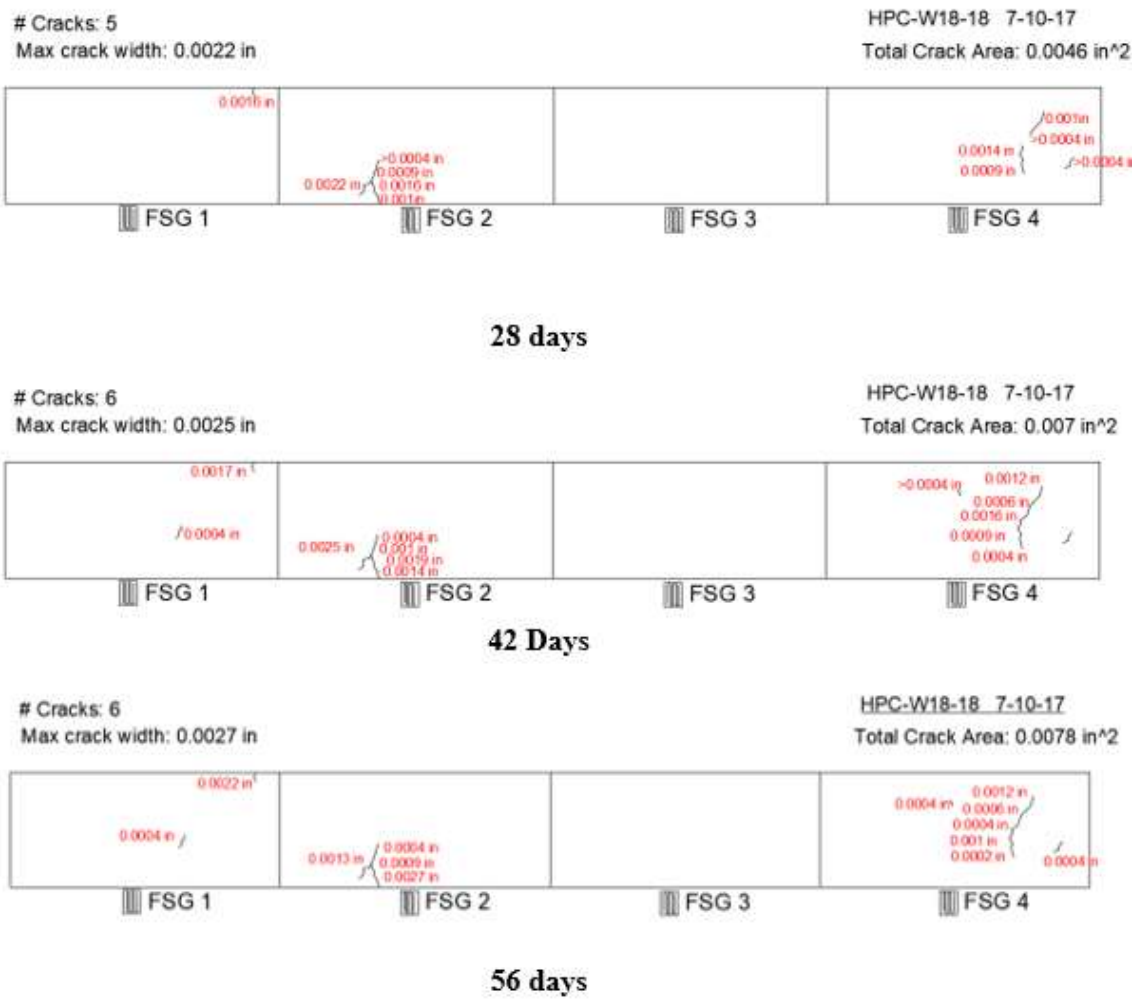

Figure 5.15 HPC-b Ring #1 Crack Maps

The cracking here is substantially larger than that seen from the previous FR-HPC-b ring. The difference is visibly large for both cracking area and maximum crack width. The overall comparison will come at the end of this section. Number of cracks is seemingly unaffected by the fiber addition. For Ring 1 of the HPC-b set, more initial cracking is seen at the 28-day mark, paired with a slower increase in both area and crack width when compared to its previous measurement. From day 28 to 42 there is a 45.8% increase in crack area, and from day 42 to 56 there is only an 11.4% increase in total crack area. This progression is clearly much slower than that of the FR-HPC-b; however,

the initial point of reference for the cracking area is significantly larger for HPC-b at 28 days.

Ring #2 for this subset was set up similar to ring #2 of the initial set, where both foil strain gages and vibrating wire strain gages were implemented. Again, this will lead to more significant cracking, but this mark can be easily compared to ring #2 of the first set. The strain data is as follows:

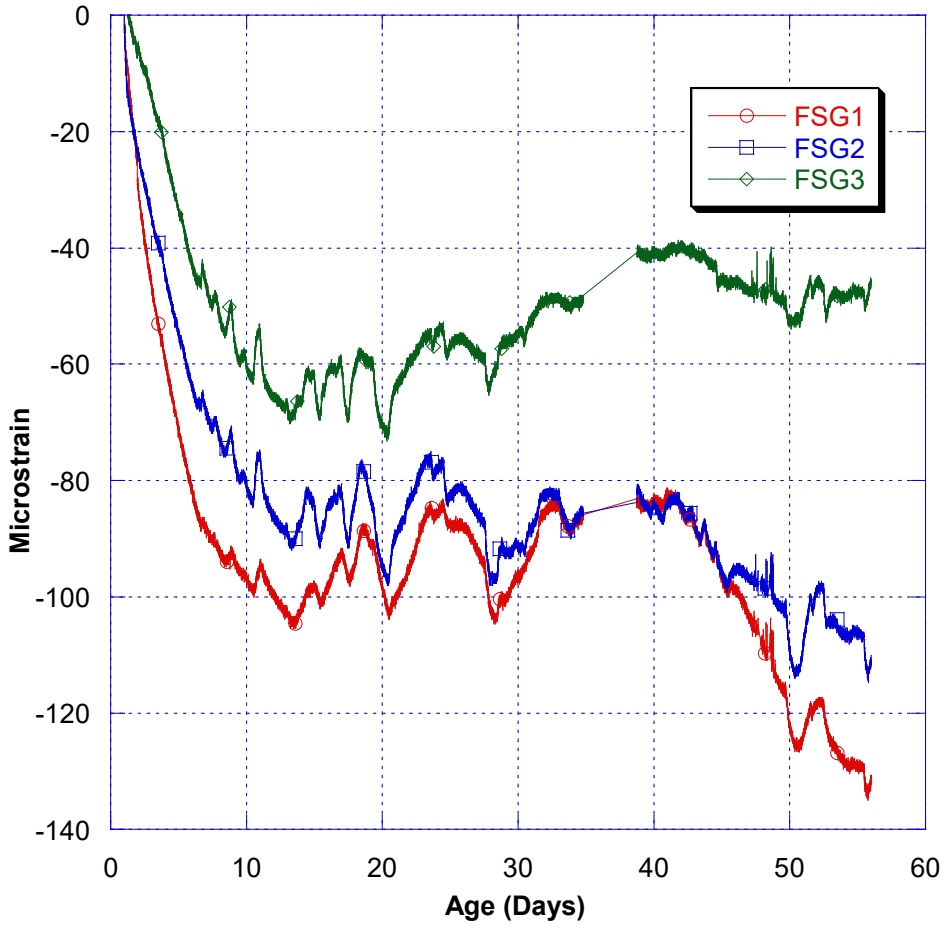

Figure 5.16 HPC-b Ring #2 FSG Data

Signs of cracking in this specimen can be seen slightly before its counterpart without vibrating wires. Initial signs appear at approximately 8 days in strain gages #1

and #2. Again, in this specimen, no full cracks were developed in the testing period. The cracking area over time can still be compared to other experiments of similar design. The most applicable comparison will be FR-HPC-b Ring #2 due to the similar use of vibrating wires and the noticeable difference in crack area that comes with them. Unfortunately, the vibrating wire data itself was corrupted due to temperature concerns, similar to ring #2 of the FR-HPC-b subset, and cannot be considered valid or applicable in defining a more effective equation for relating the strain experienced by the steel to the concrete strain. The crack maps will be shown here and the data will be appropriately compared after all of the rings have been individually analyzed.

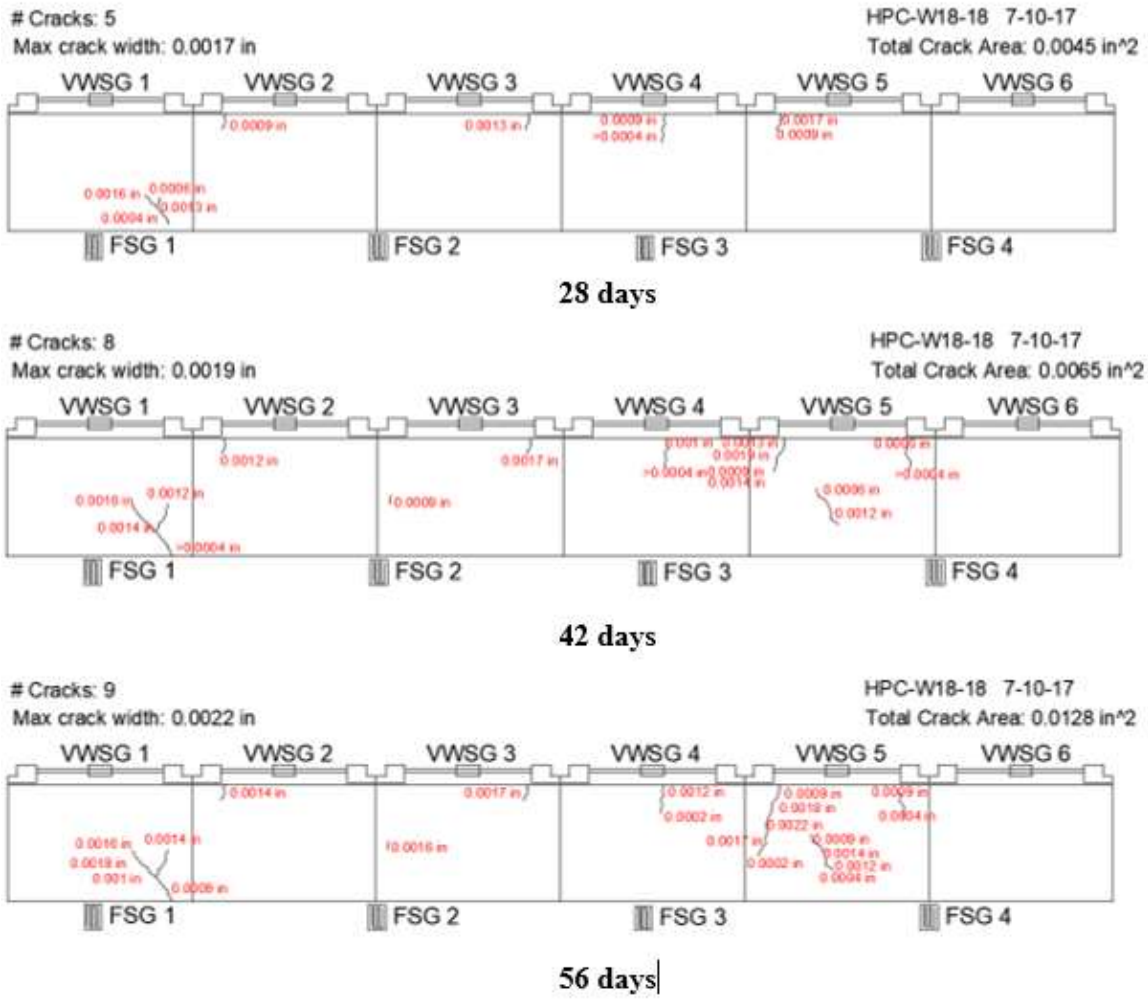

Figure 5.17 HPC-b Ring #2 Crack Maps

The pattern here remains similar to the last time a ring with a vibrating wire set up was compared to one without it. There is a significant increase in cracking area, crack width, and number of cracks, although the difference in number of cracks is less significant here than the previous comparison. Another viewpoint can be established when looking at the HPC-b Ring #2 and comparing it to FR-HPC-b Ring #2. The FR-HPC-b sample shows more cracks and more cracking area, but the maximum crack width remains similar in both samples. This will be shown in more detail later.

5.4.5.3. FR-HPC-b (Pump) Ring

The last ring from the field will be a singular FR-HPC-b ring cast from a pump being monitored by only foil strain gages. This ring was taken to attempt to see if there is a difference in cracking potential when these mixes are pumped instead of pouring from a chute. The mix needs to be considered applicable for both pumping and pouring from a chute for ease-of-use purposes. All things considered, a similar result to FR-HPC-b ring #1 will be the optimal result. This would prove no difference between the two application methods. This ring was cast exactly one week after the ring it will be compared to, and was kept under the exact same curing conditions to ensure an equal and appropriate comparison. The strain data is as follows:

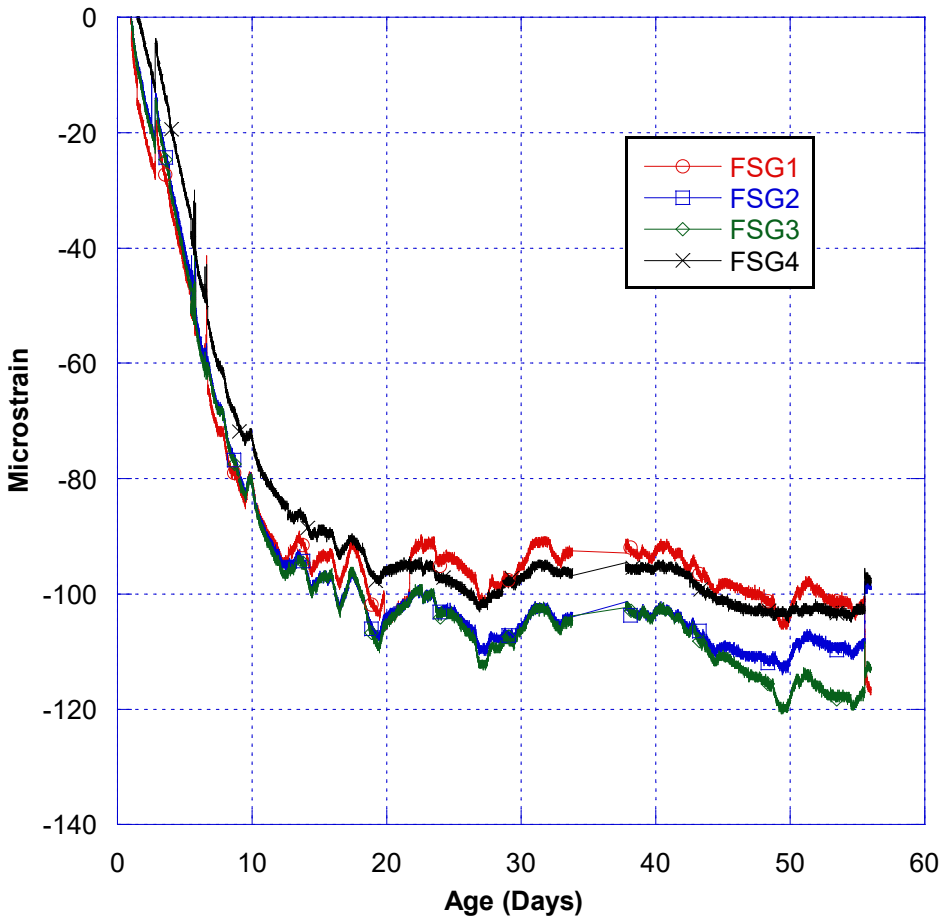

Figure 5.18 FR-HPC-b (Pump) Ring FSG Data

The average strain pattern here is similar to the FR-HPC-b ring poured from a chute. The average strain overtime and the first sign of initial cracking occur at approximately 11 days, just like its counterpart. In this case however, cracking is not observed until after the 28-day mark. It should be noted that the strain pattern here is much more consistent from gage to gage than the not pumped ring, but that could be caused by several factors. These signs alone aren't enough to completely verify the applicability of the mix if pumped, so a further look into the cracking tendencies will also occur and be analyzed. Again, no full cracks were developed in the sample. The

maximum crack width, crack area, and number of cracks will instead be compared. The crack map survey results are as follows:

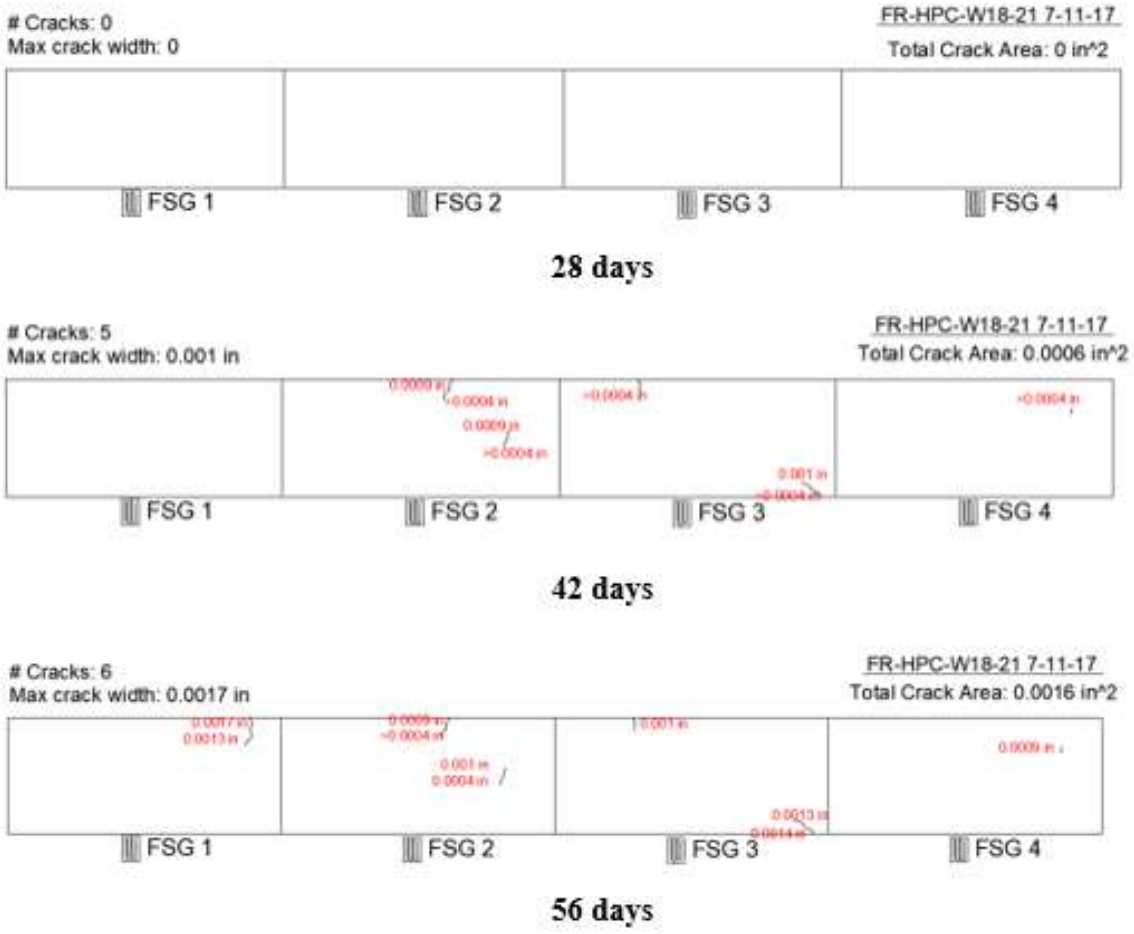

Figure 5.19 FR-HPC-b (Pump) Ring Crack Maps

The interesting thing about this set of surveys was the fact that 0 cracking had occurred at the 28-day mark. This prompted a second crack mapping survey to occur, which again produced the same result. By the 56-day mark, the number of cracks and the crack width were practically equivalent between this sample and the FR-HPC-b Ring #1. The major difference came in crack area. The ring poured from the chute accrued three

times the total amount of crack area. Taking these things into consideration, it can and should be concluded that this mix can be pumped without any issues regarding crack potential.

5.4.5.4. Comparison

The comparison here will primarily focus on the restrained rings without vibrating wires, as each set can be included in this comparison. This will provide the most accurate depiction of the effects fibers have on the cracking potential of HPC. Simple tables and graphs will be provided to effectively represent the differences of the samples in question. First, the crack area over time will be tabulated and graphically represented for the three rings without vibrating wires.

Age	*FR-HPC-b Ring #1*	*HPC-b Ring #1*	*FR-HPC-b (Pump) Ring #1*
28	0.0045	0.0456	0.0000
42	0.0187	0.0702	0.0063
56	0.0446	0.0776	0.0159

Table 5.5 Total Crack Area Comparison

This comparison can provide a plethora of information. The difference in tendencies is drastic, and obvious issues of consistency can be assumed. When mixing in the field, no mix is ever going to be perfect. Therefore, a disparity can be seen between the two field FR-HPC-b mixes. This could be because of any number of human errors, inconsistencies in the weather, casting errors, etc. The overall trend seen is more apparent, and it is the fact that the fiber additions have a significant reduction effect in terms of cracking area by more effectively reducing the crack propagations. Each ring experienced a similar number of cracks, but the propagation of the HPC-b cracks was clearly more significant. The cracking area of HPC-b Ring #1 shows a 156.5% increase over the average between the two FR-HPC-b rings from the field mixes at 56 days. The

difference is even more drastic at earlier ages. The variations against time are also depicted in the following graph.

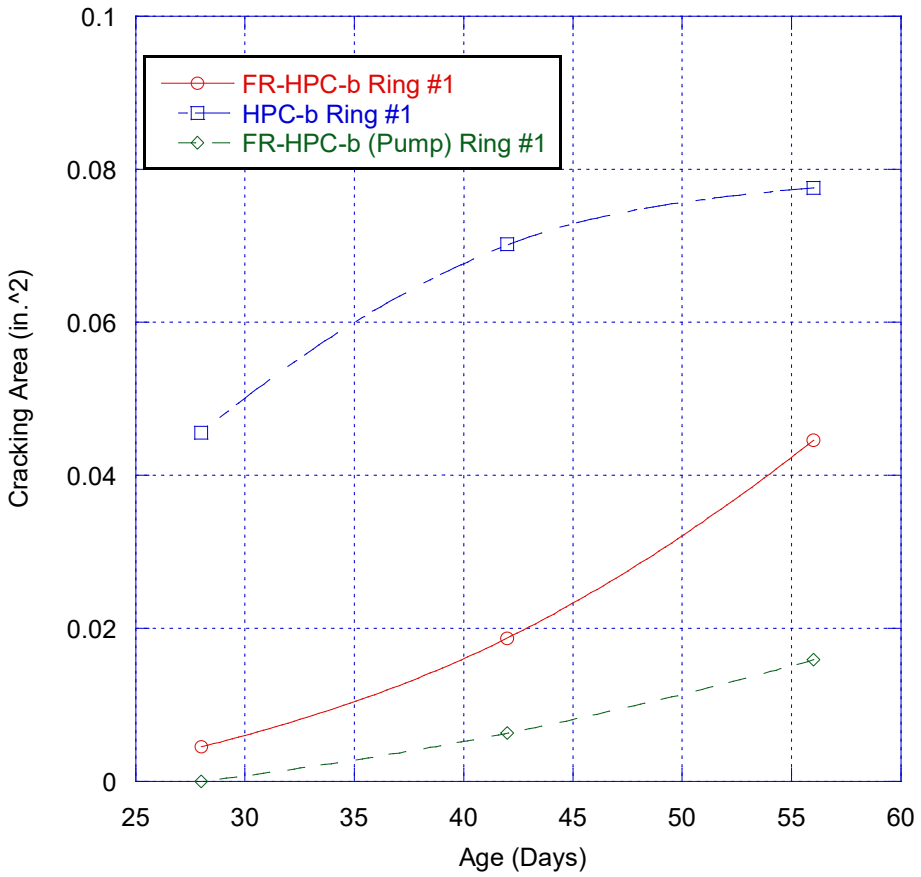

Figure 5.20 Cracking Area versus Time (Field)

The graphical representation helps to show the drastic difference that synthetic macro fiber additions appear to make in terms of the crack density of the individual samples. It also would appear that crack density begins to increase earlier in HPC-b mixes based on the graph. This is the opposite of what was experienced in the lab work, where the fibrous mixes experienced higher cracking at earlier ages and did not propagate as fast as what was seen in the base mixes. This could be further researched by crack mapping samples at further time intervals (90, 120, 180, etc.) to detect more of a pattern

indicative of long term restrained shrinkage cracking of the samples in question. In terms of the time period these samples were monitored, macro fiber reinforcement shows immense promise. Crack width and crack area are both seen to be reduced, while any adverse effects from the additions appear negligible from the given results.

Age	*FR-HPC-b*	*HPC-b*	*FR-HPC-b (Pump)*
28	6	5	0
42	6	6	5
56	6	6	6

Table 5.6 Number of Cracks per Ring

Less variation can be seen when comparing the number of cracks in this section. The one notable difference is that FR-HPC-b had zero visible cracks at 28 days. The difference from these rings cannot be linked to a variation in the number of cracks.

Age	*FR-HPC-b*	*HPC-b*	*FR-HPC-b (Pump)*
28	.0004	0.0022	0.0000
42	.0010	0.0025	0.0010
56	.0018	0.0027	0.0017

Table 5.7 Maximum Crack Width (in.)

Maximum crack width appears to show a similar trend. Both fiber mixes show a significant improvement in maximum crack width at 56 days. It is even more pronounced than the work in the lab, with reductions of 33.3% and 37.0% respectively. This difference as a large effect on the overall outcome when looking at the cracking area of these specimens.

5.4.6. Rapid Chloride Permeability and Surface Resistivity

Rapid Chloride Permeability and Surface Resistivity Testing were done for the simple reason of seeing the effects these macro synthetic polypropylene fibers will have on the permeability of the concrete. The results are depicted in the following table.

SRT				
Age	**FR-HPC-b**	**HPC-b**	**FR-HPC-b (Pump)**	**HPC-b (Pump)**
7	9.8	11.7	9.7	9.5
14	17.1	23.9	20.8	16.9
28	25.5	39	30.3	24.8
56	39.8	61.1	45.4	36.4
RCPT				
28	1657	1020	1301	1962
56	1023	566	1191	1287

Table 5.8 SR and RCPT Results

In terms of surface resistivity, a higher result is indicative of a lower permeability. The mixes will be compared in pairs. For the mixes that weren't pumped, the FR-HPC-b shows significantly more permeability than the HPC-b, but it is still well within the guidelines for use under these circumstances. The pumped mixes were extremely similar in result, with the FR-HPC showing slightly less permeability than the HPC-b. The pumping of the mixes however did cause a slight issue in terms of permeability. The limit for RCPT is set at 1100 coulombs and was slightly eclipsed by both pumped mixes**.** The FR-HPC-b results are negligible in difference from not pumped to pumped, while there is a significant jump in the HPC-b mixes in question. This again points to issues with the mix or the sampling thereof for the pumped HPC-b.

5.4.7. Crack Mapping

One of the last steps for this evaluation was returning to the field to physically crack map the decks poured by hand to verify the results. This procedure was done with the help of half a dozen graduate and undergrad students, seeing as over 12,000 square feet was to be surveyed. There were eight separate spans to be considered in total. Each pour alternated between fiber and no fiber. The number of cracks and crack width were the most important things taken into consideration. The crack mapping in this case was

performed at two separate ages, while the adjacent lanes remained open and loaded. The first set of mapping was completed by an outside contractor at the ages of 20-25 days. The second set of mapping was completed by Rutgers at 33-43 days. In terms of the physical number of cracks, there is not much difference to be seen between the findings for HPC-b and FR-HPC-b. If anything, the FR-HPC-b has a slight advantage in the number of cracks at the given ages. The following table gives some insight in terms of the number of total cracks observed, and the findings in terms of crack width and area will be summarized after.

Str. #	Span	Concrete Mix	Date Poured	Outside Contractor		Rutgers	
				Age (days)	# of Cracks	Age (days)	# of Cracks
N2.01	Slab #1	**HPC**	7/10/17	**23**	44	**43**	58
N2.02	Slab #2	**FR-HPC**	7/11/17	**22**	41	**42**	50
N2.03	Slab #3	**HPC**	7/12/17	**21**	39	**41**	47
N2.04	Slab #4	**FR-HPC**	7/17/17	**21**	42	**36**	48
N2.05	Slab #5	**HPC**	7/18/17	**20**	56	**35**	60
N2.06	Slab #6	**FR-HPC**	7/19/17	**19**	40	**34**	40
N2.07	Slab #7	**HPC**	7/20/17	**25**	43	**33**	44
N2.08	Slab #8	**FR-HPC**	7/25/17	**21**	34	**28**	36
Crack Severity (length = 200 ft per 3-span)		**HPC**		182 cracks 0.23 crack/LF		209 cracks 0.26 crack/LF	
		FR-HPC		157 cracks (13.7% reduction)		174 cracks (16.7% reduction)	

Table 5.9 Field Crack Survey Summary

The number of cracks is inherently less important that the maximum and average crack width and the overall crack density for these slabs. In terms of the crack widths, a clear majority of cracks found in the FR-HPC-b slabs were smaller in size than the cracks seen in HPC-b slabs. This is also reflected and amplified when comparing the crack densities of the comparable slabs in question. This information will be looked at in much more detail in the following pages.

Span (Mix) H**PC or** F**R-HPC**	**Age (days)**	**Mean**	**Std.**	**Max**	**Min**
Slab #1(H)	43	0.019	0.005	0.030	0.010
Slab #2(F)	42	0.015	0.006	0.030	0.005
Slab #3(H)	41	0.014	0.015	0.090	0.005
Slab #4(F)	36	0.009	0.008	0.050	0.005
Slab #5(H)	35	0.008	0.005	0.016	0.001
Slab #6(F)	34	0.009	0.010	0.060	0.004
Slab #7(H)	33	0.008	0.002	0.012	0.004
Slab #8(F)	28	0.007	0.002	0.010	0.004
All HPC	**-**	**0.012**	**0.009**	**0.090**	**0.001**
All FR-HPC	**-**	**0.010**	**0.008**	**0.060**	**0.004**

Table 5.10 Field Crack Width Statistical Data (Positive Moment Region)

Span (Mix) H**PC or** F**R-HPC**	**Age (days)**	**Mean**	**Std.**	**Max**	**Min**
Slab #1(H)	43	0.015	0.004	0.020	0.010
Slab #2(F)	42	0.015	0.004	0.020	0.010
Slab #3(H)	41	0.009	0.002	0.015	0.005
Slab #4(F)	36	0.005	0.003	0.010	0.001
Slab #5(H)	35	0.012	0.004	0.016	0.002
Slab #6(F)	34	0.006	0.002	0.010	0.003
Slab #7(H)	33	0.006	0.002	0.010	0.004
Slab #8(F)	28	0.006	0.002	0.010	0.004
All HPC	**-**	**0.011**	**0.005**	**0.020**	**0.002**
All FR-HPC	**-**	**0.009**	**0.005**	**0.020**	**0.001**

Table 5.11 Field Crack Width Statistical Data (Negative Moment Region)

The previous tables detail the mean, standard deviation, maximum and minimum crack widths for each slab at the time the crack mapping surveys were performed. The tables are split into the positive moment areas and negative moment areas because of the continuity of the deck. Comparing the two regions separate instead of simultaneously is more appropriate. The results verify that cracks forming in the FR-HPC decks remain smaller than the cracks forming in HPC decks on average. This information however can only tell you some much. Histograms were also created for both moment regions to show a distribution of cracks in terms of width.

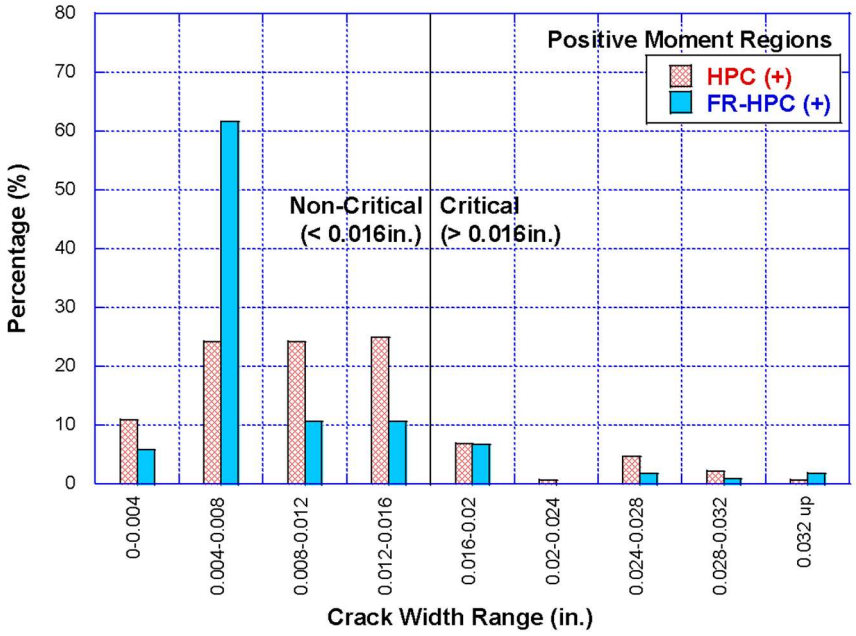

Figure 5.21 Crack Width Histogram (Positive Moment Region)

Critical cracks are defined by ACI Building Code 318 at 0.016 inches. Setting this minimum and looking at the histogram clearly shows a more significant proportion of HPC-b cracks being above the limit and close to the limit, while more than 60% of the cracks found in the FR-HPC decks are 50% of the width limit or less. The 33.3% reduction in maximum crack width, 16.7% reduction in average crack width, higher

proportion of smaller cracks, and the comparative percentage of critical cracks all point to FR-HPC mixes leaving a significant positive effect on transverse bridge deck cracking in positive moment regions.

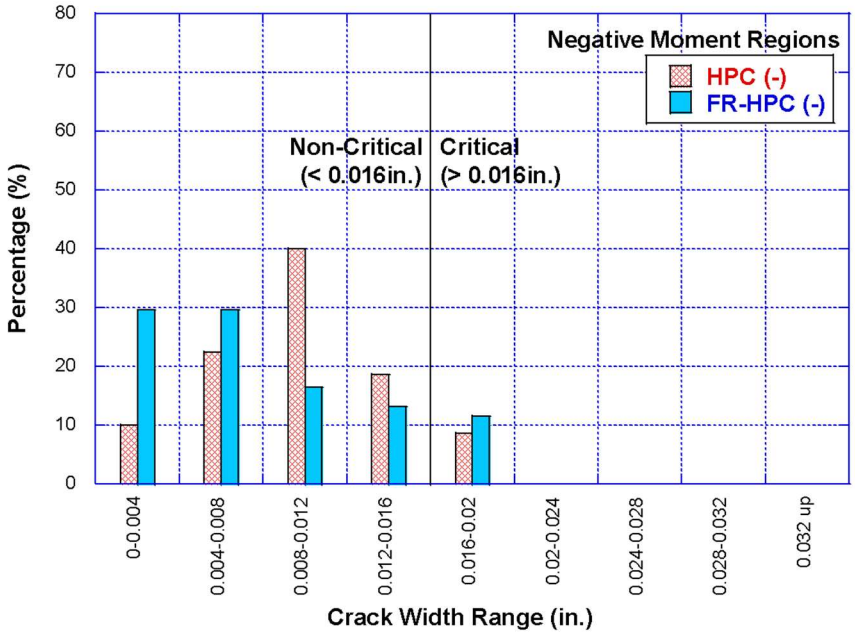

Figure 5.22 Crack Width Histogram (Negative Moment Region)

Displaying the cracks located in negative moment regions in the same format as positive moment regions shows us that the FR-HPC has a similarly skewed effect on the crack width data. While the crack width distribution remains relatively normal for the HPC deck area, The FR-HPC data is clearly heavily skewed to the right. While there is no reduction in the maximum crack widths from these regions (both showed cracks at 0.02 inches in width), the average crack width is still decreased by 18.2% for the fibrous sections of the deck. Overall, the fibers have a more tangible effect in the positive moment regions on the propagation of cracks. While less drastic in the negative moment regions, the skew presented in the histogram along with a reduction in the average still show some positive effects for fiber reinforcement.

The last comparison to be made will be made in a broader sense, and will look at the overall cracking area and cracking intensity for all the decks in question. Crack area will be taken as the mean crack width multiplied by the number of cracks. Cracking intensity is defined as the cracking area divided by the total surface area, or in this case, the bridge deck area. The results show a 16.7% reduction in total number of cracks, a 16.7% decrease in the average width of said cracks, no significant length difference, a 33.4% reduction of both cracking area and intensity.

	No. of Cracks	**Mean Crack Width (in.)**	**Mean Crack Length (ft.)**	**Cracking Area (in^2)**	**Cracking Intensity (in^2/ft^2)**
HPC	209	0.012	5.85	171.3	0.027
FR-HPC	174 (-16.7%)	0.010 (-16.7%)	5.89 (+0.7%)	114.1 (-33.4%)	0.018 (-33.4%)

Table 5.12 Cracking Area and Intensity

6. Summary and Conclusions

The effects of introducing fiber to approved HPC mixes in an effort to reduce the cracking potential of these mixes when applied as bridge decks was analyzed in two steps. In the lab, a total of seven mix designs were tested. These designs include HPC, HPC-b, FR-HPC, three FR-HPC-b variants with different fibers, and class A. The mixes were tested for compressive strength, tensile strength, modulus of elasticity, shrinkage with a dry cure, shrinkage with fourteen days of curing, permeability, surface resistivity, and restrained shrinkage. The second phase of this experiment involved the implementation of said mixes in field. Alternating decks of HPC-b and FR-HPC-b were poured along the southbound shoulder of a prominent bridge in New Jersey. These three span continuous slabs were cast and samples were taken to test the same set of parameters that were tested for in the laboratory portion of this trial. The field work also included the crack mapping of the physical decks over time. Eight three span continuous slabs were crack mapped simultaneously by a group of graduate students, and the data was further analyzed to strengthen any conclusions to be made. The results will be summarized in bullet points below.

In the laboratory portion of this experiment, the following conclusions can be made:

- The blend of aggregates used reduced compressive strength by 13.6%. Fiber implementations also resulted in a reduction of compressive strength ranging from 3.3% to 14.9%.

- When looking at tensile strength, aggregate blending resulted in a 13.2% improvement over HPC. The combination of blending and fiber additions also resulted in a net improvement over HPC ranging from 2.1% to 6.9%. A variation in failure mechanisms is also noted. Fiber reinforced concrete has the ability to hold a residual load for an elongated period of time while plain concrete fails more abruptly.
- Modulus of Elasticity was not affected by the blending used. Fiber additions did decrease the modulus of elasticity in the range of 2.9 to 8.3%.
- Shrinkage samples cured for 14 days display the desired effects additions made. Blending resulted in a reduction by 16.1% while fiber additions further reduced shrinkage by up to 11.5%. Euclid 2" fibers show the best shrinkage results when the samples are cured for 14 days.
- Shrinkage samples that did not undergo any further curing show negligible differences when looking at the effects of blending. The synthetic Sika fibers show minimal reduction as well. Sika steel fibers show a 23.6% reduction in shrinkage when the samples are not cured and Euclid PPE fibers help reduce the shrinkage by 11.0%
- Permeability and resistivity is only a concern when it comes to the mixes which include steel fibers. This permeability concern should be addressed before any further implementation.
- AASHTO restrained rings provide a relative comparison of the mixes cracking potential. The blending of aggregates shows a negligible difference in total cracking area (+2.5%) when compared to HPC, but it also shows a

10.7% reduction to the maximum crack width at 56 days. Euclid 2" PPE Macro fibers provided a 31.2% decrease in cracking area when implemented in the not blended mix and a 23.2% reduction in total area and 12% reduction in maximum crack width when used in the blended mix design. Sika steel fibers provided a 26.3% reduction to cracking area and 8% reduction to the maximum crack width when compared to HPC-b. Sika synthetic fibers only provide a 4.8% reduction in cracking area at 56 days.

In the field portion of this experiment, the following conclusions can be made:

- Undocumented additions to promote pumping of mixes can cause a disparity in the strength and durability properties of concrete if not approached carefully.
- Compressive strength is reduced by 3.3% when fibers are implemented in the poured set of mixes. The opposite shows for the pumped mixes. This could be a result of said undocumented additions. Pumping also reduced the strength of each concrete variant. FR-HPC-b was reduced by 8.8% while HPC-b was reduced by 18.2%.
- The addition of fiber reinforcement promoted a 15.1% reduction in tensile strength. Pumping negatively affects the HPC-b mix, resulting in a 21.8% reduction in tensile capacity. Pumping shows little to no effect when comparing the FR-HPC-b results.
- FR-HPC-b shows a 14.9% reduction in modulus of elasticity to HPC-b. FR-HPC-b shows little difference when pumped or poured while HPC-b experienced a 15.3% decrease in modulus of elasticity.

- FR-HPC-b, HPC-b, and FR-HPC-b all performed relatively similar in terms of free shrinkage when cured properly.
- When analyzing the results from the AASHTO restrained rings, a higher disparity of results is observed than what was seen in the lab. Certain influences in the field reinforce the effectiveness of fiber implementation. Reductions in total cracking area of 42.5% for poured FR-HPC-b and 79.5% for the pumped FR-HPC-b were observed at 56 days. There was also a significant decrease in the maximum crack with. FR-HPC-b showed a 33.3% improvement while the pumped FR-HPC-b shows a reduction of 37.0%. The pumped FR-HPC-b offers better results than the poured. This is likely due to a combination of similar tensile strength, slight improvements to shrinkage, reduction of the modulus of elasticity, and a reduction in compressive strength
- Crack mapping of the 8 bridge decks in question shows a positive effect in both the negative and positive moment regions. Overall, a reduction of 16.7% to the number of cracks, a 16.7% decrease in average maximum crack width and a reduction of 33.4% to total cracking area and cracking intensity at the time of crack mapping.

Lastly, a comparison will be forged between the field and lab results in terms of the cracking potential observed from the AASHTO restrained rings. When overlaying both sets of results for total cracking area, the following graph is formed.

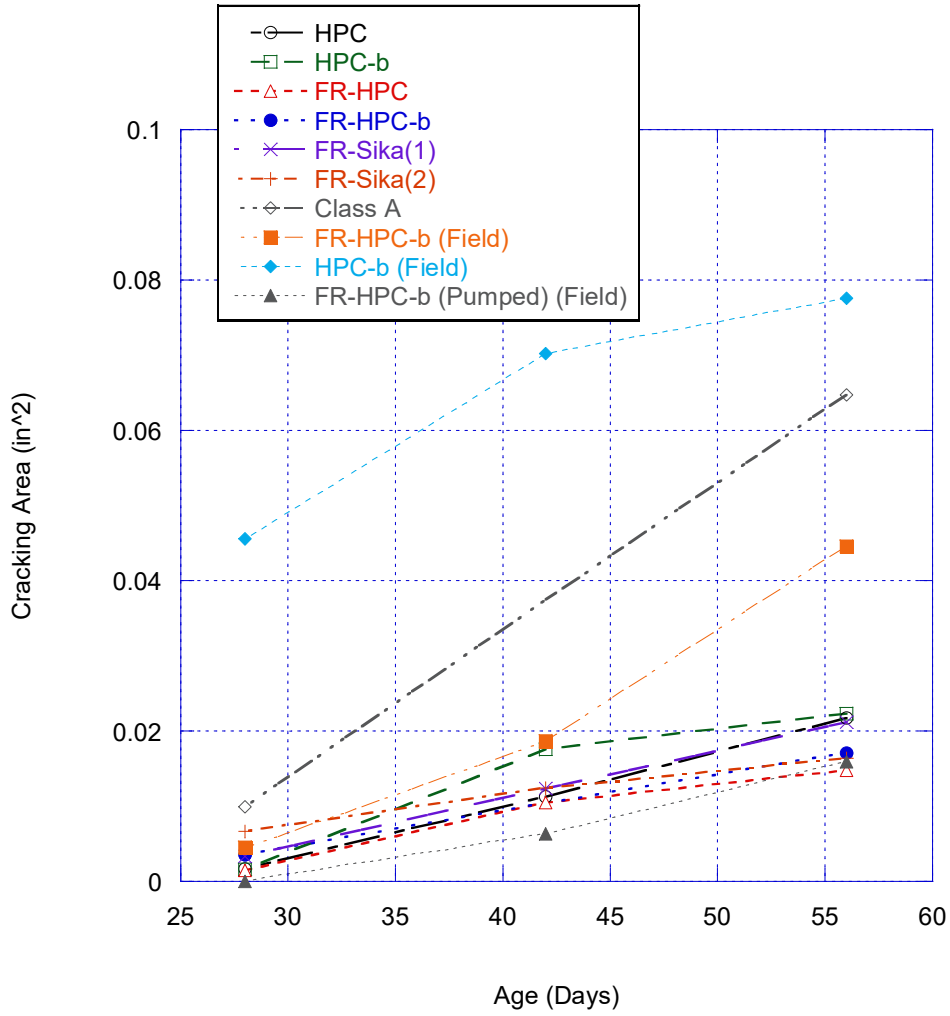

Figure 6.1 Field vs Lab Cracking Area Comparison

The field rings clearly experienced more cracking on average than the rings cast in the laboratory. This could be due to the influences from the ambient conditions where the samples remained in the field, the uncertainties and approximations made in construction, or the inconsistencies in mix designs. In terms of cracking area, the mixes from the lab and the field do not align. The field mix designs overall saw a lower water:cement ratio. The pumped FR-HPC-b ring does however show a similar result to the FR-HPC-b ring from the lab portion of this experiment. The undocumented additions made to this mix appear to have caused its result to mimic the lab result very closely.

Maximum crack width is the most appropriate facet in which this comparison can be made from field to lab. The size of the cracks is the most important factor when corrosion is involved. Smaller cracks result will result in less of a corrosion effect over time. The data is as follows:

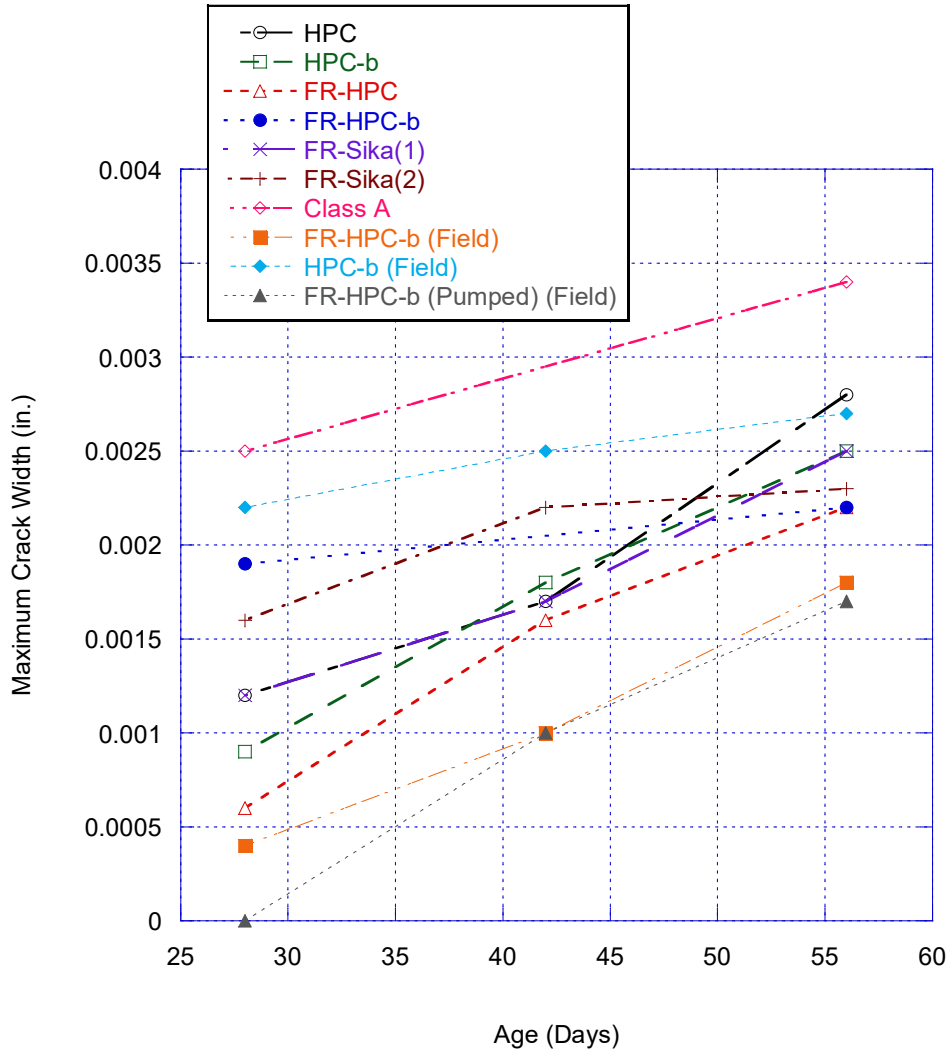

Figure 6.2 Field vs Lab Maximum Crack Width Comparison

Even with the disparity seen in cracking area between the field and laboratory mixes, a clear conclusion can be made when observing the maximum crack widths for fiber mixes. Blended HPC resulted in maximum crack widths of 0.0025 inches to 0.0027

inches for the lab and field mixes, while Euclid 2” PPE macro fiber implementation resulted in maximum widths ranging from 0.0017 inches to 0.0022 inches. Through the 56-day mark, fibers clearly have a resounding positive effect on reducing maximum crack width regardless of being tested in the lab or in the field.

Fiber additions have proven their effectiveness throughout this experimentation. Their inherent reduction of both compressive strength and modulus of elasticity paired with the post cracking behaviors observed all culminate to the final result. Both the steel hooked fibers and the Euclid PPE macro fibers proved immensely effective in the reduction of cracking area and crack width. Further into this topic should include the variation of both fiber concentrations, fiber lengths, and fiber types. Each of these variables can greatly affect the outcome. In order to optimize a design to mitigate crack propagation, all avenues should be explored. Fiber hybridization should also be explored. Micro fibers are known to positively influence shrinkage strain. Pairing these fibers with a mix that has already proven its positive influence on cracking could further improve the results. A study should also be conducted on a longer schedule. This crack mapping only occurred up to 56 days, and at this point some trends can be seen. Monitoring the progress past this mark can lead to further insight on the long-term effects of fiber additions. This holds true for both the restrained rings and the decks already placed.

7. Bibliography

Aitcin, P.C., *High Performance Concrete*, Modern Concrete Technology 5, p. 22-29, 2004.

Adi Abu-Obeidah, Hani Nassif, Chaekuk Na, Jean Laird and Scott Johnsen, *Application of the Maturity Method in Predicting Concrete Strength in Early Age,* Transportation Research Board 95th Annual Meeting Compendium of Papers, 2016.

Benjamin A. Graybeal, and Turner-Fairbank Highway Research Center. *High Performance Concrete Bridge Deck Investigation*. McLean, VA: U.S. Dept. of Transportation, Federal Highway Administration, Research, Development, and Technology, Turner-Fairbank Highway Research Center, 2009.

Ei-ichi Tazawa, Autogenous Shrinkage of Concrete, Proceedings of the International Workshop organized by Japan Concrete Institute, 1998.

Faisal Fouad Wafa, *Properties and Applications of Fiber Reinforced Concrete*, JKAU: Eng. Sci., Vol. 2, pp. 49-63, 1990.

F. H. Wittmann, *Creep and Shrinkage Mechanisms,* Creep and Shrinkage in Concrete Structures, Chapter 6, 1982.

G.L. Guerrini, *Applications of High-Performance Fiber-Reinforced Cement-Based Composites*, Applied Composite Materials V. 7, pp. 195-207, 2000.

Hakan Bolat, Osman Simsek, Mustafa Cullu, Gokhan Durmus, and Omer Can, *The Effects of Macro Synthetic Fiber Reinforcement Use on Physical and Mechanical Properties of Concrete,* Composites: Part B 61, p. 191-198, 2014.

Indrajit Ray; Zhiguo Gong; Julio Davalos; Arkamitra Kar, *Shrinkage and Cracking Studies of High Performance Concrete for Bridge Decks,* Construction and Building Materials, Vol. 28, Issue:1, p. 244-254, 2012.

J. Saliba, E. Roziere, F. Grondin, A. Loukili, *Influence of shrinkage-reducing admixtures on plastic and long-term shrinkage*, Cement Concrete Composites 33, p. 209-217. 2011.

J. L. Granju and S. Ullah Balouch, *Corrosion of Steel Fibre Reinforced Concrete from Cracks*, Cement and Concrete Research 35, p. 572-577, 2005.

James L. Sheard, *Fiber Reinforced Concrete,* US Patent N. US3616589A, November 1971.

Kevin J. Folliard and Neal S. Berke, *Properties of High Performance Concrete Containing Shrinkage Reducing Admixture*, Cement and Concrete Research, Vol. 27, pp. 1357-1364, 1997.

Marco di Prisco, Giovanni Plizzari, and Lucie Vandewalle, *Fiber Reinforced Concrete: New Design Perspectives*, Materials and Structures 42 pp. 1261-1281, 2009.

Menashi D. Cohen, Jan Olek and William L. Dolch, *Mechanism of Plastic Shrinkage Cracking in Portland Cement and Portland Cement-Silica Fume Paste and Mortar*, Cement and Concrete Research Volume 20, pp. 103-119, 1990.

Michael D. Brown, Greg Sellers, Dr. Kevin Folliard and Dr. David Fowler, *Restrained Shrinkage Cracking of Concrete Bridge Decks: State of the Art Review*, Federal Highway Administration Technical Report TX-0-4098-1, 2001.

M. J. Hasan, M. Afroz and H. M. I. Mahmud, *An Experimental Investigation on Mechanical Behavior of Macro Synthetic Fiber Reinforced Concrete*, International Journal of Civil and Environmental Engineering, Vol. 11 No. 3, p 18-23, 2011.

M. N. Soutsos, T.T. Le, A. P. Lampropoulos, *Flexural Performance of Fiber Reinforced Concrete made with Steel and Synthetic Fibers*, Construction and Building Materials 36, pp. 704-710, 2012.

M. Pigeon and F. Saucier, *Durability of Repaired Concrete Structures,* Proceedings of the International Conference on Advances in Concrete Technology, pp. 741-773, 1992.

Nicola Buratti, Claudio Mazzotti, and Marco Savoia, *Post-Cracking Behaviour of Steel and Macro-Synthetic Fibre-Reinforced Concretes*, Construction and Building Materials 25, p. 2713-2722, 2011.

Pablo Pujadas, Ana Blanco, Sergio Cavalaro, Albert de la Fuente and Antonio Aguado, *Fibre Distribution in Macro-plastic Fibre Reinforced Concrete Slab-panels,* Construction and Building Materials 64, pp. 496-503, 2014.

Paul D. Krauss, and Ernest A. Rogalla. *Transverse cracking in newly constructed bridge decks*. No. Project 12-37 FY'92. 1996.

P. Kumar Mehta and Richard W. Burrows, *Building Durable Structures in the 21st Century,* Indian Concrete Journal p. 437-443, 2001.

P. S. Song and S. Hwang, *Mechanical Properties of High-Strength Steel Fiber-Reinforced Concrete*, Construction and Building Materials 18, p. 669-673, 2004.

Rambod Hadidi and M. Ala Saadeghvaziri, *Transverse Cracking of Concrete Bridge Decks: State-of-the-Art*, Journal of Bridge Engineering p. 503-510, 2005.

Ronald F. Zollo, *Fiber-Reinforced Concrete: An Overview after 30 Years of Development*, Concrete and Cement Composites 19 p. 107-122, 1997.

Saber Fallah and Mahdi Nematzadeh*, Mechanical Properties and Durabiltiy of High Strehgth Concrete Containing Macro-polymeric and Polypropylene Fibers with Nano-silica and Silica Fume,* Construction and Building Materials Volume 132, pp. 170-187, 2017.

S. Slatnick, K.A. Riding, K.J. Folliard, M.C.G. Juenger, A.K. Schindler, *Evaluation of autogenous deformation of concrete at early ages*, ACI Mater J. 108 – p. 21-28, 2011.

T. Plague, C Desmettre and J.P. Charron, *Influence of Fiber Type and Fiber Orientation on Cracking and Permeability of Reinforced Concrete Under Tensile Loading*, Cement and Concrete Research 94, p. 59-70, 2017.

V. Baroghel-Bouny and P.-C. Aitcin, *Shrinkage of Concrete: Shrinkage 2000*, Proceedings of the International RILEM Workshop, 2000.

W. B. Ashraf and M. A. Noor, *Performance-Evaluation of Concrete Properties for Different Combined Aggregate Gradation Approaches*, Procedia Engineering (14), pp. 2627-2634, 2011.

Youping Liu and Richard E. Weyers, *Modeling the Time-to-Corrosion Cracking in Chloride Contaminated Reinforced Concrete Structures*, Materials Journal V. 95, pp. 675-680, 1998.

Zongcai Den and Jianhui Li, *Mechanical Behaviors of Concrete Combined with Steel and Synthetic Macro-Fibers*, International Journal of Physical Sciences Vol. 1 (2), pp. 57-66, 2016.